

ผลของการเติมโลหะและการใส่สีย้อมที่มีต่อการเปลี่ยนเฟสของอะลูมินา  
ซึ่งเตรียมโดยวิธีการตกตะกอน



นางสาวเบญจพร เมืองสมบัติ

สถาบันวิทยบริการ

จุฬาลงกรณ์มหาวิทยาลัย

วิทยานิพนธ์นี้เป็นส่วนหนึ่งของการศึกษาตามหลักสูตรปริญญาวิศวกรรมศาสตรมหาบัณฑิต

สาขาวิชาวิศวกรรมเคมี ภาควิชาวิศวกรรมเคมี

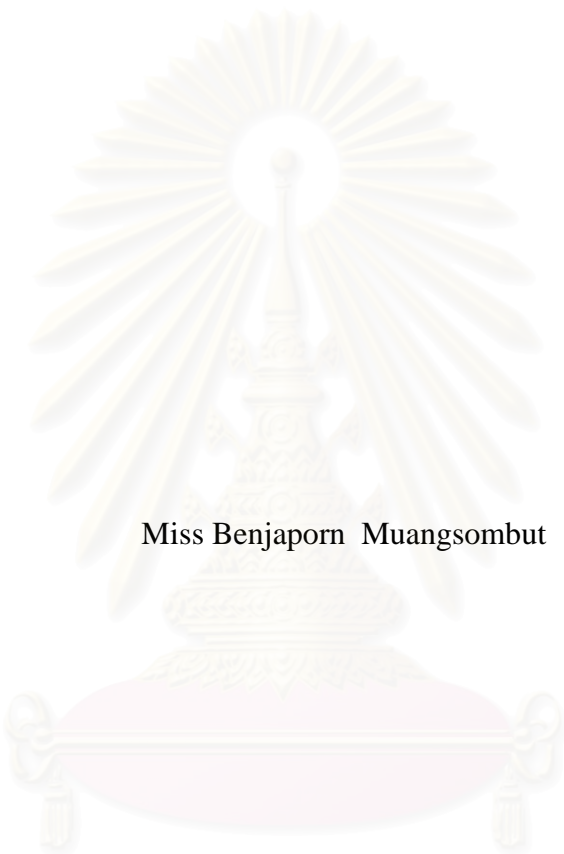
คณะวิศวกรรมศาสตร์ จุฬาลงกรณ์มหาวิทยาลัย

ปีการศึกษา 2548

ISBN 974-53-2644-5

ลิขสิทธิ์ของจุฬาลงกรณ์มหาวิทยาลัย

**EFFECTS OF METAL DOPING AND SEED INTRODUCTION  
ON PHASE TRANSFORMATION OF ALUMINA PREPARED  
BY PRECIPITATION METHOD**



Miss Benjaporn Muangsombut

สถาบันวิทยบริการ  
จุฬาลงกรณ์มหาวิทยาลัย

A Thesis Submitted in Partial Fulfillment of the Requirements  
for the Degree of Master of Engineering Program in Chemical Engineering

Department of Chemical Engineering

Faculty of Engineering

Chulalongkorn University

Academic Year 2005

ISBN: 974-53-2644-5

Thesis Title            EFFECTS OF METAL DOPING AND SEED  
                                 INTRODUCTION ON PHASE TRANSFORMATION OF  
                                 ALUMINA PREPARED BY PRECIPITATION METHOD


By                            Miss Benjaporn Muangsombut

Field of Study            Chemical Engineering

Thesis Advisor           Assistant Professor Varong Pavarajarn, Ph.D.

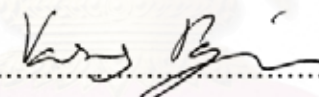
---

Accepted by the Faculty of Engineering, Chulalongkorn University in Partial  
Fulfillment of the Requirements for the Master's Degree

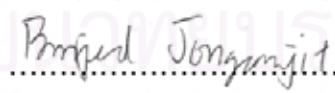
  
..... Dean of the Faculty of Engineering  
(Professor Direk Lavansiri, Ph.D.)

THESIS COMMITTEE

  
..... Chairman  
(Associate Professor Suttichai Assabumrungrat, Ph.D.)

  
..... Thesis Advisor  
(Assistant Professor Varong Pavarajarn, Ph.D.)

  
..... Member  
(Associate Professor Tawatchai Charinpanitkul, Ph.D.)

  
..... Member  
(Assistant Professor Bunjerd Jongsomjit, Ph.D.)

เบญจพร เมืองสมบัติ: ผลของการเติมโลหะและการใส่สีย้อมที่มีต่อการเปลี่ยนเฟสของอะลูมินาซึ่งเตรียมโดยวิธีการตกตะกอน (EFFECTS OF METAL DOPING AND SEED INTRODUCTION ON PHASE TRANSFORMATION OF ALUMINA PREPARED BY PRECIPITATION METHOD) อ. ที่ปรึกษา: ผศ.ดร. วงศ์ ปวรอาจารย์, 117 หน้า. ISBN: 974-53-2644-5

ผงอะลูมินาที่มีขนาดผลึกในระดับนาโนเมตรได้ถูกสังเคราะห์จากวิธีตกตะกอน โดยได้ทำการศึกษาปัจจัยของการเติมโลหะ และการใส่สีย้อม ที่มีผลต่อการเปลี่ยนเฟสโครงสร้างผลึก ความหนาแน่น สี ขนาดและการกระจายขนาดของอนุภาค นอกจากนี้ได้เติมโลหะตัวที่สองเข้าไปโดยการผสมเกลือไนเตรตของเหล็ก โคโรเมียม อิทเทรียม หรือ แมกนีเซียม เข้าไปในสารละลาย ด้วยความเข้มข้นต่างๆ ในช่วง 0.1 ถึง 10 เปอร์เซ็นต์ของสารตั้งต้นที่ทำปฏิกิริยา การให้ความร้อนทำให้ผลิตภัณฑ์ตั้งต้นเปลี่ยนโครงสร้างผลึก เป็นแกมมาอะลูมินา และอัลฟาอะลูมินา ตามลำดับ การเติมโลหะในปริมาณเล็กน้อยมีผลให้อุณหภูมิในการเปลี่ยนเฟสจากแกมมาเป็นอัลฟาอะลูมินาสูงขึ้นที่อุณหภูมิ 1000 องศาเซลเซียส ซึ่งงานที่ขึ้นรูปได้ถูกเผาผนึกในอากาศที่อุณหภูมิ 1550 องศาเซลเซียส เป็นเวลา 2 ชั่วโมงพบว่า ค่าความหนาแน่นสัมพัทธ์ของชิ้นงานอะลูมินาที่เตรียมมาจากตัวอย่างต่าง ๆ มีค่าอยู่ในช่วงร้อยละ 90-96 ของความหนาแน่นทางทฤษฎี และมีขนาดเกรนอยู่ในช่วง 1-1.5 ไมโครเมตร

## สถาบันวิทยบริการ จุฬาลงกรณ์มหาวิทยาลัย

ภาควิชา.....วิศวกรรมเคมี.....  
สาขาวิชา.....วิศวกรรมเคมี.....  
ปีการศึกษา.....2548.....

ลายมือชื่อนิสิต.....เบญจพร เมืองสมบัติ.....  
ลายมือชื่ออาจารย์ที่ปรึกษา.....  
ลายมือชื่ออาจารย์ที่ปรึกษาร่วม.....

## 4770333221 : MAJOR CHEMICAL ENGINEERING

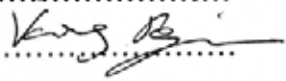
KEY WORDS : PRECIPITATION, ALUMINA, PHASE TRANSFORMATION, METAL DOPING

BENJAPORN MUANGSOMBUT: EFFECTS OF METAL DOPING AND SEED INTRODUCTION ON PHASE TRANSFORMATION OF ALUMINA PREPARED BY PRECIPITATION METHOD. THESIS ADVISOR: ASSISTANT PROFESSOR VARONG PAVARAJARN, Ph.D., 117 pp. ISBN: 974-53-2644-5

Nanocrystalline alumina is synthesized by precipitation method. The effects of metal doping and sol-seeding on the phase transformation, crystal structure, density, color, size and size distribution of powder are investigated. The secondary metal doping is done by incorporating the nitrate salt of iron, chromium, yttrium or magnesium into the solution with various metal concentrations, in the range of 0.1-10 wt% of the metal precursor. The precipitate transforms to  $\alpha$ -alumina upon the calcination at high temperature via the formation of metastable  $\gamma$ -alumina. It is found that small amount of the secondary metal doping is sufficient to increase the phase transformation temperature from  $\gamma$ - to  $\alpha$ -alumina up to 1000°C. Fabrication of undoped alumina, sol-seeded alumina and metal-doped alumina are also investigated. The compacted bodies were sintered at 1550°C for 2 h in air. The relative density of sintered specimens prepared from various samples is in the range of 90-96% of theoretical density and grain size is in the range of 1-1.5  $\mu\text{m}$ .

สถาบันวิทยบริการ  
จุฬาลงกรณ์มหาวิทยาลัย

Department ..... Chemical Engineering .....  
Field of Study ..... Chemical Engineering .....  
Academic year ..... 2005 .....

Student's signature ..... Benjaporn Muangsombut .....  
Advisor's signature .....  .....  
Co-advisor's signature .....

## ACKNOWLEDGEMENTS

The author would like to express her sincere gratitude and appreciation to her advisor, Assistant Professor Dr. Varong Pavarajarn, for his invaluable suggestions, stimulating, useful discussions throughout this research and devotion to revise this thesis otherwise it can not be completed in a short time.

The author is similarly grateful to Professor Shigetaka Wada, Mr. Nirut Wangmuklang and Mr. Soontorn Tansungnoen for their kind suggestion throughout this work. In addition, the author would also be grateful to Associate Professor Suttichai Assabumrungrat, as the chairman, and Associate Professor Dr. Tawatchai Charinpanitkul and Assistant Professor Dr. Bunjerd Jongsomjit, as the members of the thesis committee.

The author would like to acknowledge to Thailand Research Fundd (TRF), Thailand Japan Technology Transfer Project (TJTTP), Graduate School of Chulalongkorn University and National Nano-Technology Center (NANOTEC) for their financial support.

The author wishes to thank the members of the Center of Excellence on Catalysis and Catalytic Reaction Engineering, Department of Chemical Engineering, Faculty of Engineering, Chulalongkorn University for their assistance especially Dr. Okorn Mekasuwandumrong and Miss Tanitta Prasitwuttisak.

Finally, the author would like to express her highest gratitude to her parents who always pay attention to her all the times for suggestions and have provided her support and encouragement. The most success of graduation is devoted to her parents.

สถาบันวิทยบริการ  
จุฬาลงกรณ์มหาวิทยาลัย

# CONTENTS

	<b>PAGE</b>
ABSTRACT (IN THAI).....	iv
ABSTRACT (IN ENGLISH).....	v
ACKNOWLEDGMENTS.....	vi
CONTENTS.....	vii
LIST OF TABLES.....	x
LIST OF FIGURES.....	xi
CHAPTER	
I INTRODUCTION.....	1
II THEORY AND LITERATURE REVIEWS.....	3
2.1 Alumina (Al <sub>2</sub> O <sub>3</sub> ).....	6
2.2 Precursors for Metastable Alumina Synthesis.....	7
2.2.1 Aluminum trihydroxides.....	8
2.2.2 Aluminum monohydroxides.....	8
2.2.3 Tohdite: 5Al <sub>2</sub> O <sub>3</sub> .H <sub>2</sub> O.....	9
2.2.4 Amorphous anodic Al <sub>2</sub> O <sub>3</sub> film.....	9
2.2.5 Alumina melt.....	10
2.3 Formation and Crystal Structure of Active Aluminas.....	10
2.3.1 Dehydration of aluminum trihydroxides.....	12
2.3.2 Dehydration of aluminum monohydroxides.....	13
2.4 Preparation of Alumina Powder by Precipitation Method .....	14
III EXPERIMENTAL.....	27
3.1 Chemicals .....	27
3.2 Experimental procedure.....	28
3.2.1 Synthesis of alumina powder.....	28
3.2.2 Fabrication of alumina article .....	29
3.3 Characterizations .....	30
3.3.1 X-Ray Diffraction (XRD).....	30
3.3.2 Scanning Electron Microscopy (SEM).....	30

	<b>PAGE</b>
3.3.3 Fourier transform infrared spectroscopy (FTIR).....	30
3.3.4 Particle size distribution analysis (PSD).....	30
3.3.5 X-Ray photoelectron spectroscopy (XPS).....	31
3.3.6 UV/Visible spectrophotometry (UV/Vis).....	31
3.3.7 Surface area measurement.....	31
3.3.8 Thermogravimetric analysis (TGA).....	31
<b>IV RESULTS AND DISCUSSION .....</b>	<b>32</b>
4.1 Properties of Undoped Alumina Powder.....	32
4.1.1 Preparation without sol-seeding.....	33
4.1.2 Effects of Sol-seeding.....	35
4.2 Effect of Secondary Metal Doping.....	38
4.2.1 Doping in low content.....	38
4.2.2 Effect of Iron.....	50
4.2.3 Effect of Magnesium.....	52
4.2.4 Effect of Yttrium.....	55
4.2.5 Effect of Chromium.....	58
4.2.6 Lattice parameters of metal-doped alumina.....	61
4.2.7 XPS analysis.....	64
4.2.8 Introduction of both metal and sol-seed to alumina.....	67
4.3 Fabrication of Alumina Powder.....	72
<b>V CONCLUSIONS AND RECOMMENDATIONS.....</b>	<b>75</b>
5.1 Conclusions.....	75
5.2 Recommendations.....	76
<b>REFERENCES.....</b>	<b>77</b>
<b>APPENDICES.....</b>	<b>88</b>
APPENDIX A: Calculation of concentration of both reactants in precipitation method.....	89
APPENDIX B: Calculation of amount of chromium precursor for chromium doped alumina.....	91
APPENDIX C: Calculation of the crystallite size.....	95
APPENDIX D: Phase transformation behavior of products calcined at various temperatures.....	98



	<b>PAGE</b>
APPENDIX E: Conditions for ball mill and dispersion of powder.....	109
APPENDIX F: Density.....	110
LIST OF PUBLICATION.....	112
VITAE.....	117



สถาบันวิทยบริการ  
จุฬาลงกรณ์มหาวิทยาลัย

## LIST OF TABLES

TABLE		PAGE
2.1	Causes of color in corundum.....	23
4.1	Mass concentration of dopant for as-synthesized and calcined powder, analyzed by XPS.....	39
4.2	Phase of products doped with 0.1 wt.% of metal and calcined at various temperatures.....	39
4.3	Crystallite size of powder doped with 0.1 wt.% metal and calcined at various temperatures.....	42
4.4	Average particle size for product calcined at 1200°C.....	43
4.5	Specific surface area of alumina powder after milling.....	48
4.6	Lattice parameters of $\alpha$ -Al <sub>2</sub> O <sub>3</sub> in products doped with 0.1 wt.% of metal and calcined at 1200°C.....	62
4.7	Lattice parameters of $\gamma$ -Al <sub>2</sub> O <sub>3</sub> in products doped with 0.1 wt.% of metal and calcined at various temperatures.....	62
4.8	Density of sintered alumina specimen.....	72
4.9	Average grain size of sintered specimens.....	73

## LIST OF FIGURES

FIGURE		PAGE
2.1	Transformation sequences of aluminum hydroxides.....	11
2.2	Common processing routes resulting in formation of different metastable Al <sub>2</sub> O <sub>3</sub> structures and sequences of phase transformation toward the stable $\alpha$ -alumina.....	12
2.3	Metastable aluminas formed by dehydration of the trihydroxides.....	13
2.4	Phase transformation of metastable aluminas formed from trihydroxides in vacuum.....	13
2.5	Parameters affecting property of the precipitate.....	15
2.6	Correlation between green bulk density, final density, and forming pressure of high-purity alumina ceramics.....	17
2.7	Steps of dry pressing operation.....	18
2.8	Formation of a neck during the sintering of two fine particles.....	20
2.9	Development of the density of alumina ceramics during sintering.....	21
4.1	XRD patterns of undoped products calcined at various temperatures.....	33
4.2	FTIR spectra of undoped products calcined at various temperatures.....	34
4.3	Result from Thermogravimetric analysis (TG curve) of the precipitate...	35
4.4	XRD patterns of products produced by precipitation accompanied by sol-seeding and calcined at various temperatures.....	36
4.5	FTIR spectra of products produced by precipitation accompanied by sol-seeding and calcined at various temperatures.....	37
4.6	Result from Thermogravimetric analysis (TG curve) of the sample from precipitation accompanied by sol-seeding.....	37
4.7	FTIR spectra of precipitate for 0.1 wt.% of metal doping.....	41
4.8	SEM images of calcined powder before milling: (a) undoped alumina, (b) sol-seeded alumina, (c) 0.1 wt.%Cr-doped alumina, (d) 0.1 wt.% Fe-doped alumina, (e) 0.1 wt.%Mg-doped alumina, (f) 0.1 wt.% Y-doped alumina.....	44

<b>FIGURE</b>	<b>PAGE</b>	
4.9	SEM images of calcined powder after milling for 72 h: (a) undoped alumina, (b) sol-seeded alumina, (c) 0.1 wt.%Cr-doped alumina, (d) 0.1 wt.%Fe-doped alumina, (e) 0.1 wt.%Mg-doped alumina, (f) 0.1 wt.%Y-doped alumina.....	45
4.10	Particle size distribution of powder calcined at 1200°C: (a) before milling, (b) after 72 h milling.....	46
4.11	Reflective UV/visible spectra of calcined powders.....	49
4.12	XRD patterns of the products doped with iron in various content and calcined at 1000°C.....	50
4.13	XRD patterns of products calcined at various temperatures, which were obtained from precipitation accompanied by iron at 10 wt.%.....	51
4.14	FTIR spectra of products calcined at various temperatures, which were obtained from precipitation accompanied by iron at 10 wt.%.....	52
4.15	XRD patterns of the products doped with magnesium in various content and calcined at 1000°C.....	53
4.16	XRD patterns of the products doped with magnesium in various content and calcined at 1200°C.....	53
4.17	XRD patterns of products calcined at various temperatures, which were obtained from precipitation accompanied by magnesium at 10 wt.%.....	54
4.18	FTIR spectra of products calcined at various temperatures, which were obtained from precipitation accompanied by magnesium at 10 wt.%.....	54
4.19	XRD patterns of the products doped with yttrium in various content and calcined at 1200°C.....	56
4.20	XRD patterns of products calcined at various temperatures, which were obtained from precipitation accompanied by yttrium at 10 wt.%.....	57
4.21	FTIR spectra of products calcined at various temperatures, which were obtained from precipitation accompanied by yttrium at 10 wt.%.....	58
4.22	XRD patterns of the products doped with chromium in various content and calcined at 800°C.....	59

<b>FIGURE</b>	<b>PAGE</b>
4.23	XRD patterns of the products doped with chromium in various content and calcined at 1000°C..... 59
4.24	XRD patterns of products calcined at various temperatures, which were obtained from precipitation accompanied by chromium at 10 wt.%..... 60
4.25	FTIR spectra of products calcined at various temperatures, which were obtained from precipitation accompanied by chromium at 10 wt.%..... 61
4.26	The <i>a</i> and <i>b</i> -axis of lattice constant of $\alpha$ -Al <sub>2</sub> O <sub>3</sub> from various metal content..... 63
4.27	The <i>c</i> -axis of lattice constant of $\alpha$ -Al <sub>2</sub> O <sub>3</sub> from various metal content..... 63
4.28	The O 1s binding energy of the samples calcined at different temperatures..... 64
4.29	The Al 2p binding energy of the samples calcined at different temperatures..... 65
4.30	The metal content at the surface of sample calcined at different temperatures..... 66
4.31	XRD patterns showing phase transformation of products incorporating both iron-doping and sol-seeding, which were synthesized from: (a) Sol-seeded AAS solution mixed with iron nitrate; (b) AAS solution with iron doped sol..... 68
4.32	XRD patterns showing phase transformation of products incorporating both iron-doping and sol-seeding, which were synthesized from: (a) Sol-seeded AAS solution mixed with chromium nitrate; (b) AAS solution with chromium doped sol..... 69
4.33	XRD patterns showing phase transformation of products incorporating both iron-doping and sol-seeding, which were synthesized from: (a) Sol-seeded AAS solution mixed with magnesium nitrate; (b) AAS solution with magnesium doped sol..... 70
4.34	XRD patterns showing phase transformation of products incorporating both iron-doping and sol-seeding, which were synthesized from: (a) Sol-seeded AAS solution mixed with yttrium nitrate; (b) AAS solution with yttrium doped sol..... 71

<b>FIGURE</b>	<b>PAGE</b>	
4.35	Microstructures of alumina samples sintered for 2 h at 1550°C: (a) undoped alumina, (b) sol-seeded alumina, (c) 0.1 wt.%Cr-doped alumina, (d) 0.1 wt.%Fe-doped alumina, (e) 0.1 wt.%Mg-doped alumina, (f) 0.1 wt.%Y-doped alumina.....	74
C.1	The 012 diffraction peak of $\alpha$ -alumina for calculating the crystallite size.....	96
C.2	The graph indicating that value of the line broadening attribute to the experimental equipment from the $\alpha$ -alumina standard.....	97
D.1	XRD patterns of undoped product calcined at various temperatures.....	98
D.2	XRD patterns of the product synthesized by precipitation accompanied by sol-seeding and calcined at various temperatures.....	98
D.3	XRD patterns of the precipitate and products calcined at various temperatures, which were obtained from precipitation accompanied by iron at 0.1 wt.%.....	99
D.4	XRD patterns of the precipitate and products calcined at various temperatures, which were obtained from precipitation accompanied by iron at 0.5 wt.%.....	99
D.5	XRD patterns of the precipitate and products calcined at various temperatures, which were obtained from precipitation accompanied by iron at 1.0 wt.%.....	100
D.6	XRD patterns of products calcined at various temperatures, which were obtained from precipitation accompanied by iron at 10 wt.%.....	100
D.7	XRD patterns of the precipitate and products calcined at various temperatures, which were obtained from precipitation accompanied by chromium at 0.1 wt.%.....	101
D.8	XRD patterns of the precipitate and products calcined at various temperatures, which were obtained from precipitation accompanied by chromium at 0.5 wt.%.....	101
D.9	XRD patterns of the precipitate and products calcined at various temperatures, which were obtained from precipitation accompanied by chromium at 1.0 wt.%.....	102

<b>FIGURE</b>		<b>PAGE</b>
D.10	XRD patterns of products calcined at various temperatures, which were obtained from precipitation accompanied by chromium at 10 wt.%.....	103
D.11	XRD patterns of the precipitate and products calcined at various temperatures, which were obtained from precipitation accompanied by magnesium at 0.1 wt.%.....	104
D.12	XRD patterns of the precipitate and products calcined at various temperatures, which were obtained from precipitation accompanied by magnesium at 0.5 wt.%.....	104
D.13	XRD patterns of the precipitate and products calcined at various temperatures, which were obtained from precipitation accompanied by magnesium at 1.0 wt.%.....	105
D.14	XRD patterns of products calcined at various temperatures, which were obtained from precipitation accompanied by magnesium at 10 wt.%.....	105
D.15	XRD patterns of the precipitate and products calcined at various temperatures, which were obtained from precipitation accompanied by yttrium at 0.1 wt.%.....	106
D.16	XRD patterns of the precipitate and products calcined at various temperatures, which were obtained from precipitation accompanied by yttrium at 0.5 wt.%.....	106
D.17	XRD patterns of the precipitate and products calcined at various temperatures, which were obtained from precipitation accompanied by yttrium at 1.0 wt.%.....	107
D.18	XRD patterns of products calcined at various temperatures, which were obtained from precipitation accompanied by yttrium at 10 wt.%.....	108

# CHAPTER I

## INTRODUCTION

Alumina ( $\text{Al}_2\text{O}_3$ ) has been considered as one of the most promising advanced materials for variety of applications because of its distinctive chemical, mechanical and thermal properties. Alumina is a highly insulating material characterized by mixed ionic and covalent bonding, low concentrations of both ionic defects and electronic carriers [1], high melting point, high temperature stability, chemical inactivity, extreme hardness, and large band gap energy. It is widely used as structural material (e.g., reinforcement or matrix in composites and a diffusion barrier in coatings), microelectronic material (e.g., silicon on sapphire transistors and packaging substrates), and membranes (e.g., micro- and ultrafiltrations). Many preparation methods have been developed to prepare alumina powder that possesses the required characteristics. Examples of these method are precipitation from solution [2], sol-gel synthesis [3], hydrothermal synthesis [4], microwave synthesis [5], emulsion evaporation [6, 7] and solvothermal synthesis [8-15]. In such methods, the characteristics of alumina are taylored-made by controlling the crystal structure, crystallite size, particle shape, particle size distribution, degree of agglomeration and porosity of particles [16-23].

Alumina is known to exist in a number of metastable polymorphs in addition to the thermodynamically stable alpha-alumina ( $\alpha\text{-Al}_2\text{O}_3$ ) or corundum form. There are six principal metastable phases of alumina designated by the Greek letters chi ( $\chi$ ), kappa ( $\kappa$ ), eta ( $\eta$ ), theta ( $\theta$ ), delta ( $\delta$ ), and gamma ( $\gamma$ ), respectively. Many industrial solid catalysts are made up from active centers anchored on transition alumina supports due to the prominent characteristics of such transition aluminas, such as high porosity, high surface area, good mechanical strength and thermal stability.

Alumina ceramics are usually polycrystalline and not transparent. For transparent alumina ceramics, they can be synthesized either in single-crystal or polycrystalline forms [24]. Single crystal alumina (SCA) has been used as highly transparent material for many commercial, industrial and military applications, such



as optical windows for laser, armor part, IR-dome for infrared missile guidance system and artificial jewelry. Polycrystalline alumina (PCA) has been available for optical application since early 1962 when Coble [25] invented translucent alumina, which was composed of micrometer-sized grains. PCA is normally fabricated by sintering of alumina powder.

The cost of PCA manufacturing is much lower than SCA. It is also easier to produce PCA in large size and complicated shape. Therefore, the development of PCA can actuate a new world of artificial precious stones, which is differentiated from that of natural jewelry and, in turn, could help increasing the nation's benefits. From the background above mentioned, we are interested in the polycrystalline alumina ceramic for jewelry industry.

Nevertheless, light transmission of PCA is normally small in contrast to that of SCA, which shows a complete transparency. The low light transmission of PCA is caused by scattering of light at grain boundaries and residual pores [26]. Thus, transparency of PCA can be increased by complete elimination of the residual porosity, and reduction of the grain size to submicrometered or nanometered level [27].

It is, therefore, the objective of this research to study the precipitation method to synthesize nanocrystalline alumina powder suitable for the production of transparency polycrystalline alumina. Effect of metal doping and seed introduction during alumina synthesis are investigated. Alumina powders are also fabricated into alumina articles by sintering at high temperature, in order to investigate the effect of the synthesis powder on properties of the sintered article.

## CHAPTER II

### THEORY AND LITERATURE REVIEW

Alumina ( $\text{Al}_2\text{O}_3$ ) exists in many metastable phases before transformation to the stable  $\alpha\text{-Al}_2\text{O}_3$  (corundum form). The metastable alumina can be divided into two groups, i.e. the face-centered cubic (fcc) and the hexagonal close packing (hcp) arrangement of oxygen anions. The distribution of aluminum cations depends on the structure of the polymorphs [28]. The  $\text{Al}_2\text{O}_3$  structures based on fcc packing of oxygen include  $\gamma$ -,  $\eta$ -,  $\theta$  -, and  $\delta$ -phases, whereas the  $\text{Al}_2\text{O}_3$  structures based on hcp packing of oxygen are the  $\alpha$ -,  $\kappa$ - and  $\chi$ -phases.

The excellent stability of  $\text{Al}_2\text{O}_3$  makes it an important constituent for many protective oxide scales of the surface of high-temperature metal and alloy. The dominant (and stable) phase in these scales is  $\alpha\text{-Al}_2\text{O}_3$ , which also contributes to adhesion and coherence of the scale. Thus, understanding of the metastable intermediate polymorphic structures and the transformation mechanisms that result in the formation of  $\alpha\text{-Al}_2\text{O}_3$  is important for heat treatment to promote stable-scale formation. Understanding of the mechanisms of polymorphic phase transformation is also important for the sintering of nanosized  $\text{Al}_2\text{O}_3$  powder, in which the starting material is usually metastable alumina and consequently transformed to  $\alpha\text{-Al}_2\text{O}_3$  during sintering process. Both the sintering and the grain-growth behavior relate strongly on the phase transformation.

Boehmite is one of the polymorphs of  $\text{AlO}(\text{OH})$  which often involves in transformation pathway of alumina. The so-called pseudoboehmite is microcrystalline boehmite which has extra water content due to the surface hydroxyl groups. Pseudoboehmite, one of the most widely used precursors to produce alumina can be decomposed to form transition alumina. Phase transformation from pseudoboehmite to various forms of alumina such as  $\gamma$ -,  $\delta$ -,  $\theta$ - and finally  $\alpha$ - phase takes place by heat treatment at various temperatures. This phase transformation is the major cause for loss of surface area [29].

Transition aluminas normally start losing the surface area even at temperature below 800°C due to the elimination of micro-pores during heat treatment. However, drastic loss occurs at temperature higher than 1000°C when the crystallization to the thermodynamically stable  $\alpha$ -Al<sub>2</sub>O<sub>3</sub> occurs [30].

The phase transformation of  $\theta$ - to  $\alpha$ -Al<sub>2</sub>O<sub>3</sub> is believed to occur via a nucleation and growth process [31, 32]. Investigations on the critical crystallite size for the transformation have been previously reported [20, 33-38], although there are substantial discrepancies among them. Recent studies on the nanosized alumina powder have reported that the transformation process from  $\theta$ - to  $\alpha$ -Al<sub>2</sub>O<sub>3</sub> requires critical size of  $\theta$ -Al<sub>2</sub>O<sub>3</sub> at the nucleation stage to initiate the formation of the  $\alpha$ -Al<sub>2</sub>O<sub>3</sub> nucleus. During the transformation,  $\theta$ -crystallites grow to the critical size and remain as monodispersed crystallites before the transformation to  $\alpha$ -Al<sub>2</sub>O<sub>3</sub> nucleus. Then, the  $\alpha$ -Al<sub>2</sub>O<sub>3</sub> nucleus grow drastically before the polycrystalline  $\alpha$ -Al<sub>2</sub>O<sub>3</sub> particles are formed by sintering [39, 40].

Morinaga et al. (2000) studied the phase transformation occurring during the thermal decomposition of ammonium aluminum carbonate hydroxide into  $\alpha$ -alumina [41]. Amorphous,  $\gamma$ - and  $\theta$ -alumina were identified as intermediate species. They have found that type of gas used in calcination affects grain size distribution of the final  $\alpha$ -alumina particles.

Other studies have reported on methods to enhance the rate of phase transformation [42]. The effect of defects on the transformation behavior has been reported in many papers. Shek et al. reported that  $\gamma$ -alumina produced by nanosized amorphous alumina directly transformed to stable  $\alpha$ -alumina [43]. This behavior was explained by the reduction of defects and lattice distortion during the relaxation process, which released large amount of energy and thus promoted the nucleation of  $\alpha$ -Al<sub>2</sub>O<sub>3</sub>.

Previous studies have focused on the correlation between the phase transformation of transition aluminas to  $\alpha$ -alumina and sinterability of the final material [42, 44-46]. The stabilization of transition alumina is also a challenge for

other applications, such as the ceramic membranes or the support used for catalytic conversion of automotive exhaust gas [47-49]. To prevent or delay alumina phase transformation, addition of doping elements has been extensively used [50-52]. Rossignol et al. reported that an introduction of doping element in form of nitrate salt to alumina synthesized by sol-gel method could prolong the transformation from  $\theta$ - to  $\alpha$ -alumina to take place at higher temperature [53].

Several studies have been carried out on the direct phase transformation of alumina from one phase to another. The mechanism of the direct phase transformation from  $\gamma$ -alumina to  $\alpha$ -alumina, which involves the conversion of the cubic close packing of oxygen ions into the stable hexagonal close packing, has been examined [54, 55]. It is known that the temperature triggering the  $\gamma$ - to  $\alpha$ -alumina transformation can be influenced by the presence of cation additive. The influence of the cation additive on the transformation temperature has been related to the respective radii and charge of the specific cations. The temperature, at which the phase transformation to  $\alpha$ -alumina takes place, can be lowered by addition of  $\text{Fe}^{3+}$  ions or  $\alpha$ - $\text{Al}_2\text{O}_3$  grains acting as seeds to alumina, respectively [56, 57].

Seeding is a general approach to enhance the anisotropic growth of alumina grains, which may increase fracture toughness of alumina. In 1984, Kumagai and Messing reported that they succeeded in lowering the formation temperature of  $\alpha$ -alumina by introducing seed particles of alumina to corundum structures [42]. Seabaugh et al. used  $\alpha$ - $\text{Al}_2\text{O}_3$  platelets as seeds to induce the growth of plate-like alumina [58]. Recently, Yoshizawa et al. reported that alumina ball abrasives, which was introduced into aluminum hydroxide as seeds, enhanced the phase transformation to  $\alpha$ - $\text{Al}_2\text{O}_3$  [59]. Moreover, the hydroxide in the abrasives could transform into  $\alpha$ - $\text{Al}_2\text{O}_3$  at temperature lower than  $1000^\circ\text{C}$ , which is much lower than the conventional thermal phase transformation ( $\approx 1200^\circ\text{C}$ ).

Baca et al. have described the transformation of boehmite into  $\alpha$ -alumina as a topotactic sequence, which forms several increasingly ordered transition aluminas [60]. The final transition to  $\alpha$ -alumina is a nucleation-and-growth process, in which the nucleation sites usually are oxygen vacancies and/or dislocations [61]. Corundum

( $\alpha$ - $\text{Al}_2\text{O}_3$ ) seeds enable an epitaxial growth of the corundum phase. According to the works done by Xie et al. [62, 63], seeds can efficiently reduce the transformation temperature of aluminum hydroxide to  $\alpha$ - $\text{Al}_2\text{O}_3$ . Grain size as well as size distribution of the calcined powder are closely related to size and distribution of seeds introduced. It also changes the sintering behavior and microstructure of the calcined powder.

Yoldas extensively studied the formation of aluminum hydroxide sols by the hydrolysis of aluminum alkoxide using several acidic catalysts [64]. Moreover, Youn et al. found that an addition of alumina-sol into  $\gamma$ -alumina enabled the onset of the  $\gamma$ - to  $\alpha$ -alumina transformation at temperatures as low as  $600^\circ\text{C}$  [65]. This phenomenon was designated as the “sol-effect”.

## 2.1 Alumina ( $\text{Al}_2\text{O}_3$ )

Alumina is an important material in many fields because of its excellent and wide range properties. Study of alumina has been a subject of great interest for many decades. It is one of the most common crystalline materials to be used as adsorbent, coating, soft abrasives, catalyst and catalyst support because of its fine particle size, high surface area, catalytic activity, distinctive chemical, mechanical and thermal properties. The details described in this part are based on a review of Levin and Brandon [54] and a text book from Lippens and Steggerda [66].

Alumina is widely used as material in field of catalytic technology because of its good and important properties. It has high surface area with fine particle size, good adsorbent, catalytic activity and high melting point (above  $2000^\circ\text{C}$ ) which is also desirable for the support. For catalytic applications, alumina can be used in three functions: as catalyst, co-catalyst and support. For example, alumina is used as catalyst in the reaction of steam reforming process at high temperature. Alumina is used as co-catalyst in the catalytic reforming of gasoline and as support in many cases, such as in catalytic converter and in membrane technology.

Although corundum ( $\alpha$ - $\text{Al}_2\text{O}_3$ ) is recognized as the thermodynamically stable polymorph of alumina at ambient pressure, this phase is not readily synthesized at temperature lower than  $1100^\circ\text{C}$  [28, 29, 54]. Corundum can be synthesized from

various kinds of hydroxide precursors (gibbsite, bayerite, and boehmite), which can be directly derived from the Bayer process. The hydroxide precursors decompose to nanocrystalline transition aluminas upon dehydration at temperature in the range of 300 to 600°C. With increasing temperature, metastable products from the decomposition progress through additional series of phase transformation until corundum is finally formed above 1100°C [28, 29, 54, 67]. Similarly, transition phases are also formed during the direct decomposition or oxidation of aluminum salts, alkoxides, and metal organics [28, 29, 54].

$\gamma$ -Alumina is an enormously important material in catalysis. It is frequently used as a catalyst in hydrocarbon conversion (petroleum refining), and as a support for automotive and industrial catalysts. It is one of the metastable polymorphs of transition alumina, which is normally obtained by decomposition of boehmite. Boehmite transforms to  $\gamma$ -alumina at temperature in the range of 500-800°C and consequently to  $\delta$ -alumina at 900°C.

## **2.2 Precursors for Metastable Alumina Synthesis**

Aluminum trihydroxide ( $\text{Al}(\text{OH})_3$ ) and aluminum monohydroxide ( $\text{AlOOH}$ ) exhibit polymorphism and exist in many forms of structure. The structure of all aluminum hydroxides consists of double oxygen-stacking layers with aluminum cations locating in octahedrally coordinated interstices. The packing of oxygen ions inside the layer can be either hexagonal or cubic, whereas the symmetry of the overall structure for each hydroxide is determined by the distribution of hydrogen atoms. It has been also suggested that the relative distance between hydroxyl groups, both within and between the layers, controls the mechanism of dehydration for the particular hydroxide. The structures of common alumina hydroxides are briefly summarized below.

### 2.2.1 Aluminum trihydroxides

#### a) *Gibbsite (hydrargillite): $\gamma\text{-Al(OH)}_3$*

Gibbsite is the best known aluminum trihydroxide. Technically, it is the most important form because it is an intermediate for the production of aluminum metal from bauxite (Bayer process). The crystal structure of gibbsite is based on double layers of closely-packed hydroxyl ions in ABAB stacking sequence with aluminum cations sandwiched in octahedrally coordinated interstices between the layers [68].

#### b) *Bayerite: $\alpha\text{-Al(OH)}_3$*

Bayerite is rarely found in nature, but it can be synthesized in laboratory by many processing routes [28]. The oxygen coordination in the bayerite structure is similar to that in gibbsite. However, hydrogen atoms in bayerite, form an AB-AB stacking sequence of the O-H layers.

#### c) *Nordstrandite: $\beta\text{-Al(OH)}_3$*

Nordstrandite is one of three polymorphs of aluminum trihydroxides which relatively rare in nature, but it can be synthesized in laboratory. The layer stacked sequence of nordstrandite is similar to gibbsite (ABBA stacking).

### 2.2.2 Aluminum monohydroxides

#### a) *Boehmite: $\gamma\text{-AlOOH}$*

Boehmite is the major constituent of many bauxite minerals. It can also be synthesized in laboratory by neutralizing aluminum salts at temperature close to the boiling point of water, by treating activated aluminum with boiling water or by hydrothermal reaction. Crystal structure of boehmite consists of cubic-packing oxygen ions with aluminum cations sandwiched between adjacent oxygen layers. Nevertheless, the distribution of hydrogen atoms in the structure makes it an

orthorhombic unit cell. The lattice parameters of boehmite are  $a = 2.861$ ,  $b = 3.696$  and  $c = 12.233$  [69].

In addition to the stoichiometric crystal structure described above, the name of boehmite has been used to describe the product of aluminum hydroxide gel aging, better referred as pseudoboehmite or gelationous boehmite [28]. Pseudoboehmite typically contains 15% excess water comparing to the stoichiometric composition of  $\text{AlOOH}$ , but the exact location of the excess water in pseudoboehmite structure is not certain. In boehmite, Al atoms are surrounded by a distorted octahedral group of O atoms, which are linked together to form complex layered structure.

#### *b) Diaspore: $\alpha\text{-AlOOH}$*

Diaspore exists in nature in clay and bauxite, which is the interesting material for preparation of  $\alpha$ -alumina. Diaspore structure consists of hexagonal layers of oxygen, which are significantly distorted. Aluminum cations are located in octahedral coordinated interstices between the adjacent oxygen layers. Diaspore possesses orthorhombic symmetry with lattice parameters of  $a = 4.4$ ,  $b = 9.43$ ,  $c = 2.84$ . The structure has four formula units per unit cell [68].

### **2.2.3 Tohdite: $5\text{Al}_2\text{O}_3 \cdot \text{H}_2\text{O}$**

The crystal structure of tohdite, determined by Yamaguchi et al., consists of oxygen close-packing layers, stacking in ABACBAC fashion [70, 71]. The hexagonal unit cell of tohdite has lattice parameters of  $a = 5.567$  and  $c = 8.768$ . Each unit cell contains ten aluminum cations, eight of which are in octahedrally coordinated and two in tetrahedrally coordinated interstices.

### **2.2.4 Amorphous anodic $\text{Al}_2\text{O}_3$ film**

Amorphous  $\text{Al}_2\text{O}_3$  film can be formed by anodization of aluminum in acid solution. Nonporous  $\text{Al}_2\text{O}_3$  film is formed in solutions that do not dissolve  $\text{Al}_2\text{O}_3$ . The structure of  $\text{Al}_2\text{O}_3$  films synthesized by anodization has been studied by both X-ray adsorption fine structure (EXAFS) [72] and electron energy loss fine structure



(EXELFS) techniques [73]. Amorphous  $\text{Al}_2\text{O}_3$  film generally has been assumed to contain a mixture of tetrahedrally and octahedrally coordinated aluminum. Results from both EXAFS and EXELFS have confirmed that dense  $\text{Al}_2\text{O}_3$  film contains 80% aluminum cations in octahedral sites and 20% in tetrahedral sites. On the other hand, aluminum cations in the porous  $\text{Al}_2\text{O}_3$  film are predominantly in tetrahedral or even lower coordination sites.

### 2.2.5 Alumina melt

The radial distribution function for  $\text{Al}_2\text{O}_3$  melt, in the temperature range of 2200-2700 K, recently has been reported by Ansell et al. [74] using X-ray synchrotron radiation.  $\text{Al}_2\text{O}_3$  undergoes structural rearrangement on melting with a change of the aluminum cations coordination from octahedral, in  $\alpha\text{-Al}_2\text{O}_3$ , to predominantly tetrahedral in the  $\text{Al}_2\text{O}_3$  melt. This result contradicts those reported earlier by Waseda et al. [75], who found octahedrally coordinated aluminum as the fundamental cluster configuration in the melt. No explanation accounting for this discrepancy has been given. However, quenching experiments do support the proposed tetrahedral coordination above the melting point, because high cooling rate ( $>10^5$  K/s) from the melt results in crystallization of either  $\gamma$ -alumina or various types of transition alumina phases, all containing tetrahedrally coordinated aluminum.

## 2.3 Formation and Crystal Structure of Active Aluminas

Alumina can exist in many metastable phases before transforming to the stable  $\alpha$ -alumina. There are six principal metastable phases of alumina designated by the Greek letters chi ( $\chi$ ), kappa ( $\kappa$ ), eta ( $\eta$ ), theta ( $\theta$ ), delta ( $\delta$ ), and gamma ( $\gamma$ ), respectively. Although the ranges of temperature, in which each transition phase is thermodynamically stable, have been reported by many researchers, they are inconsistent, depending upon various factors such as degree of crystallinity of sample, amount of impurities in the starting materials, and the subsequent thermal history of sample. Most studies on phase transformation of alumina was conducted by calcination of alumina precursor. It has been found that the difference in phase transformation sequence is resulted from the difference in the precursor structure [76, 77]. Moreover, the transformation sequence is irreversible. Nature of the product

obtained by calcination depends upon the starting hydroxide and the calcination condition. The phase transformation sequences, from metastable  $\text{Al}_2\text{O}_3$  structures to the final stable  $\alpha$ -alumina phase, reported in the literature are also approximates.

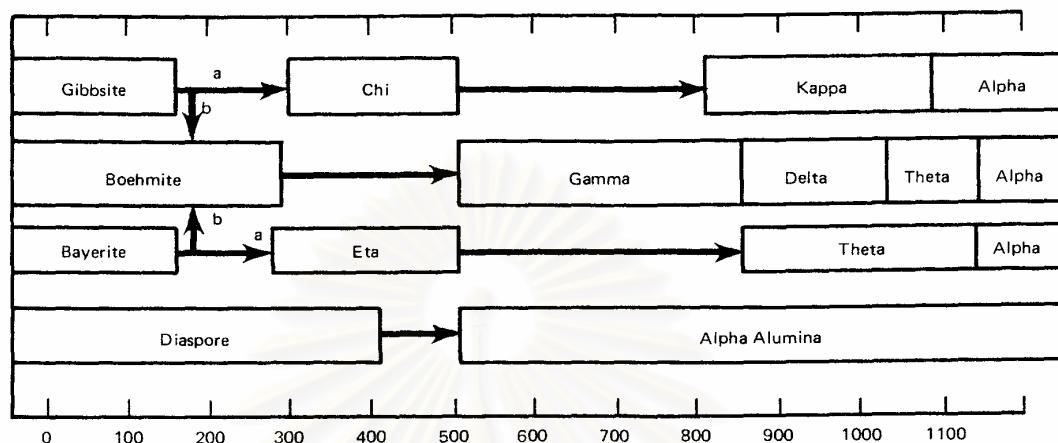


**Figure 2.1** Transformation sequences of aluminum hydroxides [29].

The phase transformation sequence normally starts with aluminum hydroxide ( $\text{Al}(\text{OH})_3$  or  $\text{AlOOH}$ ) transforming to low-temperature phase of alumina ( $\eta$  and  $\chi$ ) at temperature around  $150\text{--}500^\circ\text{C}$ , before subsequently transforming to high-temperature phase ( $\delta$ ,  $\theta$ ,  $\kappa$ ) at temperature around  $650\text{--}1000^\circ\text{C}$ . Finally, the thermodynamically stable phase,  $\alpha$ -alumina, is formed at temperature around  $1100\text{--}1200^\circ\text{C}$ . It is generally believed that  $\alpha$ -phase transformation takes place through the nucleation and growth mechanism.

Aluminas are usually obtained by dehydration of various hydroxides. Nevertheless the phase transformation sequences from various dehydration precursors are controversial, even in recent works [28, 78]. Apart from difficulties in characterization of the obtained alumina in various forms, most of the confusion arises from insufficient information concerning the reaction conditions.

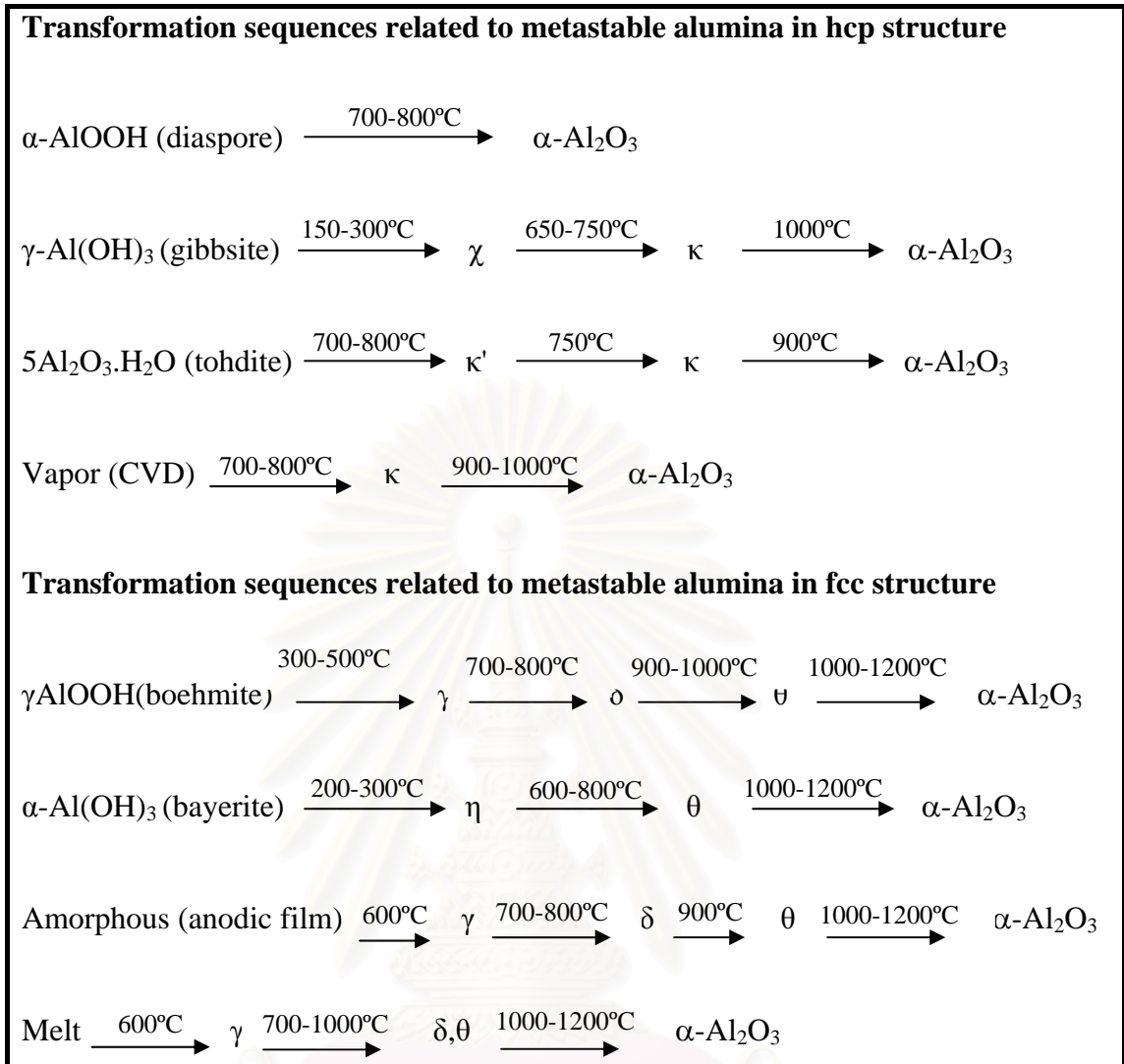


**Figure 2.2:** Common processing routes resulting in formation of different metastable  $\text{Al}_2\text{O}_3$  structures and sequences of phase transformation toward the stable  $\alpha$ -alumina.

### 2.3.1 Dehydration of aluminum trihydroxides

Dehydration of gibbsite in air or nitrogen gives the sequence of products, which are different from the dehydration of bayerite or nordstrandite. Detailed phase transformations starting from the trihydroxides are shown in Figure 2.3.

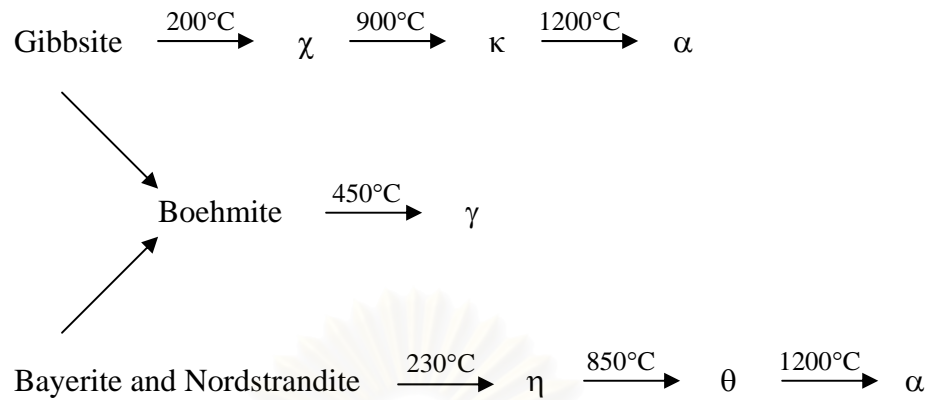


**Figure 2.3** Metastable aluminas formed by dehydration of the trihydroxides.

In vacuum, all trihydroxides mentioned above decompose into amorphous product ( $\rho$ -alumina) almost completely at low temperature.  $\rho$ -Alumina subsequently changes into  $\gamma$ -,  $\eta$ - and further into  $\theta$ -alumina upon the calcination at high temperature, as shown in Figure 2.4.

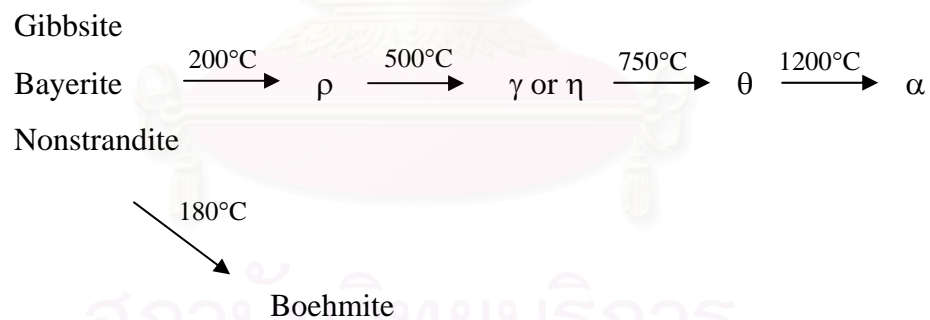
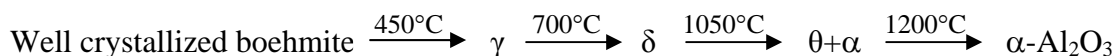


**Figure 2.4** Phase transformation of metastable aluminas formed from trihydroxides in vacuum.

### 2.3.2 Dehydration of aluminum monohydroxides

Diaspore is the only aluminum hydroxide that transforms directly into  $\alpha$ -alumina at temperature higher than  $500^{\circ}\text{C}$  [79].

The dehydration sequence of boehmite depends on its crystallinity. Well crystallized boehmite (crystal sizes  $> 1 \mu$ ) decomposes according to:



Formation of  $\delta$ -phase strongly depends on impurities and crystallinity of boehmite. Small amount of Na favors the formation of  $\theta$ -alumina, whereas Li and Mg stabilize  $\delta$ -alumina and can prevent the formation of  $\theta$ -alumina. If boehmite has low crystallinity, the formation of  $\delta$ -alumina is retarded.

Gelatinous boehmite (pseudoboehmite) decomposes at temperature around  $300^\circ\text{C}$  into alumina. Due to the poor crystallinity of pseudoboehmite, formation of  $\delta$ -alumina is hardly observed. The dehydration scheme is:



## 2.4 Preparation of Alumina Powder by Precipitation Method

There are many methods which have already been used to prepare alumina powder, such as precipitation from solution [2], sol-gel synthesis [3], hydrothermal synthesis [4], microwave synthesis [5], emulsion evaporation [6, 7, 80] and solvothermal synthesis [8-12, 14, 81, 82]. Precipitation method involves growth of solid crystals from the reaction between reactants in fluid phase. The reactants may or may not be in the same phase before the precipitation takes place. If the reactants are in the same phase, the precipitation is homogeneous, otherwise, it is heterogeneous. The homogeneous precipitation is often preferred because its behavior is more controllable [83]. Homogeneous precipitation of alumina precursor can be carried out by heating aqueous solution containing excess urea and aluminum salt approximately up to its boiling temperature [79]. Nevertheless, precipitation method is employed in this research, because of its potential to create very pure material and the flexibility of the process with respect to quality of final product.

Basically, all process parameters influence quality of the final product from the precipitation. It is usually desired to get the precipitates with specific properties. These properties may include the nature of the phase formed, chemical composition, purity, particle size, surface area, pore size, pore volume, and separability from the mother liquor. It may also include the demands which are imposed by the requirement of downstream processes, such as drying, palletizing or calcinations. It is therefore necessary to optimize the parameters in order to produce the desired material. Figure 2.5 summarizes the parameters which can be adjusted in precipitation processes and the properties which are mainly influenced by these parameters.

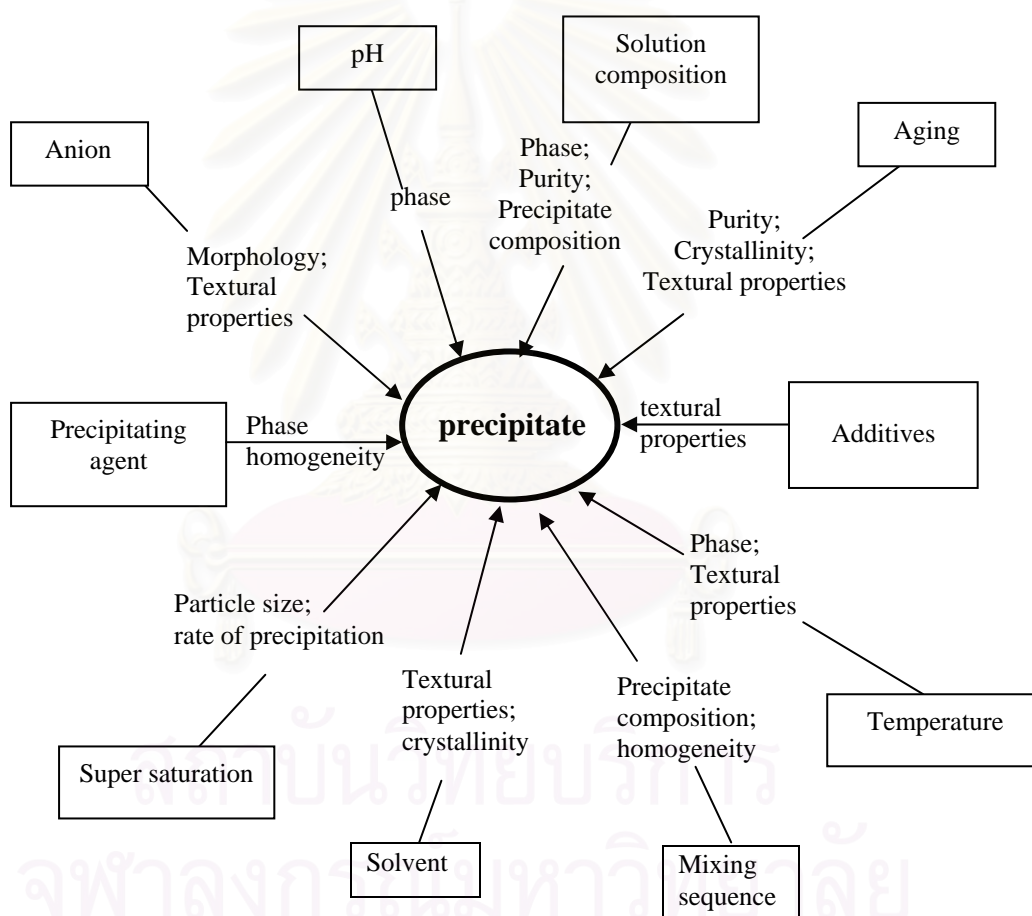


**Figure 2.5** Parameters affecting property of the precipitate [84].

Prasitwuttisak et al. [85] reported that  $\alpha$ -alumina with nanosized crystallites can be successfully synthesized by precipitation, sol-gel and solvothermal method. The morphology of calcined product is found to be loosely agglomerated powder that can be broken off by milling. The relative density of sintered specimens prepared

from various techniques were in the range of 93-98% of theoretical density. Blendel et al. [64] and Sacks et al. [64] synthesized high-purity aluminum sulfate hydrate particles by the homogeneous precipitation of aluminum sulfate solution using urea and formamide as precipitating agents.

In the precipitation method, precursors that can be easily decomposed to volatile products are usually employed. Nitrates of metal as precursors and ammonia or sodium carbonate as the precipitating agent are preferred. Since nucleation rate is extremely sensitive to a change in temperature, precipitation temperature is a decisive factor in controlling properties of the precipitate such as primary crystallite size, surface area, and phase. However, it is very difficult to state how the precipitation temperature should be adjusted to achieve a product with specific properties. The optimum precipitation temperature is usually a parameter which has to be determined experimentally. In general, most precipitation process is carried out above room temperature, often close to 100°C. Furthermore, pH directly controls the degree of supersaturation, at least in case that hydroxides are precipitated. Therefore, it is also one of the crucial factors in precipitation process. As for many other parameters, the influence of pH is not straight forward and it has to be investigated experimentally for a specific system.

Alumina powder has been prepared from ammonium aluminum carbonate hydroxide via the precipitation method as reported by Kato et al.[86]. A soluble aluminum salt was gradually added to the solution of ammonium hydrogen carbonate, and subsequently allowed the mixed solution to age for a prescribed period of time to permit growth of crystals. Then, the precipitate was separated by filtration and drying. The ammonium aluminum carbonate hydroxide obtained was decomposed at temperature in a range of 1250 to 1300°C to form  $\alpha$ -alumina.

## **2.5 Fabrication Method for Alumina Articles**

There are various methods to form shaped article from ceramic powder, for instance, dry pressing, hydrostatic molding, extrusion, injection molding, and hot pressing. The choice of the forming process depends on dimension and shape of parts to be fabricated, quantity of parts, and requirements of the final product. The forming

pressure to be applied should be approximately  $100 \text{ MN/m}^2$ , but it is usually adaptable in each type of the forming process. Bulk density of the green compacted body, as well as density of the final product after sintering, increases with increasing in forming pressure (Figure 2.6). If the forming pressure is too low, the final product will not achieve the full density. On the contrary, excessive pressure, which has the same effect as insufficient plastification or inhomogeneous distribution of the plasticizer, can lead to defects such as flaws and cracks in the compacted bodies.

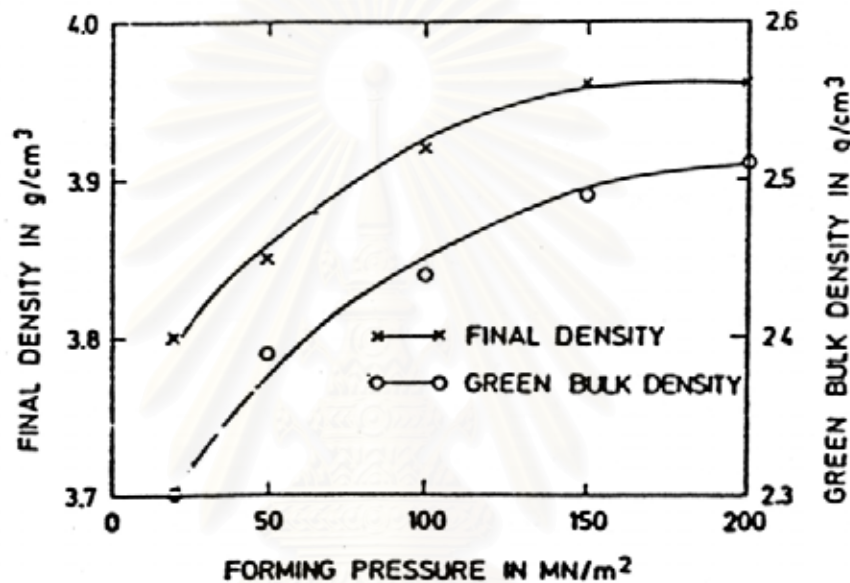


**Figure 2.6** Correlation between green bulk density, final density, and forming pressure of high-purity alumina ceramics [87].

The dry pressing technique is the most common and most economical compaction process for the fabrication of high-alumina ceramics. It is restricted, however, to parts with simple shape and to wall thickness greater than 1 mm. Dry pressing is unidirectional. Figure 2.7 illustrates the dry pressing operation using a simple ring, as well as a ring with a flange, under a pressure of  $150 \text{ MN/m}^2$ . The procedure is carried out in three basic steps. In order to develop internal stresses, the following requirements should be met.



1. It is important to get homogeneous distribution of the powder when a die is filled. This can be achieved by using suitably prepared free-flowing alumina powder and by filling the die evenly, for example, by means of a fill shoe.
2. In the pressing position, a homogeneous compaction of the powder within the desired shape should be ensured.
3. Removal of the part from the die should be simple, without any risk of damage.

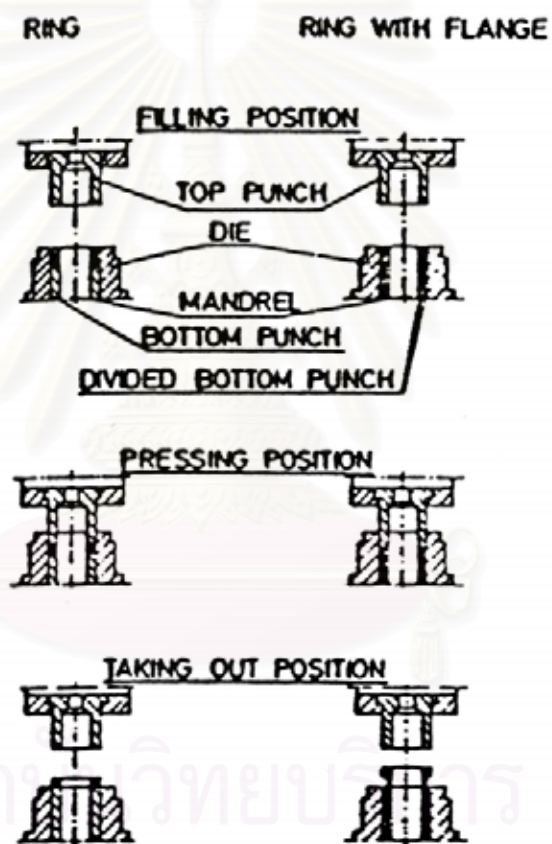


**Figure 2.7** Steps of dry pressing operation [87].

Due to the substantial tool wear caused by the extremely abrasive alumina powder, all parts of the die which are exposed to wear, such as mandrels and punches, are preferably made of cemented carbides.

The isostatic pressing is a process to form ceramic components from dry powder by uniform pressing from all directions. It is also used for fabrication of other materials, such as metals, plastics, graphite, and carbon. The process is accomplished by enclosing the powder in a deformable mold and then collapsing the mold by using a hydrostatic pressure exerted from fluid medium. For cold isostatic pressing (CIP), the process carried out at or near room temperature. On the other hand, hot isostatic pressing (HIP) is performed at elevated temperature. Cold isostatic pressing is used extensively on both laboratory and production scales. In production, it is used to form diverse array of parts, including spark plug insulator, oxygen sensor, large refractory component, and dinnerware. Furthermore, cold isostatic pressing is one of the good forming methods. It has been used in the forming of translucent alumina. It is simple and low cost operation that provides a green body of ceramic with sufficient physical strength. However, this method is not suitable to form complicated parts.

The general advantages of cold isostatic pressing are :

- Very few size or dimensional limitations, because the uniform application of pressure associated with this process obviates the size limitations of many other processes, particularly the length-to-diameter problems of dry pressing.
- Very uniform pressed compacts, due to the uniform application of pressure, which leads to very consistent density and shrinkage resulting in a reproducible process.
- Generally moderate tooling costs particularly in case of prototype and low-volume production.
- Short overall process time, because it does not require long binder burnout or drying period.

## **2.6 Sintering**

Sintering is a process by which small particles of material are bonded together by solid-state diffusion during thermal treatment. In ceramic manufacturing, this thermal treatment results in the transformation from a porous compact into a dense, coherent product. In the sintering process, particles are coalesced by solid-state diffusion at very high temperatures yet lower than melting point of the compound

being sintered [88]. Atomic diffusion takes place between the contacting surfaces of the particles so that they become chemically bonded together, as shown in Figure 2.8 [89]. As the sintering process proceeds, larger particles are formed at the expense of the smaller ones, while the porosity of the compacts decreases [90]. Finally, at the end of the process, an “equilibrium grain size” is attained.

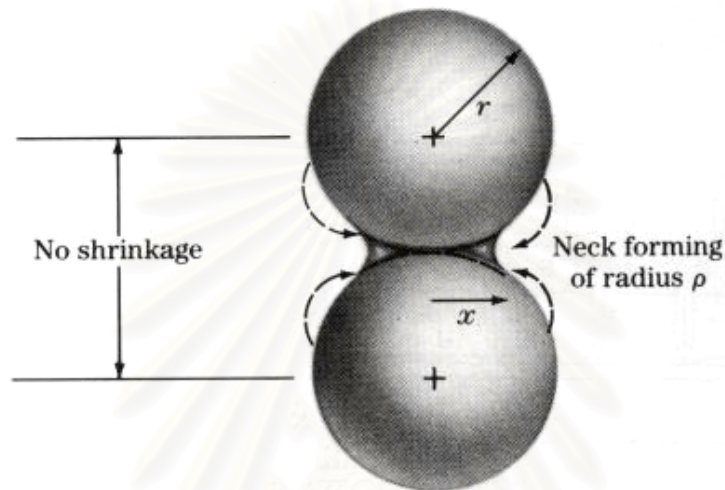


**Figure 2.8** Formation of a neck during the sintering of two fine particles.

Densification, recrystallization, and grain growth occur in the same temperature range. Therefore, strict control of the sintering process as well as small addition of grain growth inhibitor, e.g. MgO, to the alumina powders is essential to achieve a fully dense sintered body with fine-grained microstructure. In the course of sintering, the density increases with the logarithm of time, and the grain size increases with the one-third power of time.

As illustrated in Figure 2.9, the density increase linearly, according to the densification process during sintering, until it reaches saturation, where the specimen approaches its final-density. A further increase in the sintering time does not improve either the density or the mechanical properties. On the contrary, it promotes grain growth which reduces the mechanical strength. Therefore, the sintering process should be stopped as soon as the final density is obtained. Sintering in air can achieve

a maximum final density of about 99% of the theoretical density which corresponds to minimum residual porosity of about 1% from trapped air. Beyond the saturation point there is a decrease of density, due to volume-increasing reactions between the individual additives. It is very slight in the case of high-purity alumina ceramics and larger in case of alumina ceramics with high density.

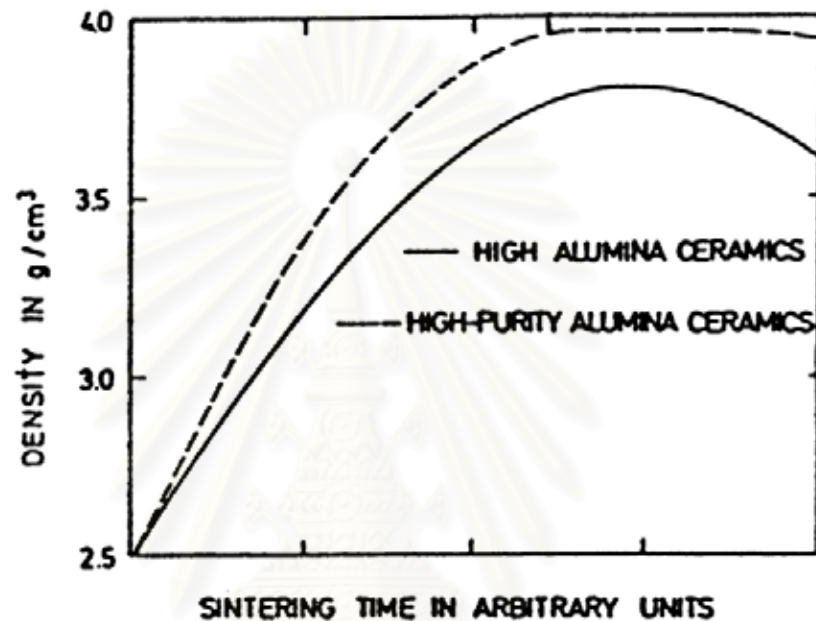


**Figure 2.9** Development of the density of alumina ceramics during sintering [87].

The nature of the sintering atmosphere may influence the rate of sintering and the residual porosity. Many additives besides temporary binders have been used in sintering process for several purposes, such as crystal growth repression, crystal growth acceleration, acceleration of sintering or shrinkage rate, reduction in maturing temperature, porosity alteration, changes in physical or chemical properties, and removal of impurities. Many researchers have studied the effects of sintering additives on the sintering process in order to improve properties of material obtained.

The choice of sintering temperature, which is usually between 1600 and 1800°C, depends on surface energy, grain size distribution, and the additives of the alumina powder. The sintering time and particularly the heating rate should be adapted to the size and the wall thickness of the body to be sintered. Larger parts

require a longer sintering time and a slower rate of heating-up. Smaller parts can be heated up more quickly, allowing a much shorter sintering time.

## 2.7 Color-Doped Alumina

Corundum is composed of aluminum oxide ( $\text{Al}_2\text{O}_3$ ) which, in its pure state, is completely colorless. However, pure corundum is rare in nature. Instead, small amount of metal impurity may impart color, either individual metal, or in combination [91].

In synthetic corundum, many different coloring agents have been used. Most color results from a peculiar group of transition elements, which also produce color in many different substances besides minerals. Electron structure of these elements contains inner unpaired electrons which can be excited to higher energy levels by absorption of visible light. The first series of transition elements in the periodic table are chromium, iron, titanium, vanadium, manganese, and copper. These are the most important instigator of gemstone coloration, which is responsible for the color of ruby, sapphire, emerald, alexandrite, tanzanite, and tsavorite.

White light or sunlight is made up of a balanced mixture of spectral colors which are violet, blue, green, yellow, orange, and red. An object does not really possess color itself. Instead, it is merely a perception based upon interaction between the light source, object, and eye. Table 2.1 shows causes of color in corundum. The color of ruby is one of the magnificent accidents of nature. Ruby is red not only by its body color due to absorption of blue and green light, but ruby also fluoresces red to daylight. This supercharges the hue into level of intensity unmatched by other red stones. Ruby's rich crimson hue is due to electron transitions involving the  $\text{Cr}^{3+}$  ion, which substitutes for Al in amounts approximating 0.1 – 3 atomic%. Ability to absorb visible light of this ion is the results from its outer electron suborbitals, in which the energy gaps are corresponding to energy of visible light. In ruby, two absorption mechanisms occur when white light passes through it. The first one involves electron transition from the ground state  $^4\text{A}_2$  to the  $^4\text{T}_2$  level (2.2 eV), which is corresponding to the absorption of yellow-green light. The second mechanism involves a transition to the  $^4\text{T}_1$  level by absorbing 3.0 eV radiation or violet light. These absorption areas

are actually bands rather than narrow lines and somewhat overlapped. Thus, there is only slight transmission in the blue, but strong transmission in the red, giving ruby its rich red color with slight purplish stones.

**Table 2.1** Causes of color in corundum

Color	Cause(s)	Reference
Red (including pink)	Electronic transition on dispersed $\text{Cr}^{3+}$ ions in octahedral coordination which have replaced $\text{Al}^{3+}$ in the corundum structure.	Fritsch & Rossman (1987)[92]
Blue	Intervalence charge transfer ( $\text{Fe}^{2+} + \text{Ti}^{4+} \rightarrow \text{Fe}^{3+} + \text{Ti}^{3+}$ ; sometimes written $\text{Fe}^{2+}-\text{O}-\text{Ti}^{4+} \rightarrow \text{Fe}^{3+}-\text{O}-\text{Ti}^{3+}$ ), where the $\text{Fe}^{2+}$ and $\text{Ti}^{4+}$ have replaced $\text{Al}^{3+}$ in the corundum structure and are in close proximity to one another.	Ferguson & Fielding (1972)[92] Fritsch & Rossman (1987)[92]
	Intervalence charge transfer ( $\text{Fe}^{2+} \rightarrow \text{Fe}^{3+}$ ), where the $\text{Fe}^{2+}$ and $\text{Fe}^{3+}$ have replaced $\text{Al}^{3+}$ in the corundum structure and are in close proximity to one another.	Schmetzer, K.(1987)[93]
Yellow	Ion pair transition on individual ions of a pair ( $\text{Fe}^{3+}-\text{Fe}^{3+}$ ).	Ferguson & Fielding (1972) [94]
	Color center (point defect) hole pair resulting from insufficient charge when any divalent impurity (such as $\text{Mg}^{2+}$ ) replaces $\text{Al}^{3+}$ in the corundum lattice. When sapphire is heat treated under highly oxidizing atmosphere, it combines with the divalent impurity, producing the +3 charge needed at the lattice site. Apparently this divalent impurity-hole pair absorbs light.	Emmett & Douthit (1993) [95]
	A variety of color centers of unknown structure.	Nassau & Valente (1987) [96]
	Color associated with an unknown element diffusing outward from exsolved particles of unknown composition.	Koivula(1987) [97] John Emmett, pers.comm.(July 5, 1994)
	Unreported mechanism involving dispersed Ni ion (synthetic only).	Nassau (1980) [98]
Orange	Combination of red color ( $\text{Cr}^{3+}$ ) and one or more of the yellow cause above.	Emmett & Douthit (1993) [95]
Violet/purple	Combination of red color ( $\text{Cr}^{3+}$ ) and one or more of the blue cause above.	Fritsch & Rossman (1988)[92]
Green	Ion pair transition on individual ions of a pair ( $\text{Fe}^{3+}-\text{Fe}^{3+}$ ), plus Intervalence charge transfer ( $\text{Fe}^{2+} + \text{Ti}^{4+} \rightarrow \text{Fe}^{3+} + \text{Ti}^{3+}$ ), as described above.	Emmett & Douthit (1993)[95]

Color	Cause(s)	Reference
	Unreported mechanism involving Co (strong reducing conditions), V and Ni ions which have replaced in the corundum structure (synthetic only)	Nassau (1980) [98]
	Combination of one or more of the blue and yellow causes described above.	Nassau, K. (pers. Comg. 19, 1994)
Color-change	Electronic transition of dispersed $V^{3+}$ ions in octahedral coordination which have replaced $Al^{3+}$ in the corundum structure. Due to balanced transmission in both the red and blue – green, the gem shifts color depending on the composition of the light source.	Schmetzer & Bank (1980) [99]
Dark Brown	Mechanical color due to dark brown color of exsolved hematite plates (mainly black star sapphire).	Weibel & wessicken (1981) [100]

In blue sapphire, iron and titanium both substitute for aluminum in the corundum structure. Iron resides either in a ferrous ( $Fe^{2+}$ ) or ferric ( $Fe^{3+}$ ) state, while titanium is found as  $Ti^{4+}$ . If both  $Fe^{2+}$  and  $Ti^{4+}$  lie in close proximity, it results in blue color. When stimulated by light, a single electron transfers from iron to titanium ion. This is illustrated by the following equation.



The intervalence charge transfer mechanism which produces blue color in sapphire is a far more efficient than the  $Cr^{3+}$  ion in ruby. Ruby requires about 0.4 – 2 atomic% of chromium for a deep red color, while only a few hundredth of one percent of iron and titanium are needed to achieve a similar depth of color in sapphire. Many sapphires possess the necessary iron and titanium, but do not have for deep blue color because the iron is in improper electronic state. Heat treatment under reducing condition can change  $Fe^{3+}$  to the required  $Fe^{2+}$  ion. Then, with  $Ti^{4+}$  already presents in the structure, a pale and cloudy stone becomes clear, with deep blue color.

For synthetic color-doped alumina, when  $Al_2O_3$  powder is sintered with coloring agents at high temperature of 1700°C or higher, metal ions diffuse into the

lattice and exchange with the Al ion, resulting in the change in ceramic color after sintering. However, at such high temperature, the grains of  $\text{Al}_2\text{O}_3$  grow over several microns. As the result, the  $\text{Al}_2\text{O}_3$  does not show good transparency. Therefore, it is very important to synthesize alumina powder in which some metal ions have already dissolved in lattice without formation of undesired porosity.

Verneuil method is known as a very popular method for synthesizing  $\text{Al}_2\text{O}_3$  single crystal. It employs ammonium alum as starting material to prepare feed powder.  $(\text{NH}_4)\text{Al}(\text{SO}_4)_2 \cdot 12\text{H}_2\text{O}$  is dissolved in hot distilled water and subsequently filtered to remove solid matter. On cooling, crystals of alum form out of the solution and impurities are left in the solution. After this process has been repeated several times, the purity of the crystals is high enough to allow the powder to be used in the crystal growth process. Chromium alum  $(\text{NH}_2)\text{Cr}(\text{SO}_4)_2 \cdot 12\text{H}_2\text{O}$  is purified in the same way to give the dopant for ruby. Two alum precursors are mixed together and fired at a temperature about  $1000\text{-}1200^\circ\text{C}$  to give the final feed powder. The feed powder needs to flow freely in the Verneuil reactor and therefore it is sieved before use. The feed powder is melted to give a characteristic boule which is a single crystal. The smooth flow of feed powder is ensured by tapping the powder container with a hammer, and the heating is achieved by a very hot flame, produced from an oxygen stream and a stream of coal gas which was available in Verneuil's time. The powder drops down through the flame. The flame touched a ceramic pedestal upon which the powder builds up a sintered cone whose tip melts and enlarges. The pedestal is lowered to give a start to the formation of the boule. The gas flow is maintained while the oxygen flow is monitored to control growth. Transparency is achieved by allowing slow growth in layers from the bottom of the boule. To prevent the formation of bubbles in the melt in many crystal and to stop cracking of the contact area of the sintered cone, the boule has to be kept small [101].

In 1817, Gay-Lussac reported that pure aluminium oxide could be obtained by heating ammonium alum. This allowed progress toward the final successful corundum growth. The work of Edmond Fremy is important because he was the first to produce clear red, though small, rubies. By using large fireclay crucibles held in heat for 20 days, thin ruby crystals were obtained [102]. Ballman, (1961) [103] described a



method for growing synthetic rubies in corundum seed in an aqueous medium containing chromium compound.

As recently, Lopez-Navarrete and Ocaña have shown the use of the spray pyrolysis technique for the synthesis of several pigment systems such as Cr-SnO<sub>2</sub> [104], Cr-SnCaSiO<sub>2</sub> [105], and Pr-CeO<sub>2</sub> [106]. In 2003, they have prepared manganese-doped  $\alpha$ -alumina pink pigments by spray pyrolysis technique [107]. They have found that the temperature required for the fully development of corundum was much lower (900°C) than that in the traditional ceramic procedure (1300°C). Nevertheless, the newly developed procedure yielded more intense color, since the amount of Mn incorporated to the corundum lattice increased with decreasing preparation temperature. In addition, the pigments obtained by this procedure require no grinding. They were consisted of uniformly shaped grains with controlled and reproducible size distribution. Furthermore, López-Navarrete, et al., (2003) [107] have investigated on the Mn valence in the Mn-alumina pigments. They have mainly used x-ray photoelectron (XPS) and X-ray adsorption spectroscopy for characterization. It was found that pink color of the pigments is mainly due to Mn(III) species dissolved in the corundum lattice, in which they form cluster containing ~2 Mn cations. The more intense color presented by the sample prepared in the presence of fluxes is due to the incorporation of a higher amount of Mn into the alumina lattice as a consequence of liquid phase presented in the system which favors the diffusion process involving in the solid solution formation.

## CHAPTER III

### EXPERIMENTAL

This chapter describes experimental system and procedures for alumina, metal doped-alumina and sol-seeded preparation. It is divided into three parts, i.e. chemicals used, preparation of samples and characterization of the obtained products, respectively.

#### 3.1 Chemicals

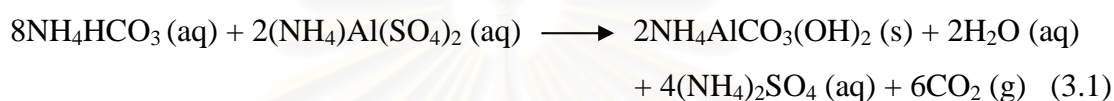
All chemicals using in this research are as follows:

1. Ammonium aluminum sulfate (99%+) ( $\text{NH}_4\text{Al}(\text{SO}_4)_2 \cdot 12\text{H}_2\text{O}$ ) available from Merck Co., Ltd., Germany.
2. Ammonium hydrogencarbonate (98%) ( $\text{NH}_4\text{HCO}_3$ ) available from Unilab.
3. Aluminium nitrate (98%) ( $\text{Al}(\text{NO}_3)_3 \cdot 9\text{H}_2\text{O}$ ) available from Aldrich Chemical Company, USA.
4. Ethyl alcohol absolute anhydrous available from Mallinckrodt Baker Co.,Ltd.
5. Chromium (III) nitrate nonahydrate (99.99%+) ( $\text{Cr}(\text{NO}_3)_3 \cdot 9\text{H}_2\text{O}$ ) available from Aldrich Chemical Company, USA.
6. Ferric (III) nitrate nonahydrate (98.0%+) ( $\text{Fe}(\text{NO}_3)_3 \cdot 9\text{H}_2\text{O}$ ) available from Sigma Chemical Company, USA.
7. Magnesium (II) nitrate hexahydrate (99%) ( $\text{Mg}(\text{NO}_3)_2 \cdot 6\text{H}_2\text{O}$ ) available from Aldrich Chemical Company, USA.
8. Yttrium (III) nitrate hexahydrate (99.9%) ( $\text{Y}(\text{NO}_3)_3 \cdot 6\text{H}_2\text{O}$ ) available from Aldrich Chemical Company, USA.

## 3.2 Experimental Procedures

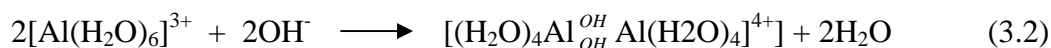
### 3.2.1 Synthesis of alumina powder

The method to produce alumina powder from ammonium aluminum carbonate hydroxide,  $\text{NH}_4\text{AlCO}_3(\text{OH})_2$ , has been invented by Shuzo et al. since 1975. Ammonium aluminum carbonate hydroxide (AACH) is synthesized from a reaction between solution of ammonium hydrogencarbonate and aluminum salt solution, according to the following equation [86]:



Ammonium aluminium sulfate (AAS) solution was gradually added to ammonium hydrogencarbonate aqueous (AHC) solution with concentration ratio of AAS to AHC of 0.5:2.0 mol/l at the temperature in a range of 40-45°C. The addition rate of AAS solution to AHC solution is 3 cc/min. The mixture was constantly stirred using magnetic stirrer rotating at 450 rpm. The pH of the mixture during the reaction was found to be constant at 9. After the reaction, the mixed solution was aged for 15 minutes to allow complete reaction. Then, the white precipitates formed were separated from the solution by centrifuging, repeatedly washed with methanol and dried in the oven at 110°C over night. Doping of the secondary metal was done by incorporating nitrate salt of metal, i.e. iron, chromium, yttrium or magnesium, into AAS solution before dropping into AHC solution in the predetermined amount. In this work, the concentration of metal investigated was 0.1, 0.5, 1.0, and 10 wt.% of aluminium salt.

In sol-seeding, alumina sol was first prepared by dissolving 24 g of aluminum nitrate nanohydrate in 50 ml of ethanol at room temperature. A homogeneous solution obtained, after mixing for approximately 10 minutes using magnetic stirrer, was transferred into a reactor equipped with a reflux-condenser and kept at temperature in the range of 70-80°C for 18 h. The first step of this process is the hydrolysis and condensation of two hexaqua complex ions to dimeric complex cations as following reaction [3]:



The obtained liquid containing alumina sol was added to AAS solution before dropping into AHC solution, to form AACH precipitates according to the procedure previously described. Doping of the secondary metal into sol-seeded product was done by either incorporating metal precursor into alumina sol during the precipitation of sol or separately adding metal precursor and undoped alumina sol into AAS solution.

All of the dried precipitates were calcined in air in a box furnace. The precipitate was heated at a rate of 10°C/min to the desired temperature and held at that temperature for 3 h.

### 3.2.2 Fabrication of alumina article

The obtained alumina powder from precipitation was milled by using ball mill for 72 h. (see Appendix C) and dried in an oven at 110°C for 24 h. The dried powder was sieved through a 100 mesh screen. Sieved powder was mixed with  $\text{Mg}(\text{NO}_3)_2 \cdot 6\text{H}_2\text{O}$  in the content of 0.03 wt.% (on the basis of MgO after decomposition) and organic binder (PVA with 9000-10000 MW) in content of 6 wt.% and passed through a 50 mesh screen. The mixture was biaxially pressed into a pallet of 13 mm in diameter followed by cold isostatic press under the pressure of 200 MPa. The green compact was dried in the oven at 105°C for 2 h. The dried green bodies were sintered at 1550°C for 2 h in air under atmospheric pressure.

### **3.3 Characterizations**

#### **3.3.1 X-ray diffraction (XRD)**

The X-ray diffraction (XRD) analysis of powder was performed by a SIEMENS D5000 X-ray diffractometer, using Ni-filtered CuK $\alpha$  radiation. The scan was performed over the  $2\theta$  range from  $20^\circ$  to  $80^\circ$ , using step size of  $0.040^\circ$ .

The crystallite size of the powder was estimated from line broadening according to the Scherrer equation. The value of shape factor,  $K$ , was taken to be 0.9 and  $\alpha$ -alumina was used as an external standard.

#### **3.3.2 Scanning electron microscopy (SEM)**

Morphology the samples was observed on JSM-5410LV scanning electron microscope. The SEM was operated using the secondary electron mode at 15 kV at the Scientific and Technological Research Equipment Center (STREC), Chulalongkorn University.

#### **3.3.3 Fourier transform infrared spectroscopy (FTIR)**

Functional groups in the samples were identified by using an infrared spectroscopy (Nicolet Impact 400). Before measurement, the sample was mixed with KBr and formed into a thin pellet.

#### **3.3.4 Particle size distribution analysis (PSD)**

The particle size and particle size distribution were analyzed by using laser scattering particle size distribution analyzer (Mastersizer S model) at the Scientific and Technological Research Equipment Centre, Chulalongkorn University.

### **3.3.5 X-Ray photoelectron spectroscopy (XPS)**

The content of metal ions on the surface of the powder was determined by using X-ray photoelectron spectroscopy (Kratos, Amicus). The analyses were carried out with these following conditions: Mg K $\alpha$  X-ray source operated at 12 kV and 20 mA, 0.1 eV/step of resolution, and the operating pressure was approximately  $1 \times 10^{-5}$  Pa.

### **3.3.6 UV/Visible spectrophotometry (UV/Vis)**

The absorption range of sample was determined by using UV/Visible spectrometer (Perkin Elmer Lambda 650), operated at wavelength 350-650 nm using step size of 1 nm.

### **3.3.7 Surface area measurement**

Specific surface area of the sample was calculated based on nitrogen uptake at liquid-nitrogen temperature, using the Brunauer-Emmett-Teller (BET) equation by the single point method.

### **3.3.8 Thermogravimetric analysis (TGA)**

The samples were subjected to differential thermal analysis (Diamond Thermogravimetric and Differential Thermal Analyzer, STA 4094) to determine the temperature of possible decomposition and phase change in the range of 20-1300°C. The analysis was performed at a heating rate of 10°C/min in 50 ml/min flow of air.

## CHAPTER IV

### RESULTS AND DISCUSSION

In this chapter, the experimental results and discussion are described. The chapter can be divided into 3 sections as follows:

Section 4.1 describes properties of undoped alumina powder prepared from precipitation method. Effect of sol-seed introduction is also discussed in this section.

Section 4.2 describes effects of metal doping on structure and morphology of alumina powder. The details of the discussion include phase change, functional groups, thermal decomposition and metal content of alumina powder.

Section 4.3 discusses application of the synthesized alumina powder in ceramic field by fabrication into sintered alumina specimen.

#### 4.1 Properties of Undoped Alumina Powder

##### 4.1.1 Preparation without sol-seeding

The XRD analysis of undoped sample, as shown in Figure 4.1, reveals that the precipitate obtained from the reaction between AAS and AHC is in fact ammonium aluminium carbonate hydroxide (AACH). All diffraction peaks are broad, indicating that the crystals are very small and imperfect, which agrees with the previous finding in literature [85].

Upon the calcination at low temperature (600°C), AACH is decomposed and transformed to amorphous form. At calcination temperature of 700°C,  $\gamma$ -Al<sub>2</sub>O<sub>3</sub> is formed, as detected by the XRD analysis. It should be noted that the diffraction peaks corresponding to  $\gamma$ -Al<sub>2</sub>O<sub>3</sub> are weak in intensity, which indicates that it is under transition from amorphous phase. The crystallinity of  $\gamma$ -Al<sub>2</sub>O<sub>3</sub> phase is improved as the calcination temperature is increased to 800°C. Phase transformation from  $\gamma$ - to  $\alpha$ -Al<sub>2</sub>O<sub>3</sub> takes place at temperature lower than 1000°C, as evidenced from the fact that the powder calcined at 1000°C is mixture of  $\alpha$ - and  $\gamma$ -phase. However, trace amount

of  $\theta$ - $\text{Al}_2\text{O}_3$  detected from the sample calcined at this temperature suggests that  $\gamma$ - to  $\theta$ -phase transformation also takes place. At temperature higher than  $1000^\circ\text{C}$ , the phase transformation is completed and only peaks corresponding to  $\alpha$ - $\text{Al}_2\text{O}_3$  are observed. Sharpness and high-intensity of  $\alpha$ - $\text{Al}_2\text{O}_3$  XRD peaks suggest the growth of crystallite grains upon the completion of phase transition [65].

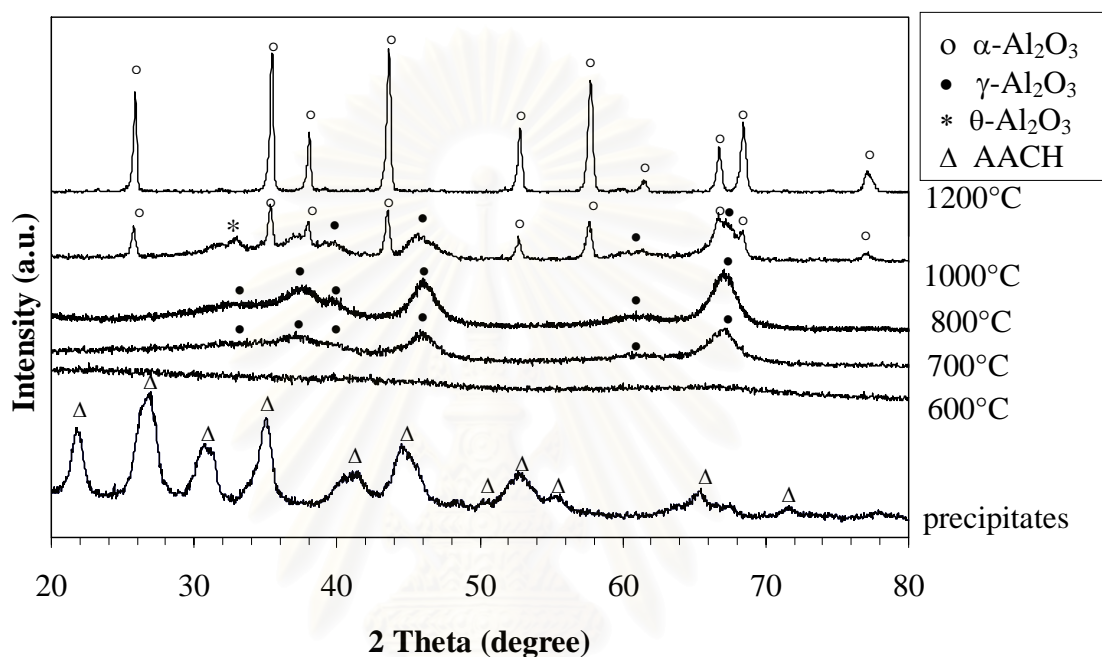


**Figure 4.1** XRD patterns of undoped product calcined at various temperatures.

FTIR spectra of sample calcined at different temperatures are shown in Figure 4.2. The presence of organic moiety in the pre-calcined precipitate can be clearly observed, e.g. the absorption from  $\text{CO}_3^{2-}$  and  $\text{NH}_4^+$  at wave number  $800$  and  $1425$   $\text{cm}^{-1}$ , respectively. These organic groups are eliminated upon the calcination. After calcination at  $600^\circ\text{C}$ , a broad and smooth absorption band at wave number ranging from  $500$  to  $900$   $\text{cm}^{-1}$  is observed. This band has been attributed to the disordered distribution of vacancies and broad distribution of bond length in amorphous alumina material [43]. This result confirms that there is no amorphous alumina in the precipitate and AACH crystals transform to amorphous alumina before the formation of  $\gamma$ -alumina. At  $700$  and  $800^\circ\text{C}$ , the infrared spectra of the products show absorption bands at  $615$  and  $747$   $\text{cm}^{-1}$ , which are specific to tetrahedral Al-O vibration from  $\gamma$ -



alumina [108]. Finally, when the calcination temperature is increased to 1000°C, the sharp absorption bands at 443, 590 and 639  $\text{cm}^{-1}$  are detected. These bands have been identified as characteristic absorption bands from octahedral Al-O vibration in  $\alpha$ - $\text{Al}_2\text{O}_3$  [108]. It can be seen that phase transformation observed by the FTIR results is in good agreement with XRD observation.

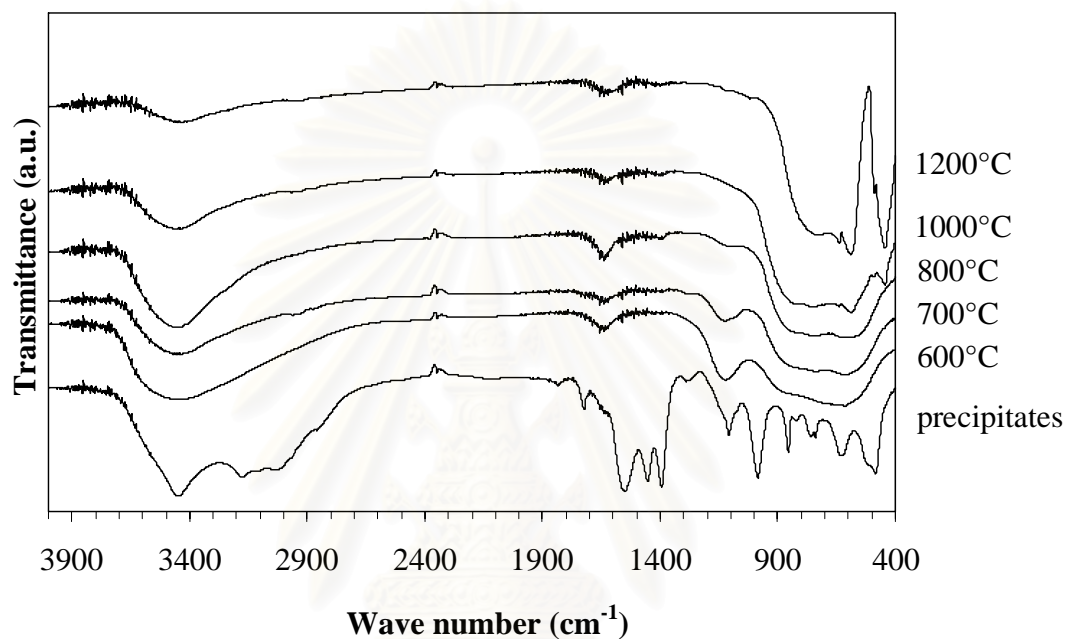


**Figure 4.2** FTIR spectra of undoped product calcined at various temperatures.

A result from thermogravimetric analysis of the undoped powder is shown in Figure 4.3. As observed, a large weight loss is detected at temperature between 40 and 250°C due to the vaporization of physically bound absorbed water and the decomposition of ammonium aluminum carbonate hydroxide (AACH) [41]. At the temperature in the range 300-600°C mass loss due to the reduction of defects and lattice distortion of amorphous  $\text{Al}_2\text{O}_3$  during transformation to  $\gamma$ - $\text{Al}_2\text{O}_3$  [108] is observed. Furthermore, a small weight loss associated with the transformation from  $\gamma$ - to  $\alpha$ - $\text{Al}_2\text{O}_3$  takes place at temperature between 800 and 1000°C. This profile of the thermogram is in agreement with the results obtained by XRD and FTIR analysis.

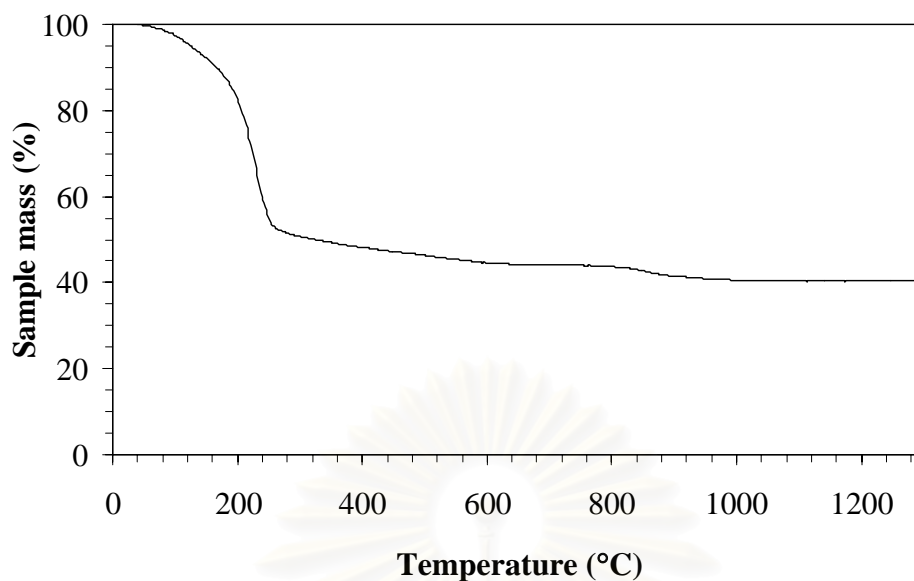


**Figure 4.3** Result from thermogravimetric analysis (TG curve) of the precipitate.

#### 4.1.2 Effects of sol-seeding

For the precipitation accompanied by sol-seeding, it is found that the precipitate is still AACH (see Figure 4.4). However, the product from the decomposition of AACH in this case remains amorphous even after calcination at 700°C. Notable amount of  $\gamma$ - $\text{Al}_2\text{O}_3$  is detected only after the precipitate is calcined at 800°C, which is higher than the case of precipitation without sol-seeding. The  $\gamma$ -phase is the sole crystalline phase observed, even in the product calcined at 1000°C. The results clearly show that the introduction of seeds results in the improvement in thermal stability of  $\gamma$ - $\text{Al}_2\text{O}_3$ . Nevertheless, at 1200°C, all  $\gamma$ -phase completely transforms into  $\alpha$ - $\text{Al}_2\text{O}_3$ . This result is in good agreement with previous report by Youn *et al.* that the sol-effect does not reduce the finishing temperature of  $\alpha$ - $\text{Al}_2\text{O}_3$  [65]. The sol-effect may be regarded as  $\text{Al}_2\text{O}_3$  self seeding.

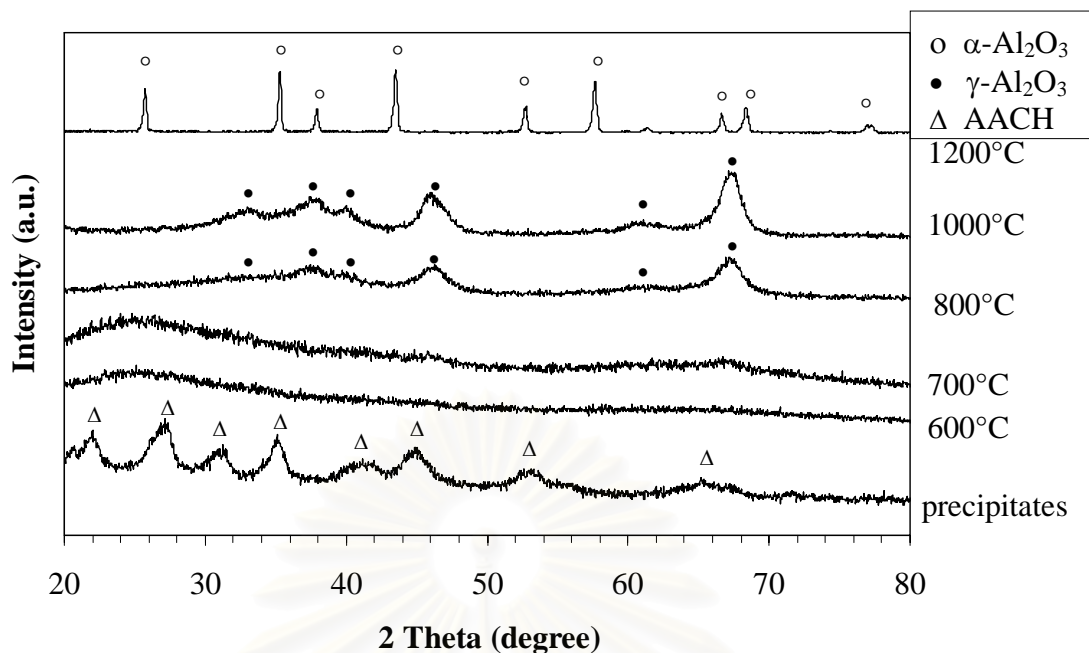


**Figure 4.4** XRD patterns of the product synthesized by precipitation accompanied by sol-seeding and calcined at various temperatures.

FTIR spectra of the precipitate obtained by reaction accompanied by sol-seeding is quite different from that of the precipitate without sol-seed (Figure 4.5). The absorption bands corresponding to organic moieties are no longer apparent and some absorption bands disappear, in which the attempt to describe was unsuccessful. Instead, the characteristic absorption bands of nitrate ion at  $1465\text{ cm}^{-1}$  [21] is observed. Moreover, the bands at  $615$  and  $773\text{ cm}^{-1}$ , which are characteristic bands of boehmite,  $\text{Al}(\text{OOH})$ , [65] are observed. It indicates that sol-seeding induces the formation of amorphous alumina in the precipitates. Nevertheless, unidentified absorption band at wave number approximately  $1130\text{ cm}^{-1}$  are detected, which disappeared after the calcination at higher temperature. However, after calcination, only absorption bands associated with  $\gamma$ - or  $\alpha$ -alumina, depending on the calcination temperature are observed. The FTIR spectra of the calcined samples are consistent with the results from the undoped samples.

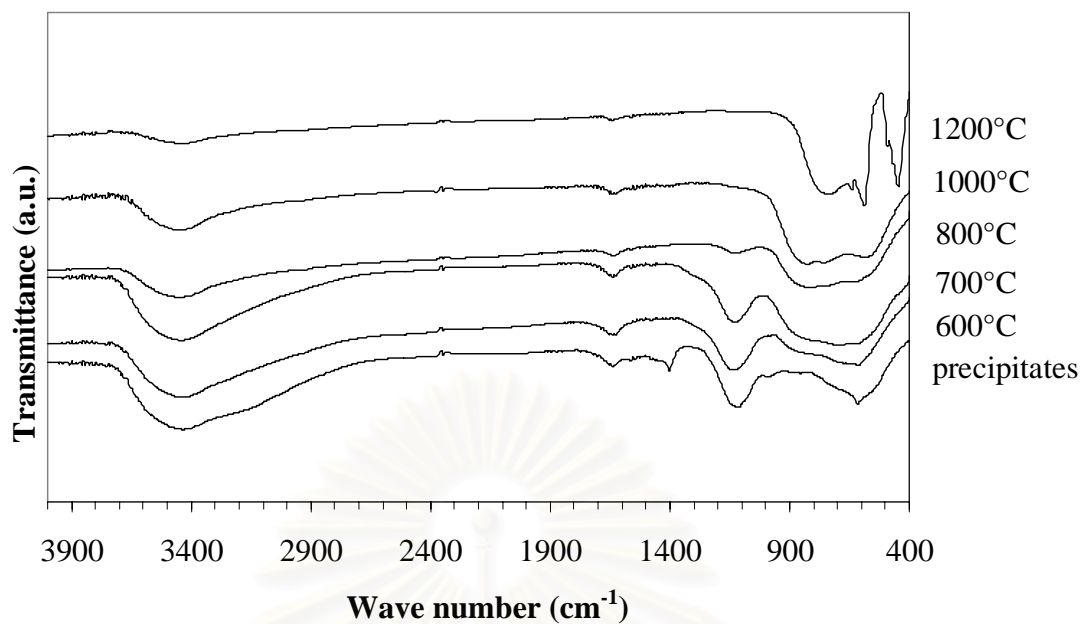


**Figure 4.5** FTIR spectra of products produced by precipitation accompanied by sol-seeding and calcined at various temperatures.

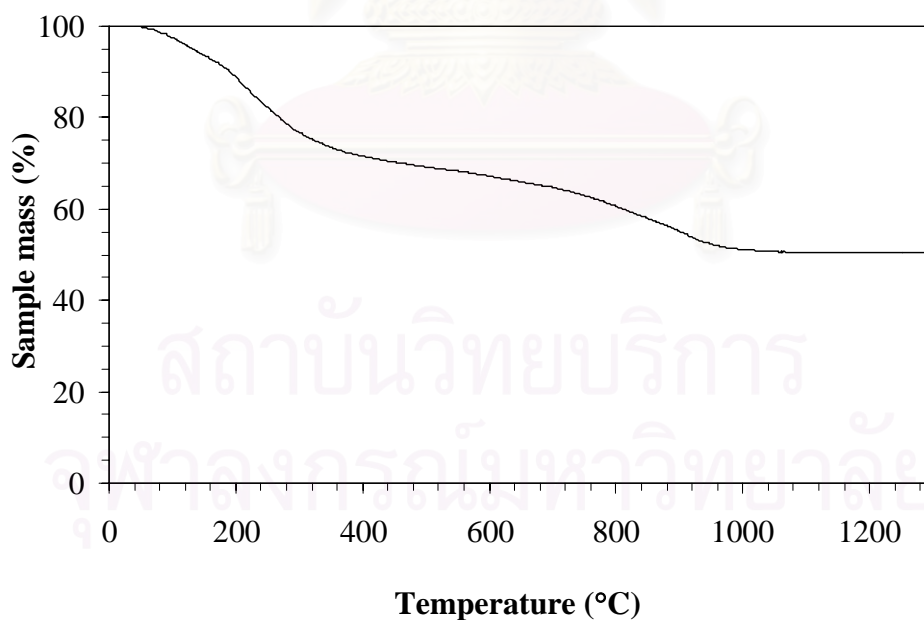


**Figure 4.6** Result from thermogravimetric analysis (TG curve) of the sample from precipitation accompanied by sol-seeding.

For thermogravimetric analysis, TG curve of the precipitate with sol-seeding (Figure 4.6) is quite different than that of the precipitate without sol-seeding (Figure 4.3). Although the extent of mass loss after TG analysis at 1200°C for both cases are roughly the same, no sudden drop in mass is observed in the TG curve in Figure 4.6. With sol-seeding, mass of the sample gradually decreases with an increase of temperature. Nevertheless, the TG curve can be divided into 3 zones. The weight loss due to physically adsorbed water elimination and decomposition of the precursor is observed at temperature between 40 and 300°C. The second weight loss is detected at temperature in the range 300-800°C due to the reduction of defects and lattice distortion of amorphous Al<sub>2</sub>O<sub>3</sub> during transformation to  $\gamma$ -Al<sub>2</sub>O<sub>3</sub> [108]. Finally, the transformation of  $\gamma$ - /  $\alpha$ -Al<sub>2</sub>O<sub>3</sub> show at the temperature in the range of 800-1000°C.

## 4.2 Effect of Secondary Metal Doping

### 4.2.1 Doping in low content

The secondary metal was doped into alumina by co-precipitation method described earlier. When low content of the dopant (0.1 wt.%) is applied, no crystalline phase other than alumina can be detected by XRD analysis, with an exception for the case of chromium doping. Nevertheless, the presence of metal in alumina powder is confirmed by the X-ray photoelectron spectroscopy analysis as shown in Table 4.1. It is found that the content of metal species decreases after calcination, which clearly indicates the incorporation of metal into alumina lattice after calcination.

**Table 4.1** Mass concentration of dopant for as-synthesized and calcined powder, analyzed by XPS.

Dopant	Mass concentration of dopant (wt.%)	
	As-synthesized powder	Powder calcined at 1200°C
Iron	0.88	0.69
Yttrium	7.22	0.97
Chromium	2.85	0.79
Magnesium	4.58	1.78

As shown in Table 4.2, it is found that the phase transformation behavior of products doped with 0.1 wt.% of iron, magnesium or yttrium is shifted toward that of alumina introduced with seeds. Detailed results are shown in Appendix D. Therefore, thermal stability of  $\gamma$ -alumina can be significantly enhanced by adding small amount of dopant as well as the effect from sol-seeding.

**Table 4.2** Phase of products doped with 0.1 wt.% of metal and calcined at various temperature.

Sample	Calcination temperature (°C)				
	600	700	800	1000	1200
pure alumina	Amorphous	$\gamma$	$\gamma$	$\gamma/\alpha$	$\alpha$
Sol-seeded alumina	Amorphous	Amorphous	$\gamma$	$\gamma$	$\alpha$
Fe-doped alumina	Amorphous	Amorphous	$\gamma$	$\gamma$	$\alpha$
Mg-doped alumina	Amorphous	Amorphous	$\gamma$	$\gamma$	$\alpha$
Cr-doped alumina	Amorphous	$\text{Cr}_2\text{O}_3$	$\gamma$	$\gamma/\alpha$	$\alpha$
Y-doped alumina	Amorphous	Amorphous	$\gamma$	$\gamma$	$\alpha$

For chromium-doped alumina,  $\text{Cr}_2\text{O}_3$  is found together with  $\gamma\text{-Al}_2\text{O}_3$  in the product calcined at temperature in the range of 700 to 800°C. It should be noted that the color of the chromium-doped powder calcined at 600-1000°C is green due to the presence of  $\text{Cr}^{3+}$  in  $\text{Cr}_2\text{O}_3$ . After calcination at temperature higher than 1000°C, the obtained powder is pink, which indicates dissolution of  $\text{Cr}^{3+}$  species into corundum structure. For  $\text{Cr}^{3+}$ , the different environment results in different color. [109].

Doping is found to be another effective approach to alter phase transformation behavior of alumina. Results from FTIR analysis as shown in Figure 4.7 reveal that FTIR spectra of the metal-doped precipitate is different from the undoped precipitate, even though the content of doping is low. The shifts in FTIR spectra observed is attributed to the change in bond structure of precipitate from the presence of metal. Further analysis shows that the FTIR spectra of iron-doped precipitate is similar to those of chromium-doped sample, while the spectra of yttrium-doped and magnesium-doped powder are similar. The absorption band around  $1300\text{ cm}^{-1}$  is disappeared when either iron or chromium is coprecipitated with AACH. On the contrary, the bands in the range of  $2850\text{-}3000\text{ cm}^{-1}$  can be clearly observed in Y- or Mg-doped samples. However, the attempt to identify functional groups associated with those bands was unsuccessful. For the absorption bands associated with  $\gamma$ - and  $\alpha$ -alumina, the results observed are in accordance with the XRD analysis, as previously discussed.

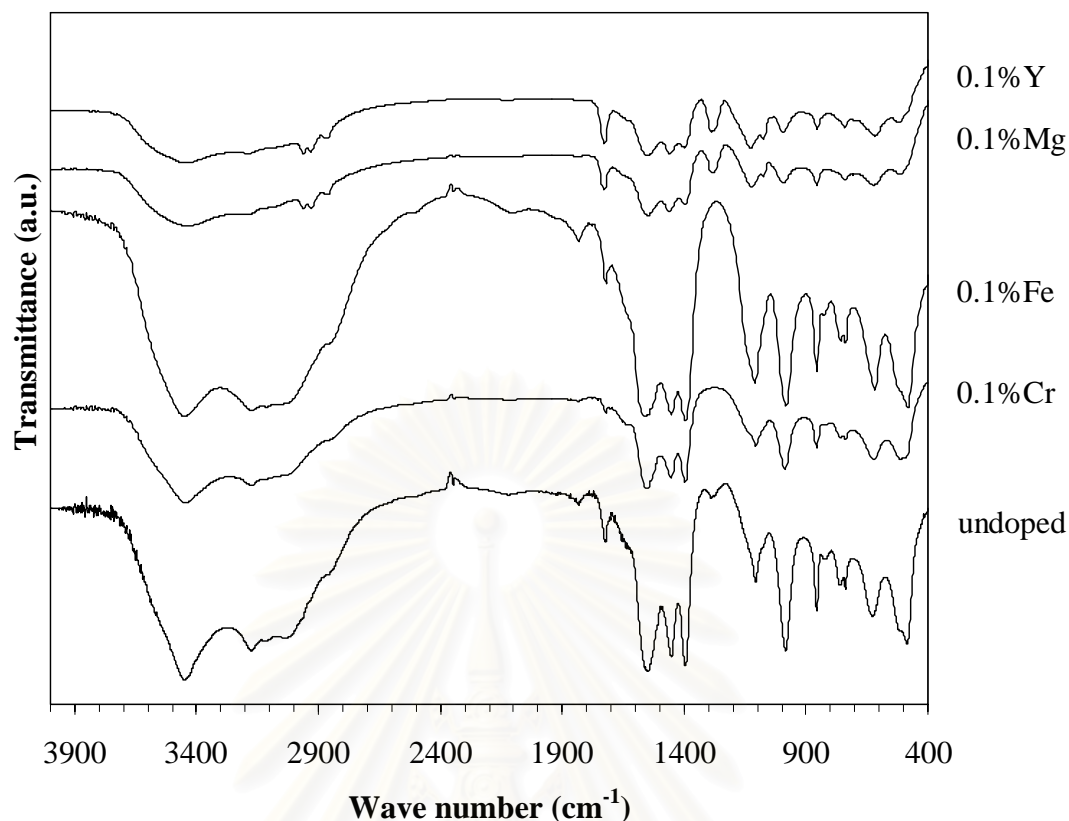


**Figure 4.7** FTIR spectra of precipitate for 0.1 wt.% of metal doping.

The crystallite size of  $\gamma$ - $\text{Al}_2\text{O}_3$  in all samples, calculated from XRD peak broadening using the Scherrer equation, is approximately 3-5 nm (Table 4.3). As the calcination temperature is increased over  $1000^\circ\text{C}$ , phase transformation from  $\gamma$ - to  $\alpha$ - $\text{Al}_2\text{O}_3$  takes place and the crystallite size of  $\alpha$ - $\text{Al}_2\text{O}_3$  is found to be one order of magnitude larger than that of  $\gamma$ - $\text{Al}_2\text{O}_3$ . The crystallite size of  $\alpha$ - $\text{Al}_2\text{O}_3$  obtained is around 50 nm. It should be noted that no significant growth of  $\gamma$ - $\text{Al}_2\text{O}_3$  crystallites is observed prior to the  $\gamma$ - to  $\alpha$ -phase transformation. The results suggest that  $\gamma$ - $\text{Al}_2\text{O}_3$  has a critical size beyond which it is unstable and undergoes phase transformation to  $\alpha$ -form. Once  $\alpha$ - $\text{Al}_2\text{O}_3$  nuclei are formed, they grow rapidly, which might be the result from sintering process. The rapid growth of  $\alpha$ -alumina has been examined by many researchers [30, 54, 110]. This behavior regarding critical size of the transition alumina has been observed from the direct phase transformation from  $\chi$ - to  $\alpha$ -alumina as well [111].



**Table 4.3** Crystallite size of powder doped with 0.1 wt.% metal and calcined at various temperatures.

Sample	Calcination temperature (°C) / Crystallite size (nm)				
	600	700	800	1000	1200
Undoped alumina	-	4.02( $\gamma$ )	4.06( $\gamma$ )	4.12( $\gamma$ ),28.17( $\alpha$ )	44.35( $\alpha$ )
Sol-seeded alumina	-	-	4.18( $\gamma$ )	4.22( $\gamma$ )	47.51( $\alpha$ )
0.1 wt.%Fe-doped alumina	-	-	4.35( $\gamma$ )	4.58( $\gamma$ )	41.21( $\alpha$ )
0.1 wt.%Cr-doped alumina	-	7.32( $\text{Cr}_2\text{O}_3$ )	3.94( $\gamma$ )	4.08( $\gamma$ )	41.78( $\alpha$ )
0.1 wt.%Y-doped alumina	-	-	4.15( $\gamma$ )	4.35( $\gamma$ )	41.56( $\alpha$ )
0.1 wt.%Mg-doped alumina	-	-	3.53( $\gamma$ )	4.58( $\gamma$ )	39.85( $\alpha$ )

#### 4.2.1.1 Morphology of alumina powder

Morphologies of products calcined at 1200°C, observed by SEM, are shown in Figure 4.8. It is obvious that the particles shown are much bigger than the crystallite size calculated from XRD line broadening (Table 4.3). This is due to agglomeration of alumina powders into larger particle, called secondary particle. The secondary particles are for all samples about 10  $\mu\text{m}$  in size (Table 4.4). It should be noted that the particle size is measured by using laser scattering technique. Nevertheless, the secondary particles of alumina synthesized via precipitation method have been reported to be very uniform in size and loosely agglomerated. The size of particle can be easily reduced by milling [112]. SEM images of the milled samples and the average particle size distributions are shown in Figure 4.9 and 4.10, respectively.

**Table 4.4** Average particle size for product calcined at 1200°C.

Sample	Mean diameter ( $\mu\text{m}$ )			
	before milling		after 72 h milling	
	D[4,3]	D[3,2]	D[4,3]	D[3,2]
undoped	13.23	8.52	0.71	0.27
sol-seeded alumina	17.38	4.64	1.90	0.33
0.1 wt.%Fe-doped alumina	13.32	8.57	1.78	0.33
0.1 wt.%Cr-doped alumina	16.33	9.19	2.15	0.36
0.1 wt.%Y-doped alumina	7.53	1.29	0.69	0.26
0.1 wt.% Mg-doped alumina	14.39	7.71	1.49	0.31

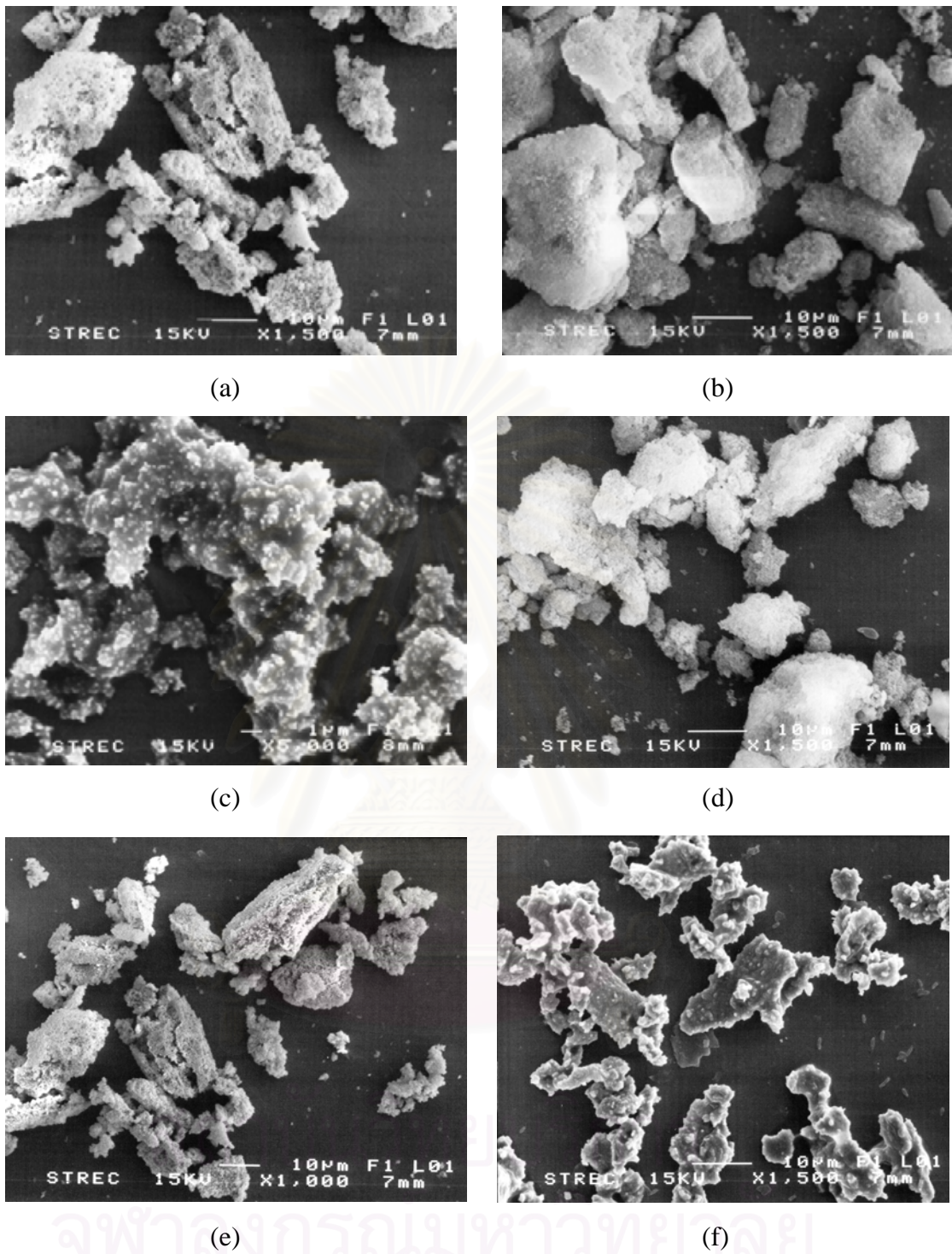


**Figure 4.8** SEM images of calcined powder before milling: (a) undoped alumina, (b) sol-seeded alumina, (c) 0.1 wt.%Cr-doped alumina, (d) 0.1 wt.% Fe-doped alumina, (e) 0.1 wt.%Mg-doped alumina, (f) 0.1 wt.% Y-doped alumina.

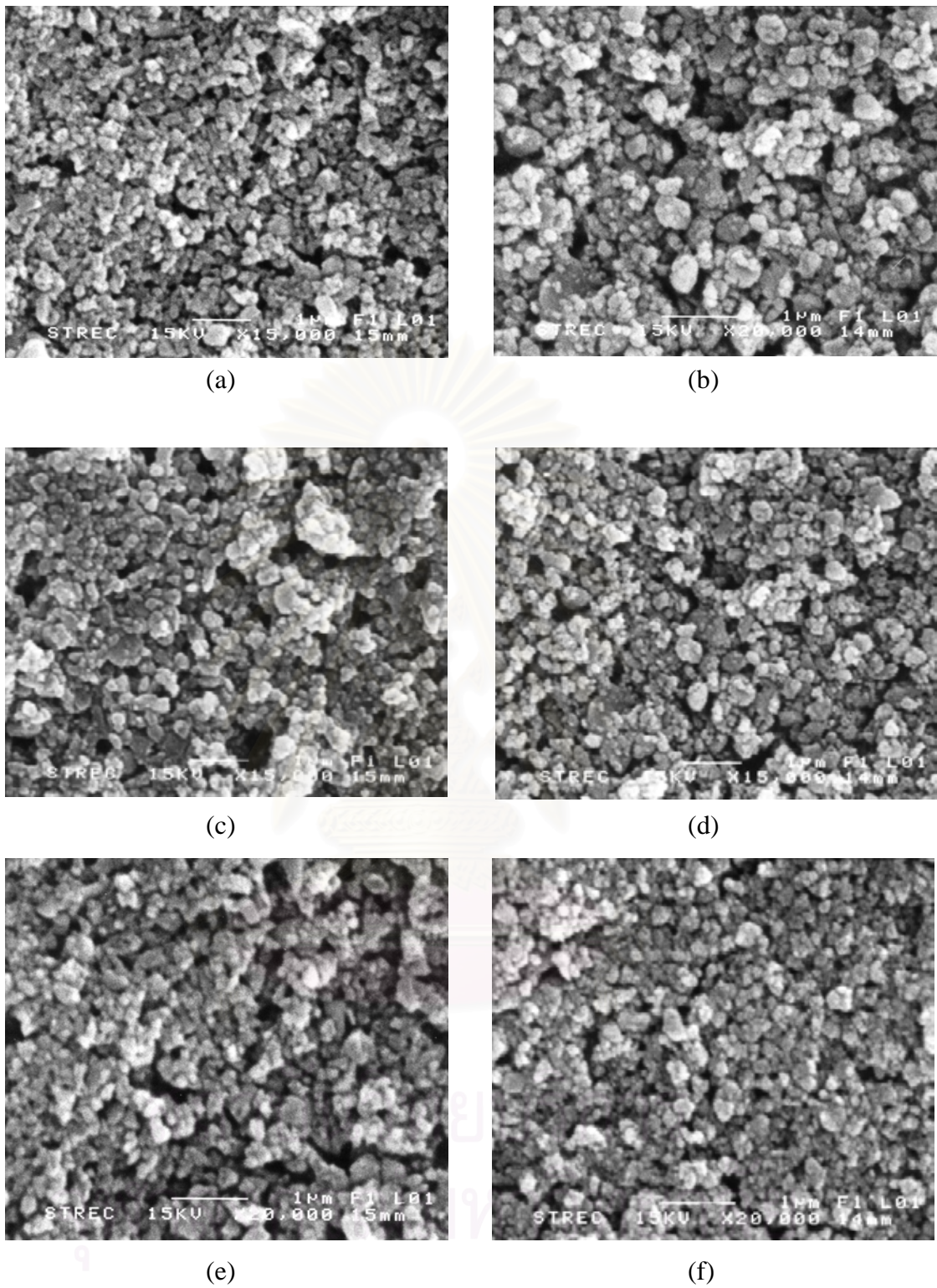
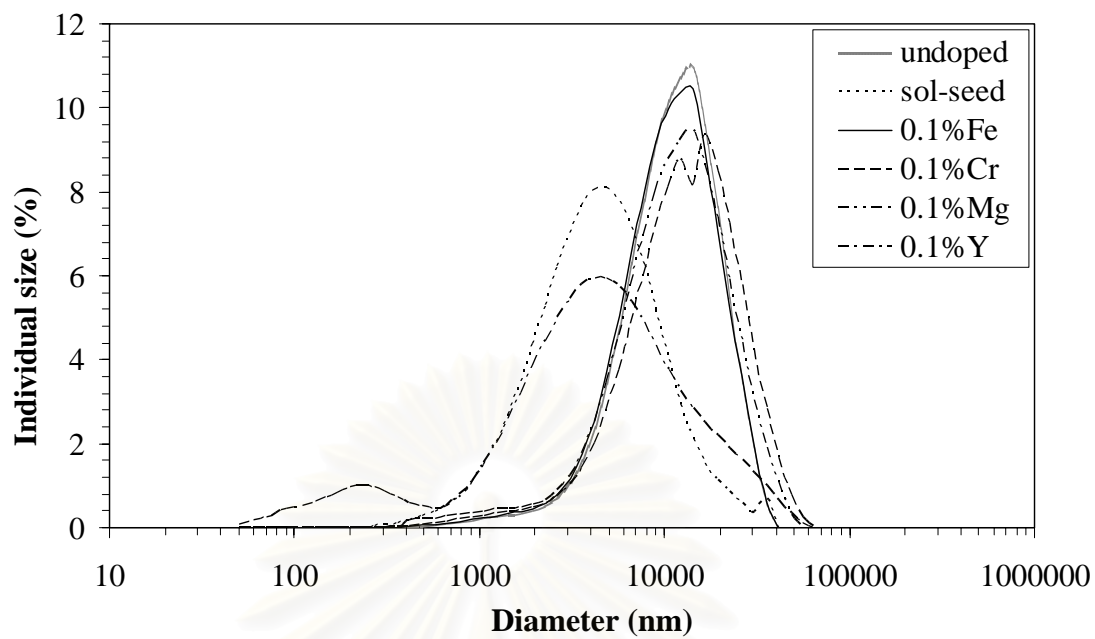
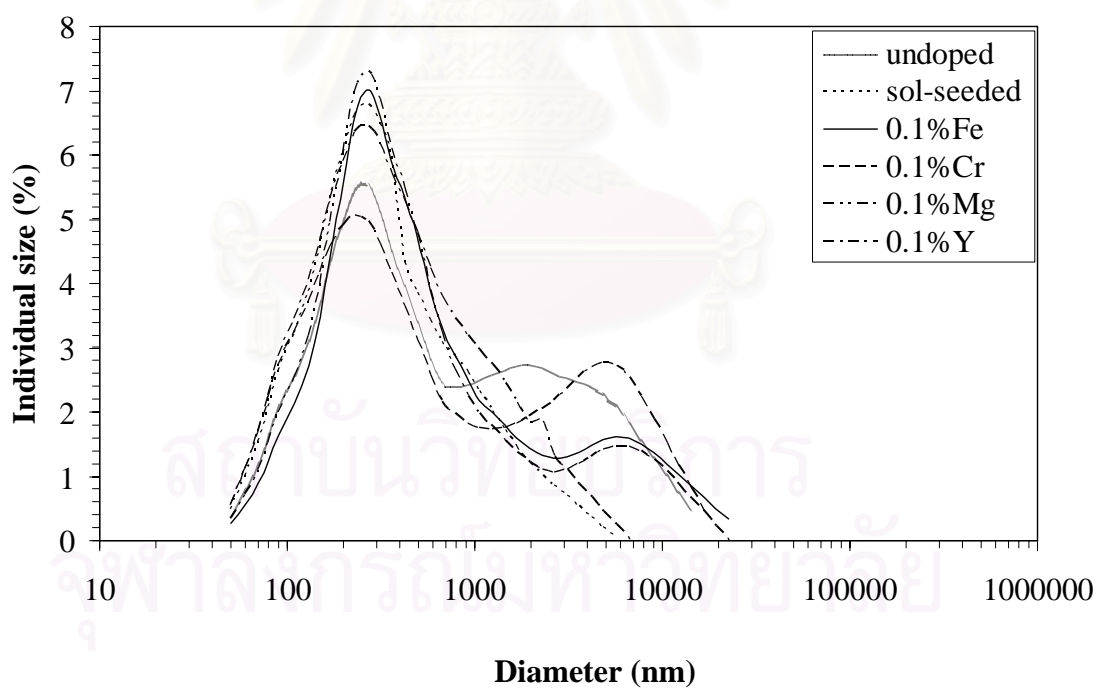


**Figure 4.9** SEM images of calcined powder after milling for 72 h: (a) undoped alumina, (b) sol-seeded alumina, (c) 0.1 wt.%Cr-doped alumina, (d) 0.1 wt.%Fe-doped alumina, (e) 0.1 wt.%Mg-doped alumina, (f) 0.1 wt.%Y-doped alumina.



(a)



(b)

**Figure 4.10** Particle size distribution of powder calcined at 1200°C:

(a) before milling, (b) after 72 h milling.

As shown in Figure 4.10b, all of the curves after milling are narrow, comparing to those before milling. It can be seen that, after milling, particle size distribution of powder synthesized with sol-seeding is unimodal, unlike the undoped alumina, of which the distribution curve splits into bimodal. Nevertheless, Table 4.4 shows that the median diameter of sol-seeded powder is higher than undoped alumina which suggests that grains of the undoped powder are highly distributive than sol-seeded alumina. On the other hand, sol behaves as seed and induces grains to come closer, which consequently affects the median diameter as well as morphology of the product.

From the particle size distribution curve of metal-doped alumina after milling (Figure 4.10b), only the distribution curve from 0.1 wt.%Y-doped alumina is unimodal, although it is bimodal before milling (Figure 4.10a). This is attributed to soft agglomeration of powder. The powder after milling is uniform in size and the median diameter is the smallest comparing to alumina doped with other metals. The size distribution of 0.1 wt.%Y-doped alumina is complement with sol-seeded alumina, which is also found to be narrow and unimodal. However, the median diameter of sol-seeded powder is much bigger, according to sol-effect as mentioned above. On the contrary, for Fe-, Mg-, and Cr-doped alumina, the distribution curves after milling apparently split into bimodal, indicated that to the powders are packed more tightly and hard to decrease into smaller size.

Specific surface area of the sample was determined based on nitrogen uptake at liquid-nitrogen temperature, using the Brunauer-Emmett-Teller (BET) equation, as described earlier. Table 4.5 shows the specific surface area of calcined powder at 1200°C. It is found that undoped alumina has the lowest surface area of approximately 10 m<sup>2</sup>/g. Since all samples have roughly the same crystallite size, the increase in specific surface area from doped alumina is suggested to be the result from pore structure in secondary particle.

**Table 4.5** Specific surface area of alumina powder after milling.

Sample	BET surface area [m <sup>2</sup> / g]
pure-alumina powder	10
sol-seed alumina powder	35
0.1%Fe alumina powder	29
0.1%Mg alumina powder	34
0.1%Y alumina powder	17
0.1%Cr alumina powder	48

As shown in Table 4.5, the sol-seeded sample has higher specific surface area than undoped alumina, of which the median particle size is smaller (Table 4.4). This result implies that the secondary particle of sol-seeded alumina is loosely agglomerated powder. There are many pores in the secondary particle of sol-seeded powder, comparing to undoped alumina, which directly results in higher BET surface area.

For metal-doped alumina, it is found that 0.1 wt.%Y-doped alumina has the lowest specific surface area with the smallest median size diameter. It can be noted that yttrium, which has the highest ionic radii, can co-precipitate with AACH in minor content. The rest of yttrium doped is located outside alumina lattice, at which it behaves like a binder to make fine particles around it agglomerate in high density with less pore formed in the secondary particle. Consequently, it shows the lowest specific surface area. For other metal-doped alumina, the high specific surface area is attributing to many pores structure in the secondary particles consisting of alumina grains with highly dispersed size distribution.

#### 4.2.1.2 Reflective UV/visible spectra of alumina powder

Figure 4.11 shows the comparison between the reflective UV/Visible spectra of the undoped alumina and the doped-alumina. For undoped, sol-seeded, 0.1%Y doped and 0.1%Mg doped powders, they show similar absorption bands which are corresponding mainly to white color. On the other hands, Cr-doped and Fe-doped powders show the reflective spectra associated with non-white color. The broad absorption band around 405-410 nm and 550 to 560 nm from 0.1%Cr doped sample are attributed to the absorption of  $\text{Cr}^{3+}$  species which results in the pink-red color, while the orange-red colors of 0.1%Fe doped sample is caused by absorption from isolated  $\text{Fe}^{3+}$  (at wavelength around 388 nm) and  $\text{Fe}^{3+}$  pairs (at absorption band at 377 nm and 450 nm, respectively) [113].

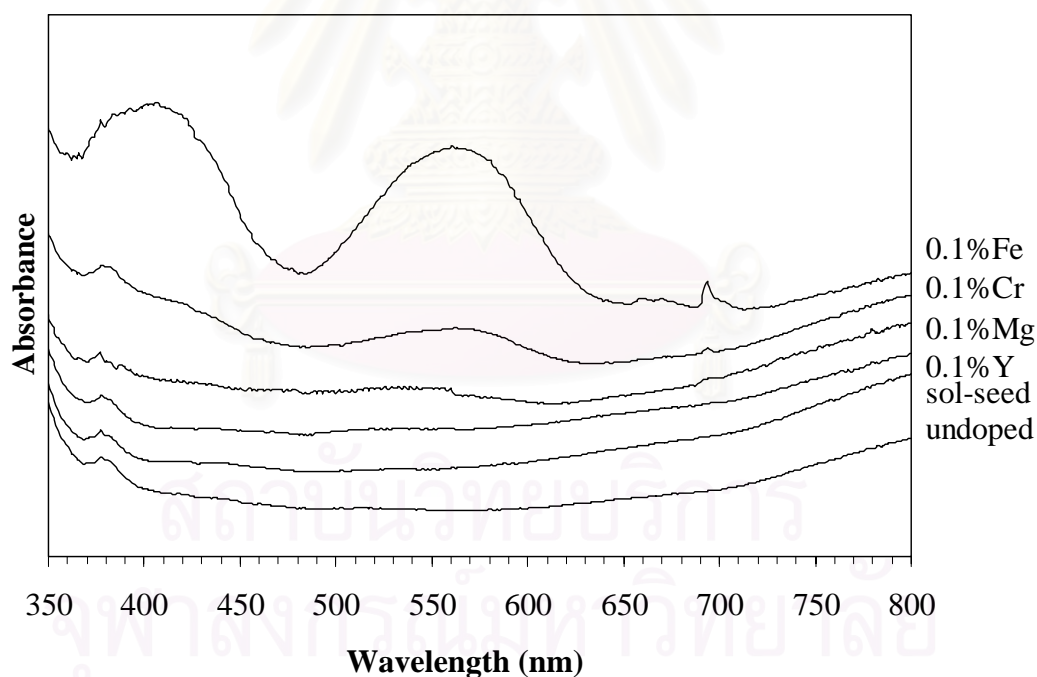


**Figure 4.11** Reflective UV/visible spectra of calcined powders.



### 4.2.2 Effect of iron

For iron doping (Figure 4.12), phase transformation of the product calcined between 600 and 800°C is not effected by the content of iron doping, i.e. phase of the product is the same as reported for 0.1 wt.% doping (Table 4.2 on page A). However, at 1000°C, the thermal stability of  $\gamma$ - $\text{Al}_2\text{O}_3$  doped with 0.5 or 1.0 wt.% iron is slightly lower than the product with only 0.1 wt.% iron. For these samples with moderate iron content, the direct phase transformation of alumina from  $\gamma$ - to  $\alpha$ -phase takes place at temperature lower than 1000°C, as witnessed from the presence of  $\alpha$ - $\text{Al}_2\text{O}_3$  in the sample calcined at 1000°C (Figure 4.12). It is found that the proportion of  $\gamma$ - to  $\alpha$ -phase is varied by the content of iron doping. Nevertheless, no iron-containing compound, such as iron oxide, is found after the heat treatment.

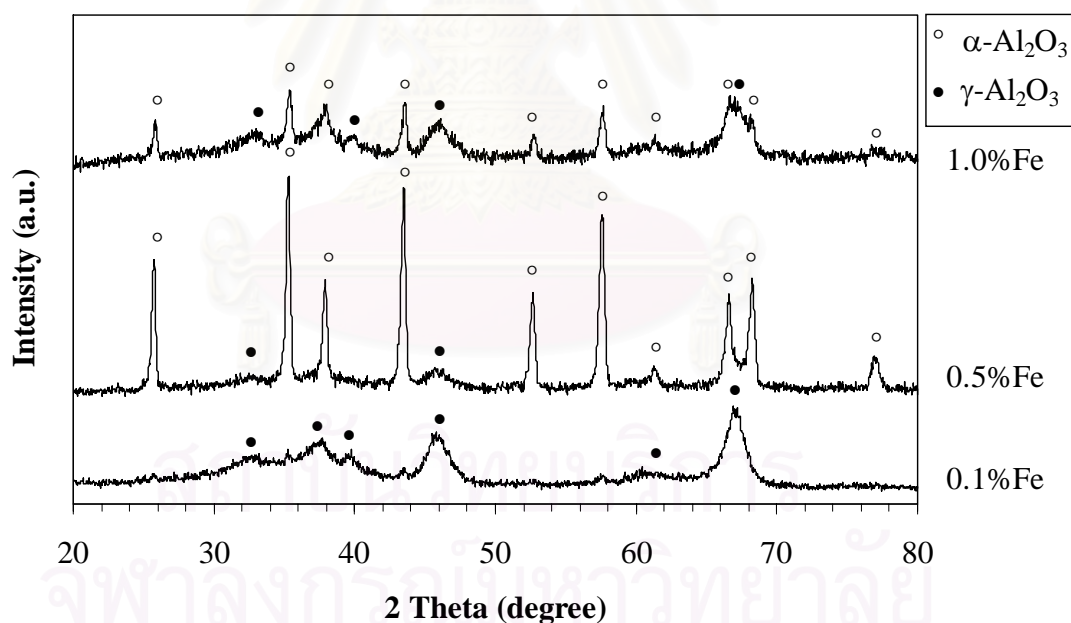


**Figure 4.12** XRD patterns of the products doped with iron in various content and calcined at 1000°C.

On the contrary, when extremely high amount of iron (10 wt.%) is co-precipitated with AACH, formation of  $\alpha$ - $\text{Fe}_2\text{O}_3$  is evolved upon the calcination at temperature higher than  $800^\circ\text{C}$ . This phase remains mixed with alumina product even after calcination at higher temperature. It should also be noted that the thermal stability of  $\gamma$ -alumina in the system with 10 wt.% iron shifts back toward that of undoped alumina, i.e.  $\gamma$ - $\text{Al}_2\text{O}_3$  can be detected in the sample calcined at  $700^\circ\text{C}$  and  $\alpha$ - $\text{Al}_2\text{O}_3$  is found after calcination at  $1000^\circ\text{C}$  (Figure 4.13). This behavior suggests that most iron separately precipitates to form  $\text{Fe}_2\text{O}_3$  without incorporation into alumina structure.

FTIR spectra of 10 wt.% iron-doped alumina powder (Figure 4.14) shows a minor band around  $621\text{ cm}^{-1}$  and an intense band at  $733\text{ cm}^{-1}$  that has been attributed to a symmetric Fe-O-Fe stretching vibration [114].

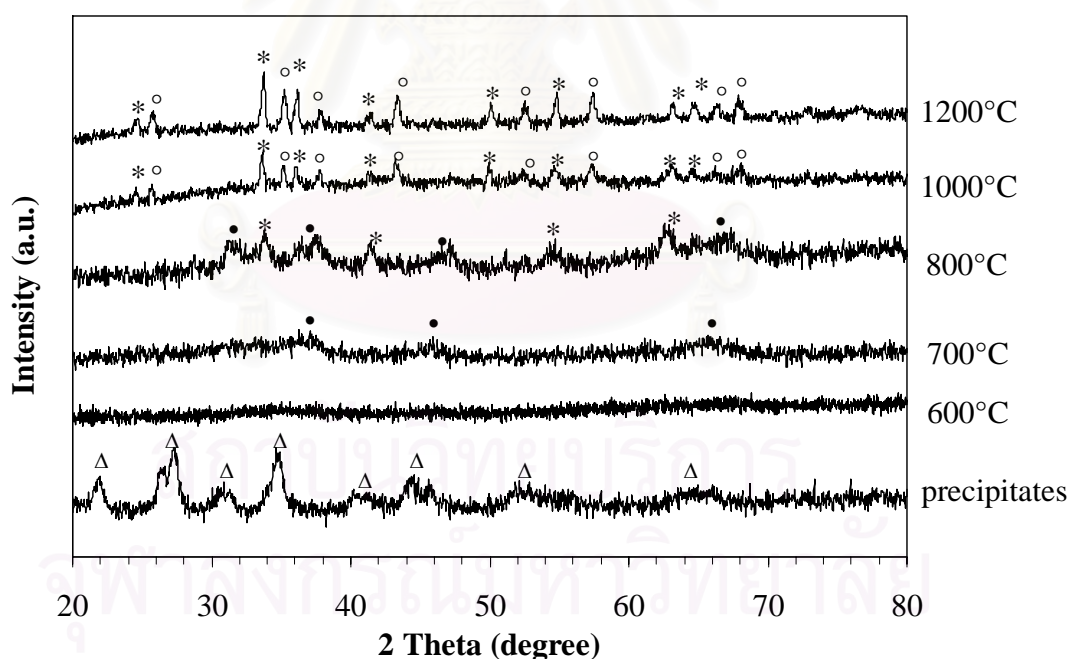


**Figure 4.13** XRD patterns of products calcined at various temperatures, which were obtained from precipitation accompanied by iron at 10 wt.% (○  $\alpha$ - $\text{Al}_2\text{O}_3$ , ●  $\gamma$ - $\text{Al}_2\text{O}_3$ , \*  $\text{Fe}_2\text{O}_3$ , Δ AACH).

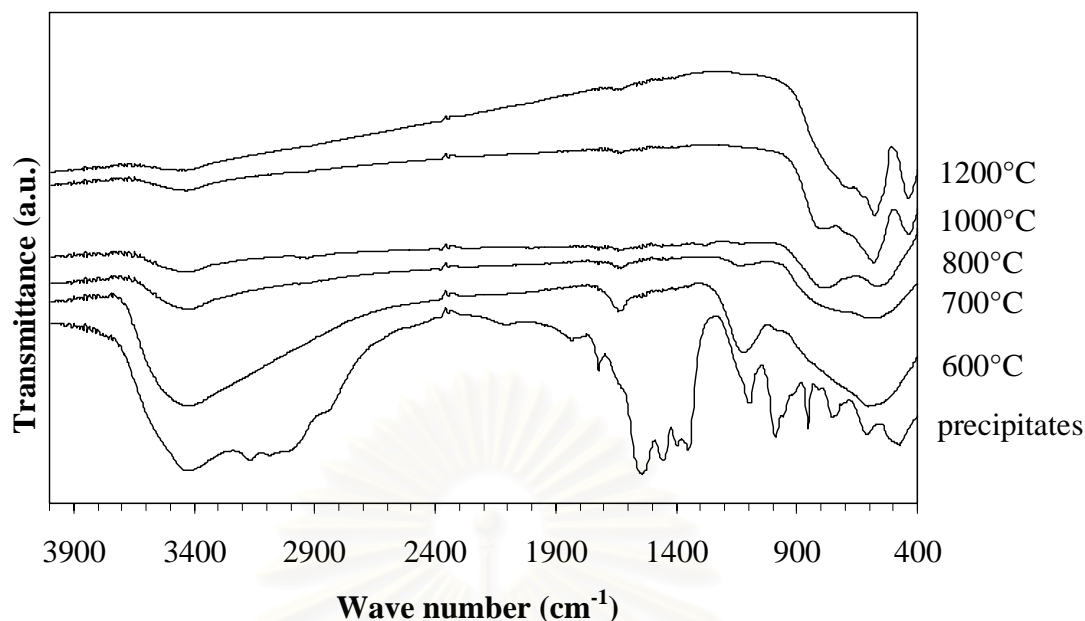


**Figure 4.14** FTIR spectra of products calcined at various temperatures, which were obtained from precipitation accompanied by iron at 10 wt.%

### 4.2.3 Effect of magnesium

For magnesium-doped alumina, in the amount corresponding to 0.5 or 1.0 wt.%, the results of phase transformation behavior at temperature between 600 and 800°C show the same as the result from 0.1 wt.% magnesium doping. However, the results from the product calcined at 1000°C (Figure 4.15) show that position of XRD peaks corresponding to  $\gamma$ -Al<sub>2</sub>O<sub>3</sub> are shifted when the content of magnesium doping is increased. This is attributed to lattice distortion in alumina structure. Therefore, it is suggested that higher amount of magnesium is incorporated into the structure of alumina at higher content of magnesium doping. After calcination at temperature higher than 1000°C (Figure 4.16), significant amount of  $\gamma$ -alumina is found only in samples doped with relatively high amount (e.g. 1.0 wt.%) of magnesium. It can be seen that thermal stability of  $\gamma$ -Al<sub>2</sub>O<sub>3</sub> can be greatly improved by increased content of magnesium doping. Nevertheless, unidentified peaks at  $2\theta$  approximately 37°, 59°

and  $65^\circ$  are detected. The higher the magnesium doping content, the higher intensities observed.

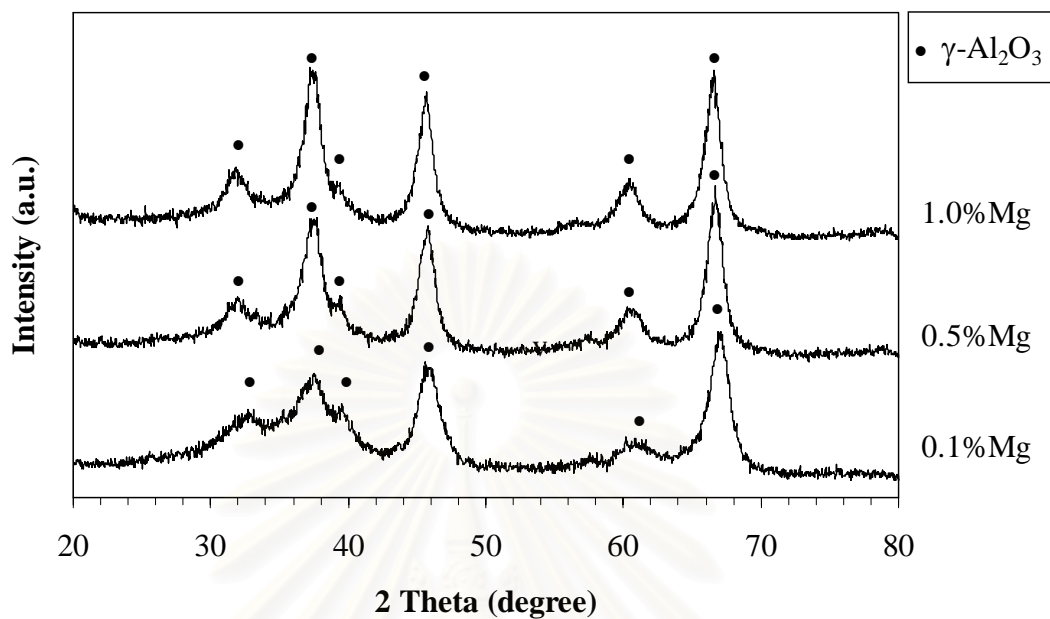


**Figure 4.15** XRD patterns of the products doped with magnesium in various contents and calcined at  $1000^\circ\text{C}$ .

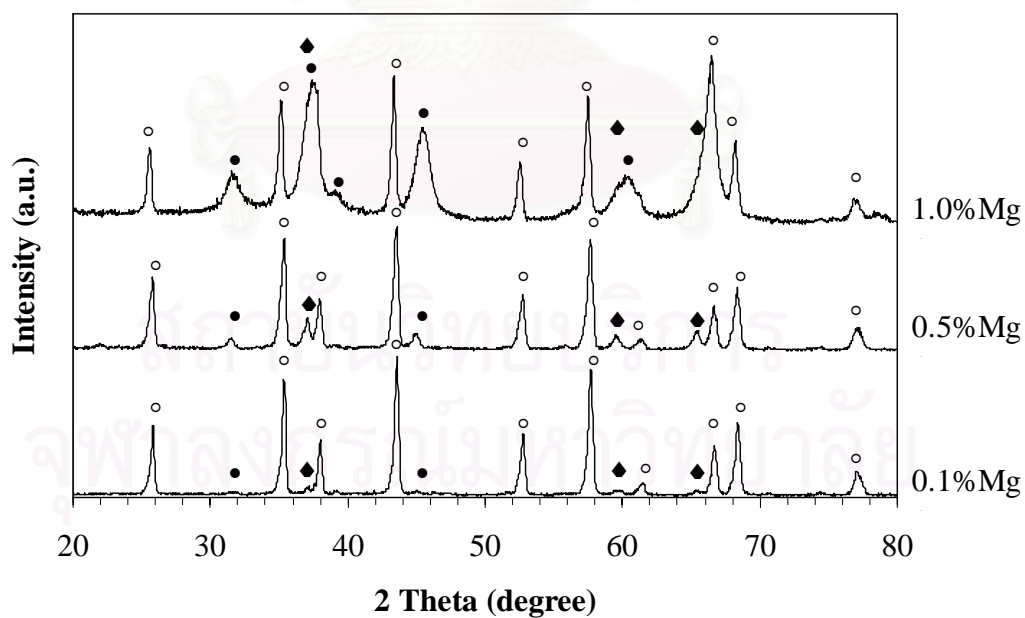


**Figure 4.16** XRD patterns of the products doped with magnesium in various contents and calcined at  $1200^\circ\text{C}$  (o  $\alpha\text{-Al}_2\text{O}_3$ , •  $\gamma\text{-Al}_2\text{O}_3$ , ◆ unidentified phase).

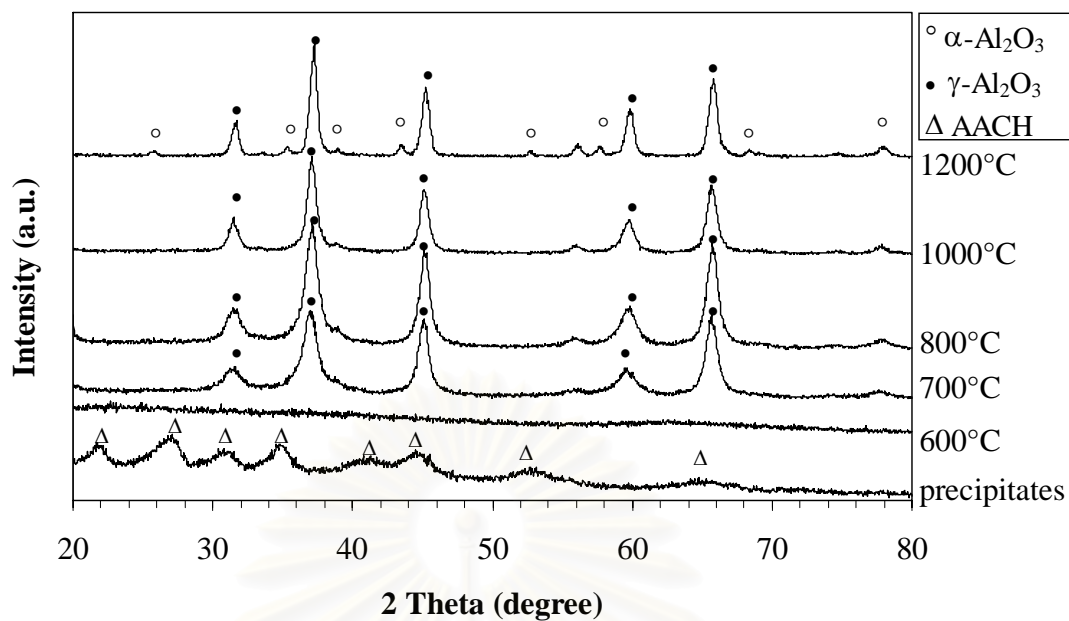


**Figure 4.17** XRD patterns of products calcined at various temperatures, which were obtained from precipitation accompanied by magnesium at 10 wt.%.

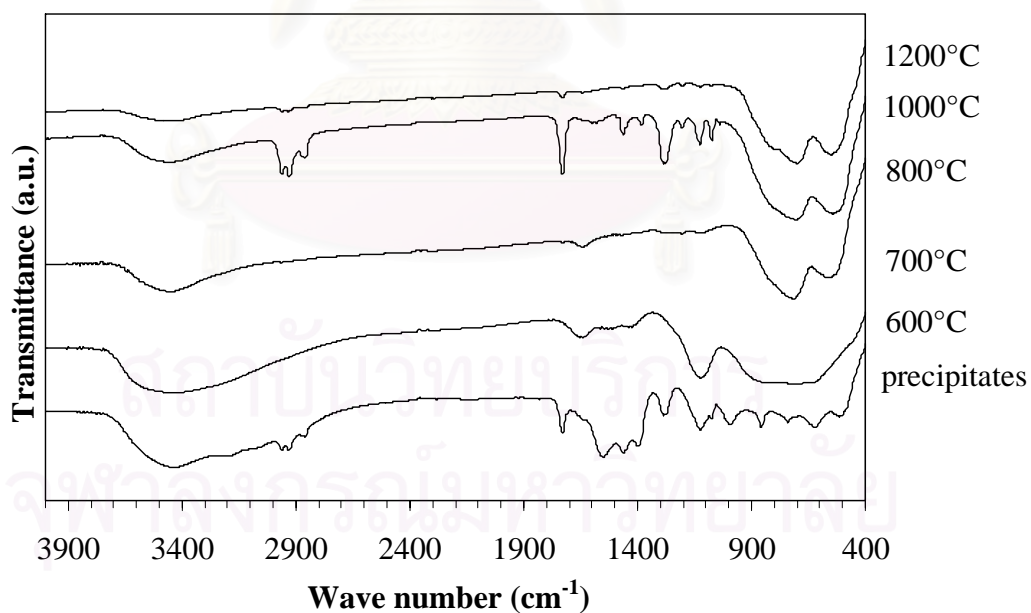


**Figure 4.18** FTIR spectra of products calcined at various temperatures, which were obtained from precipitation accompanied by magnesium at 10 wt.%.

XRD analysis of 10 wt.% magnesium doped alumina is shown in Figure 4.17. It is found that  $\gamma$ -Al<sub>2</sub>O<sub>3</sub> is quite stable even at 1200°C, although trace amount of  $\alpha$ -Al<sub>2</sub>O<sub>3</sub> is also observed. Nevertheless, the crystallite size of  $\gamma$ -Al<sub>2</sub>O<sub>3</sub> seems to be increased as observed from the sharpness of XRD peaks. Since the presence of  $\gamma$ -Al<sub>2</sub>O<sub>3</sub> at temperature higher than 1000°C is rarely observed, the result suggests that the thermal stability of  $\gamma$ -Al<sub>2</sub>O<sub>3</sub> can be significantly improved by adding high content of magnesium. FTIR spectra (Figure 4.18) reveals similar set of absorption bands as these reported for sample with 0.1% magnesium doping. However, unidentified absorption bands at wave number in the range of 1000-1800 cm<sup>-1</sup> and around 2900 cm<sup>-1</sup> are observed from the samples calcined at 1000 and 1200°C.

#### 4.2.4 Effect of yttrium

For yttrium-doped alumina, the content of doped yttrium has insignificant effect on thermal stability of  $\gamma$ -Al<sub>2</sub>O<sub>3</sub> phase at temperature between 600 and 1000°C. Doping of yttrium in the amount corresponding to 0.5 or 1.0 wt.% results in the same effect as 0.1 wt.% doping. However, at the calcination temperature of 1200°C, oxides of yttrium (i.e. Y<sub>2</sub>O<sub>3</sub>) is found in samples doped with 0.5 and 1.0% yttrium (Figure 4.19). The intensity of the XRD peaks corresponding to Y<sub>2</sub>O<sub>3</sub> increases with the content of yttrium doped.

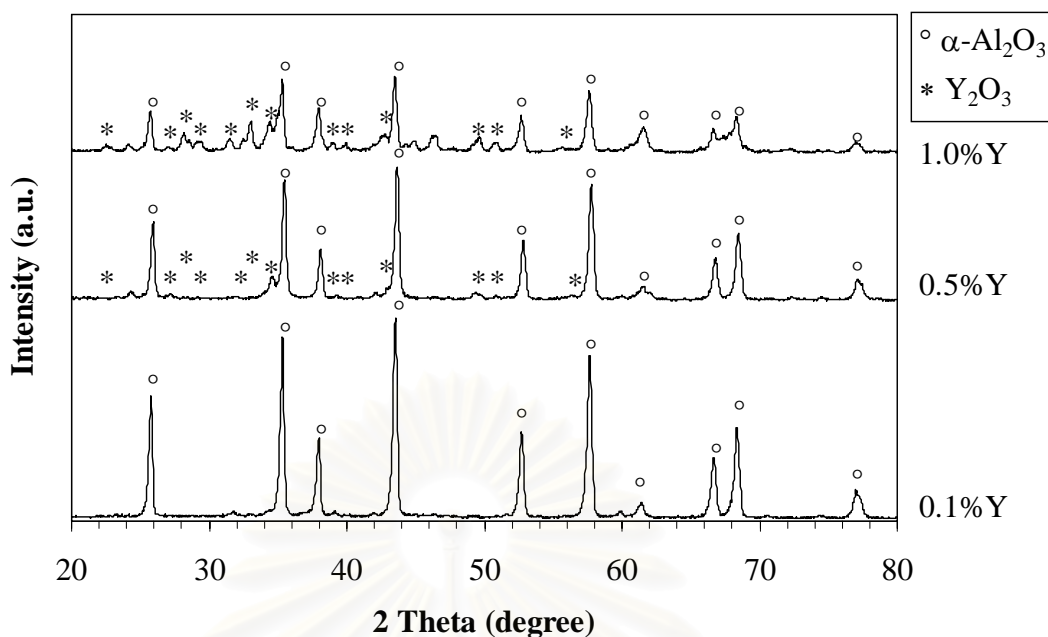


**Figure 4.19** XRD patterns of the products doped with yttrium in various contents and calcined at 1200°C.

Nevertheless, it is surprised to find no signal corresponding to any crystalline phase of alumina in the sample doped with 10 wt.% of yttrium (Figure 4.20). Instead, yttrium alumina garnet (YAG), i.e.  $Y_3Al_5O_{12}$ , can be clearly observed as the final product from the calcination at 1200°C. For the calcination at low temperature (600-800°C), unidentified peaks are detected from the XRD analysis.

According to Figure 4.21, the FTIR spectra of the 10 wt.% yttrium-doped alumina powder annealed at various temperature shows the absorption bands at 770 and 625  $cm^{-1}$ , which represent the characteristic bands of Al-O vibration. Moreover, the absorption band positioned at wave number of 708 and 551  $cm^{-1}$ , which represent the characteristic bands of Y-O vibrations [115], are detected. These results confirm the formation of YAG in the sample. It can be seen that the FTIR results are in good agreement with XRD observation.

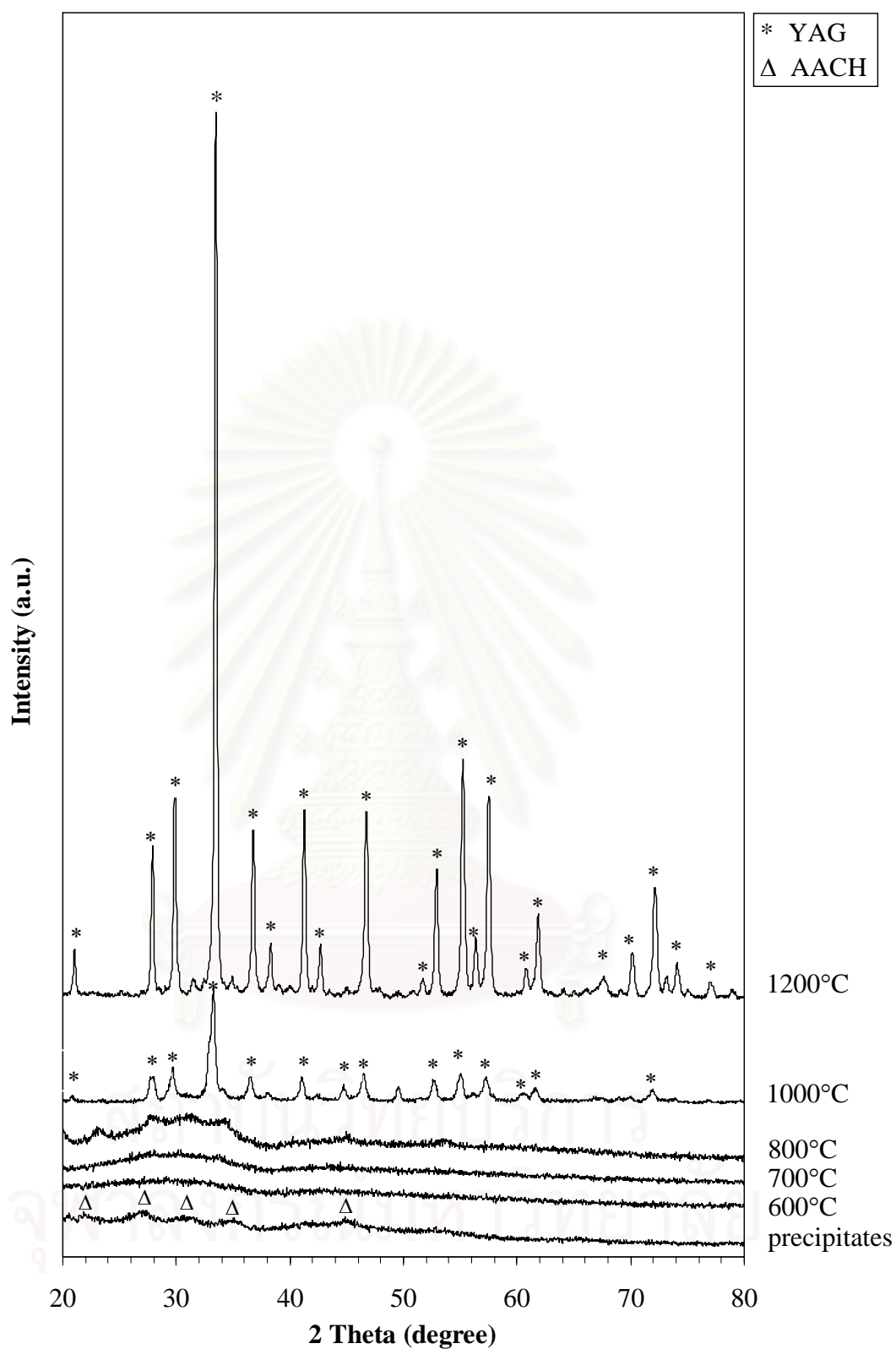


**Figure 4.20** XRD patterns of products calcined at various temperatures, which were obtained from precipitation accompanied by yttrium at 10 wt.%



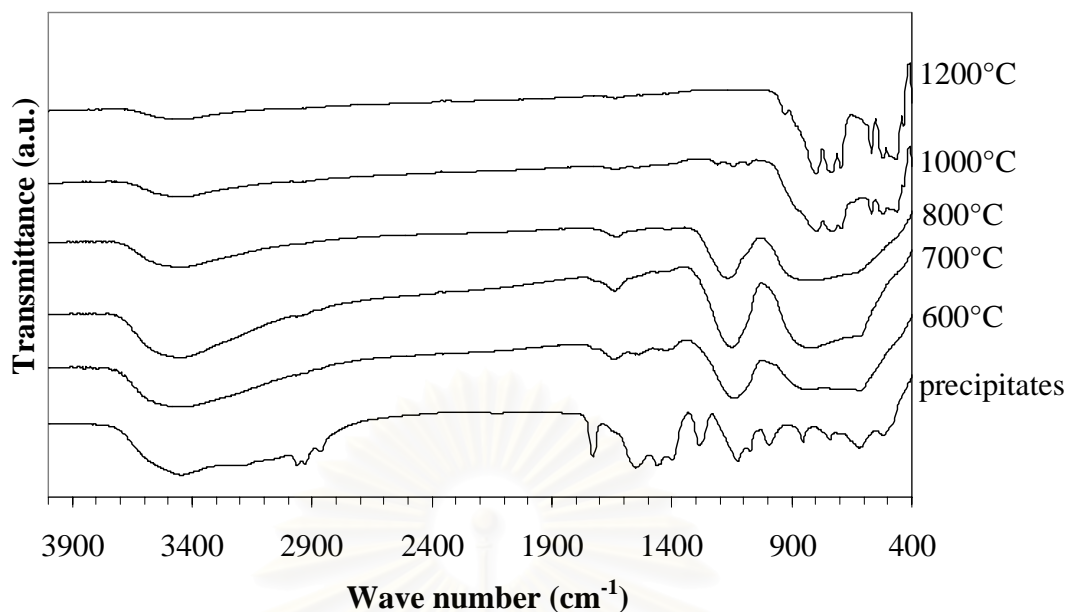


**Figure 4.21** FTIR spectra of products calcined at various temperatures, which were obtained from precipitation accompanied by yttrium at 10 wt.%.

#### 4.2.5 Effect of chromium

As reported earlier, for alumina doped with 0.1 wt.% chromium, the sample calcined at 700°C is amorphous alumina mixed with crystalline  $\text{Cr}_2\text{O}_3$ , while the product calcined at 800°C is  $\gamma\text{-Al}_2\text{O}_3$ . As the content of chromium doping is increased, it is found that the higher the chromium content, the higher the temperature at which  $\text{Cr}_2\text{O}_3$  is detected (Figure 4.22). The alumina product remains amorphous at higher temperature by the increased content of chromium doping. The signal from  $\text{Cr}_2\text{O}_3$  disappears, once the product transforms to  $\gamma$ -alumina upon the calcination at higher temperature, which indicates the incorporation of chromium into alumina product.

It is found that the temperature, at which  $\gamma$ - to  $\alpha$ - phase transformation takes place, also shifts toward higher temperature when the content of chromium is increased. Upon the calcination at temperature of 1000°C (Figure 4.23),  $\gamma\text{-Al}_2\text{O}_3$  still remains detected when the content of chromium is increased. Therefore, it can be

attributed that  $\alpha$ -phase formation is suppressed by increased chromium content. However, at the calcination of 1200°C, all  $\gamma$ - $\text{Al}_2\text{O}_3$  is converted to  $\alpha$ -phase.

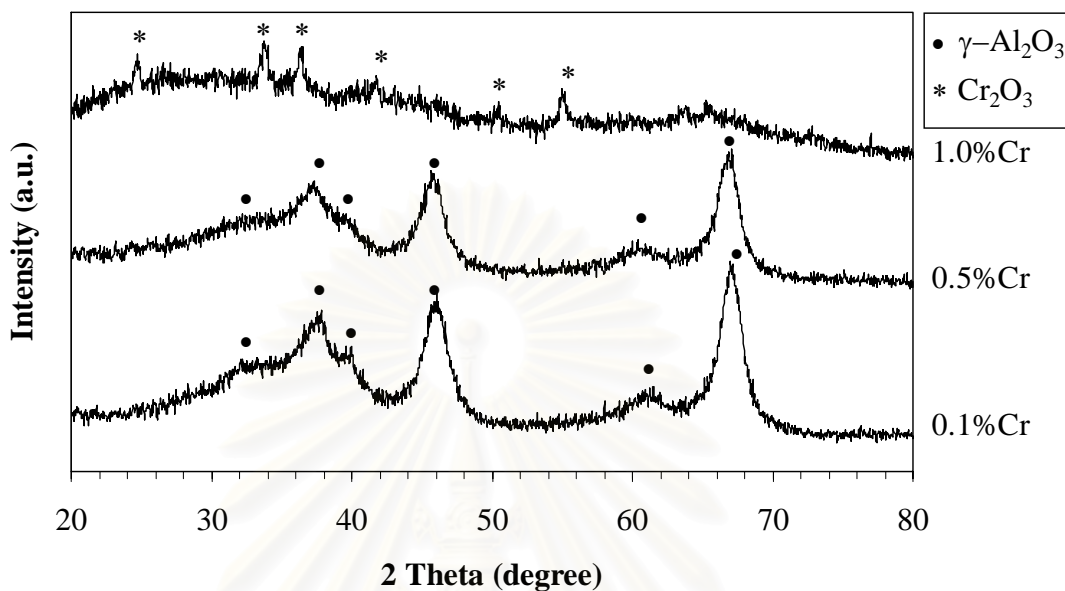


**Figure 4.22** XRD patterns of the products doped with chromium in various contents and calcined at 800°C.

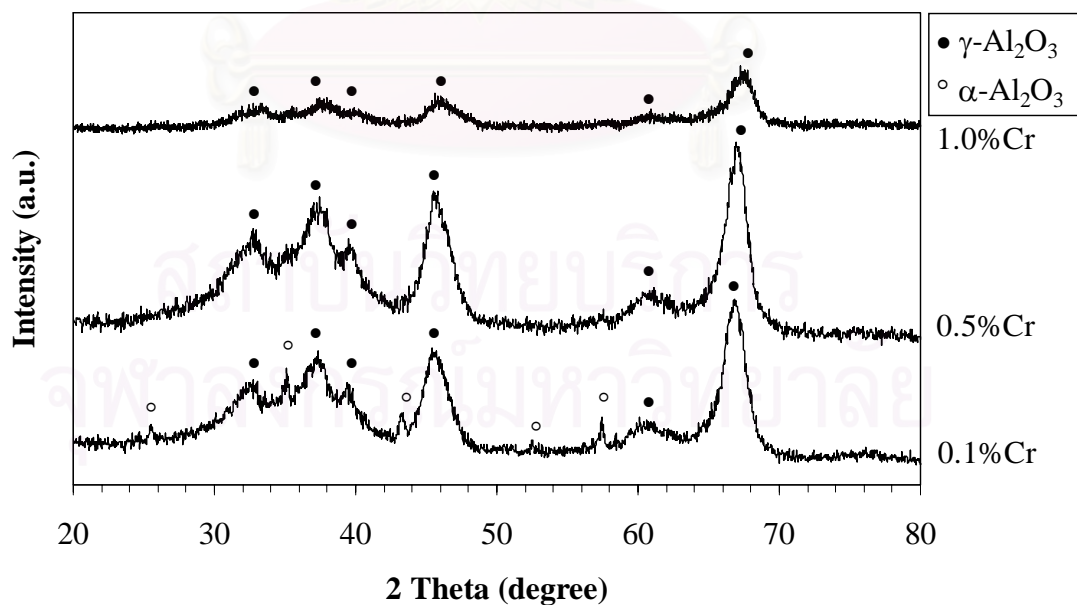


**Figure 4.23** XRD patterns of the products doped with chromium in various contents and calcined at 1000°C.

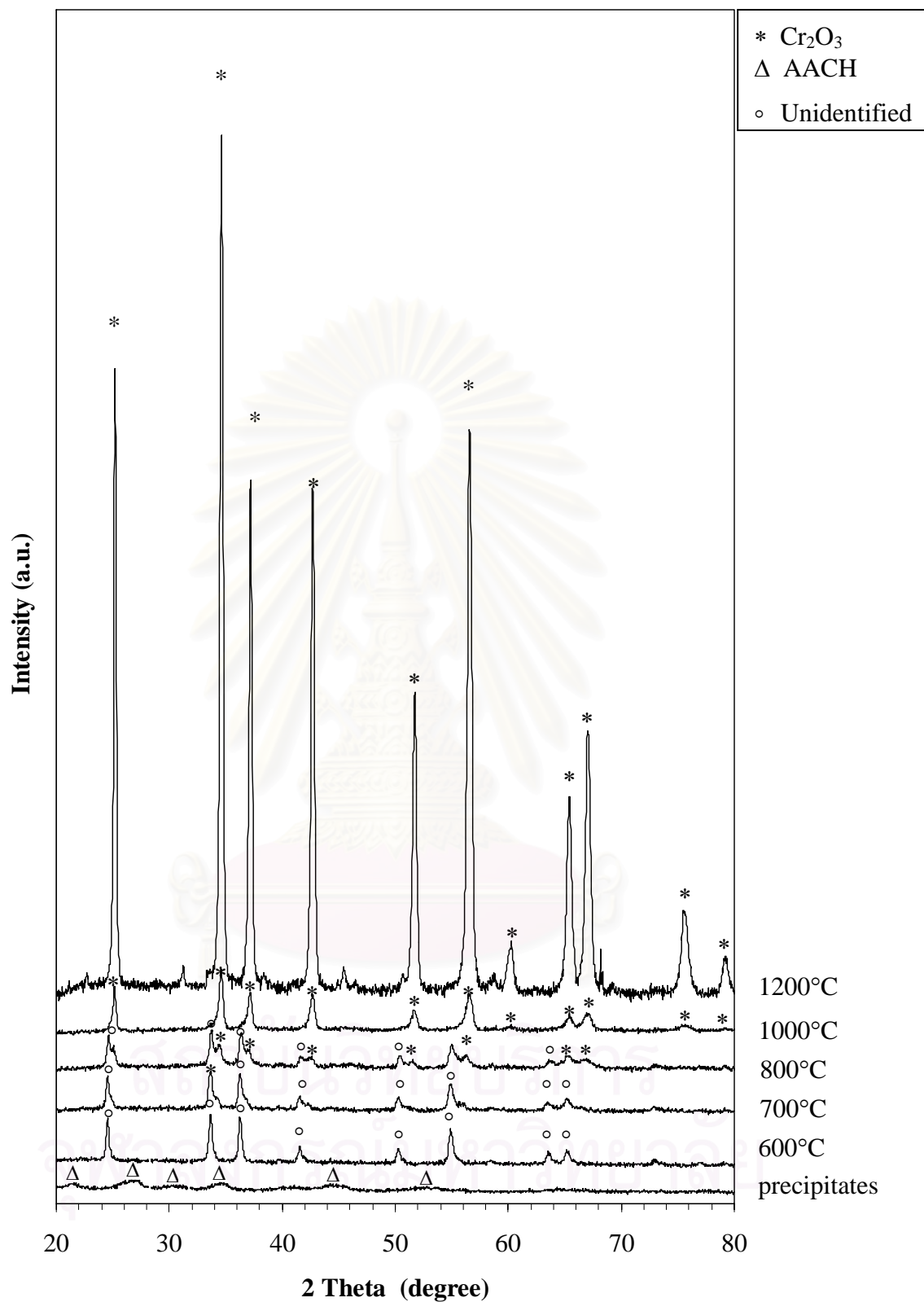


**Figure 4.24** XRD patterns of products calcined at various temperatures, which were obtained from precipitation accompanied by chromium at 10 wt.%

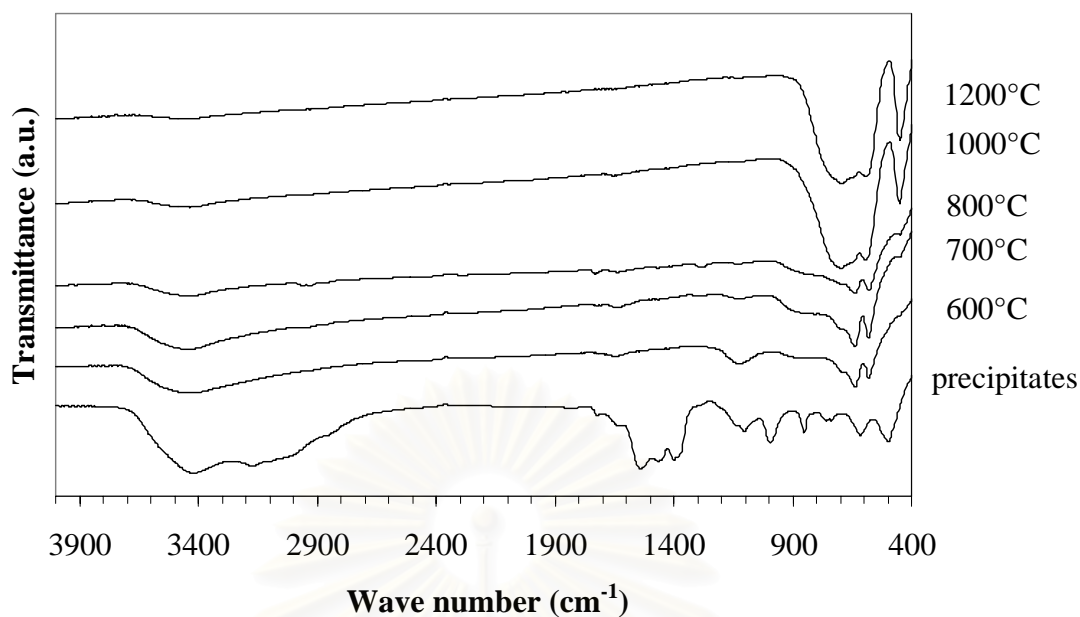


**Figure 4.25** FTIR spectra of products calcined at various temperatures, which were obtained from precipitation accompanied by chromium at 10 wt.%.

For 10 wt.% chromium-doped alumina (Figure 4.24), it is found that the unidentified peak, which is similar to  $\text{Cr}_2\text{O}_3$ , is detected at the temperature between 600 and 800°C. The formation of  $\text{Cr}_2\text{O}_3$  is observed after calcination at higher temperature. No alumina phase is detected at any calcination temperature. The IR characteristic bands of  $\text{Cr}_2\text{O}_3$  are visible at wave number of 438, 533 and 633  $\text{cm}^{-1}$  [116], as shown in Figure 4.25. The results are consistent with the XRD analysis.

#### 4.2.6 Lattice parameters of metal-doped alumina

The lattice parameters of alumina doped with low content of metal, calculated from XRD pattern, are shown Table 4.6-4.7. It can be clearly seen that the lattice parameters of metal-doped alumina are significantly deviated from those of undoped sample. The change in lattice parameters indicates the distortion of alumina lattice by the presence of metal ions in alumina structure. The fact that, for doping with all metals except chromium, the lattice parameters of  $\gamma$ -alumina are altered even after the calcination at 800°C indicates that metal is incorporated into alumina since the formation of  $\gamma$ -alumina, possibly since the formation of AACH precipitates. For

chromium doping, significant change in the lattice parameters is observed in  $\alpha$ -phase, not in  $\gamma$ -phase. Therefore, it is suggested that chromium is incorporated into alumina during  $\gamma$ - to  $\alpha$  phase transformation. This is supported by the results from XRD analysis that no metal oxide compound is detected, except for chromium doping. The change in lattice parameters with calcination temperature is suggested to be the result of relaxation process, which reduces defects and lattice distortions in alumina structure [108].

**Table 4.6** Lattice parameters of  $\alpha$ -Al<sub>2</sub>O<sub>3</sub> in products doped with 0.1 wt.% of metal and calcined at 1200°C.

Sample	$a$ and $b$ [Å]	$c$ [Å]
undoped alumina	4.5781	13.9352
Fe-doped alumina	4.5831	13.9488
Mg-doped alumina	4.5881	13.9642
Cr-doped alumina	4.5983	13.9642
Y-doped alumina	4.5932	13.9502

**Table 4.7** Lattice parameters of  $\gamma$ -Al<sub>2</sub>O<sub>3</sub> in products doped with 0.1 wt.% of metal and calcined at various temperatures.

Sample	$a, b$ and $c$ [Å]	
	800°C	1000°C
undoped alumina	7.8818	7.8800
Fe-doped alumina	7.9156	7.8992
Mg-doped alumina	7.9387	7.9089
Cr-doped alumina	7.8895	7.8789
Y-doped alumina	7.9211	7.9117

The effects of metal content on lattice parameters are shown in Figure 4.26 and 4.27. It is shown that the effect from the content of metal doping is stronger on  $c$ -axis than  $a$ - or  $b$ -axis, especially when the metal content is higher than 0.5 wt.%.

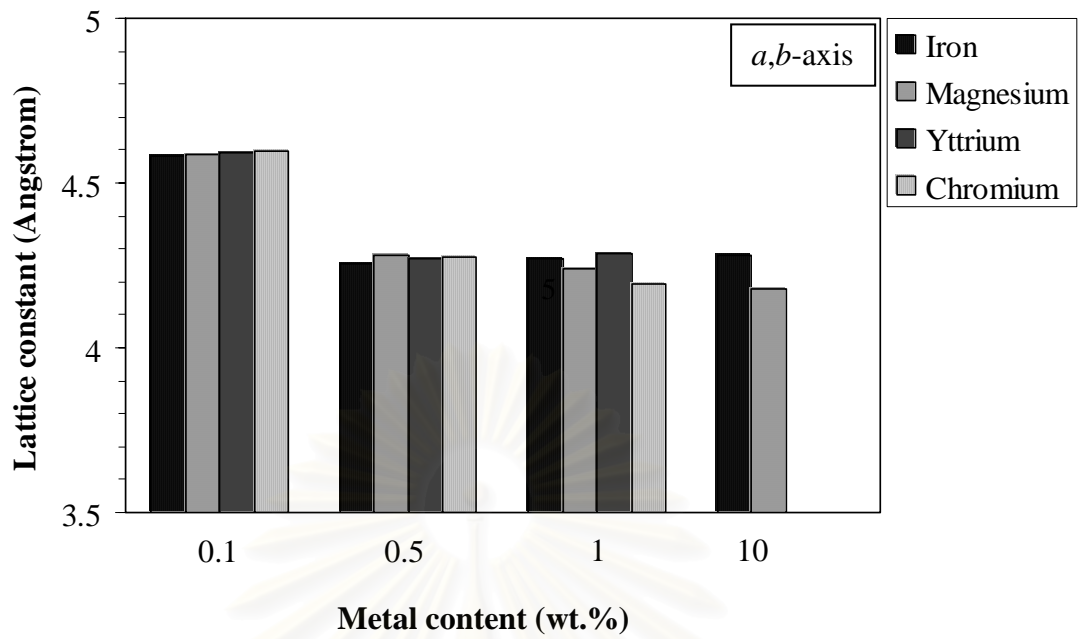


**Figure 4.26** The *a* and *b*-axis of lattice constant of  $\alpha$ -Al<sub>2</sub>O<sub>3</sub> from various metal contents.

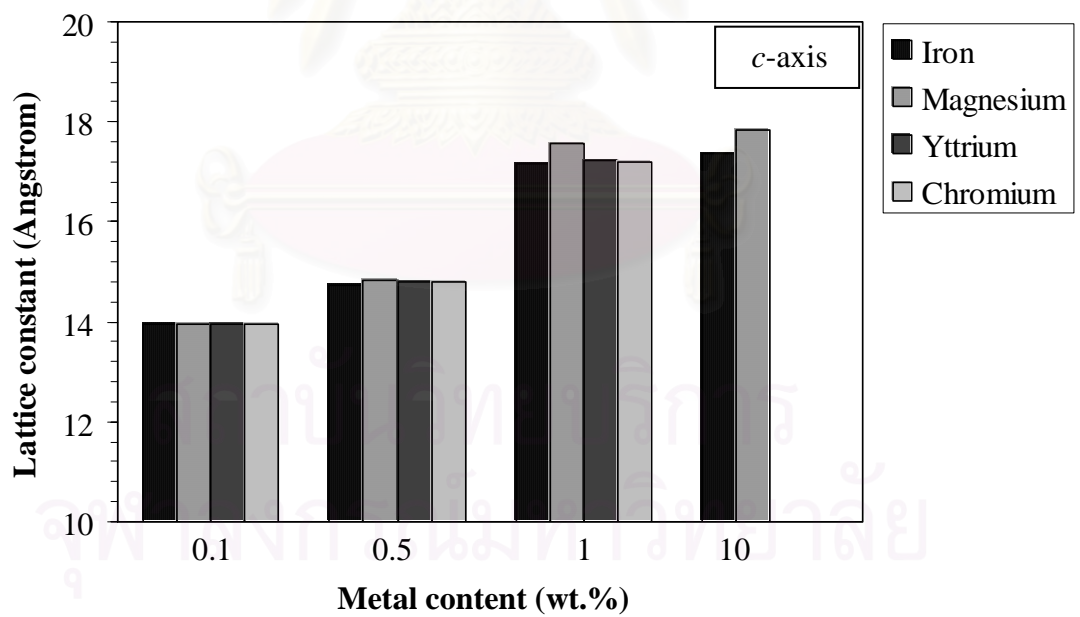


**Figure 4.27** The *c*-axis of lattice constant of  $\alpha$ -Al<sub>2</sub>O<sub>3</sub> from various metal contents.

#### 4.2.7 XPS analysis

XPS is basically a surface characterization technique. In this research, the metal-matrix interaction in metal-doped  $\text{Al}_2\text{O}_3$  was studied using XPS. Figure 4.28 and 4.29 show the binding energy of O 1s and Al 2p electrons in samples calcined at different temperatures. For undoped alumina, the XPS peak positions for both O 1s and Al 2p electrons are found to shift toward higher binding energy after the sample is calcined at higher temperature. This shift is obvious for the calcination temperature between 600 and 1000°C, which suggests that the increased binding energy is correlated with phase transformation from  $\gamma$ - to  $\alpha$ -alumina. It should be noted that trend of the change in binding energy with calcination temperature for O 1s and Al 2p electrons are the same. The observation is consistent with the relaxation of lattice parameters after heat treatment previously discussed. At 1200°C, the binding energy of O 1s and Al 2p electrons are 76 and 533 eV, respectively, which is consistent with the previous values reported for  $\alpha$ - $\text{Al}_2\text{O}_3$  [117].

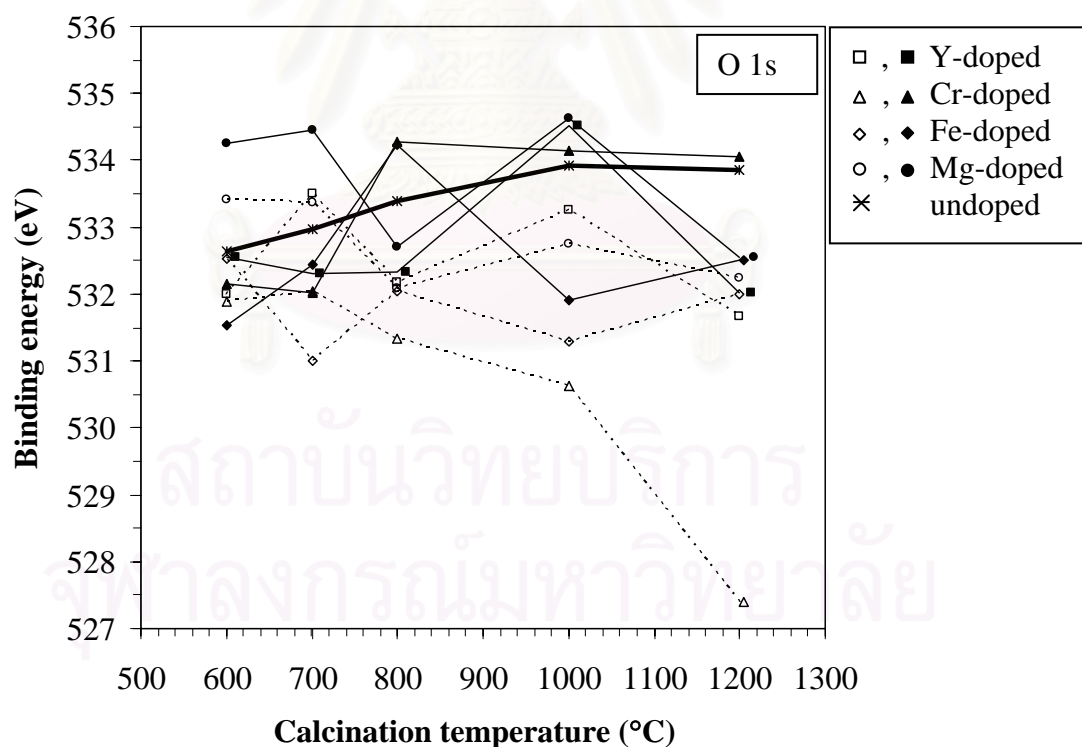


**Figure 4.28** The O 1s binding energy of the samples calcined at different temperatures: (---) alumina with doping content of 0.1%, (—) alumina with doping content of 0.5%.

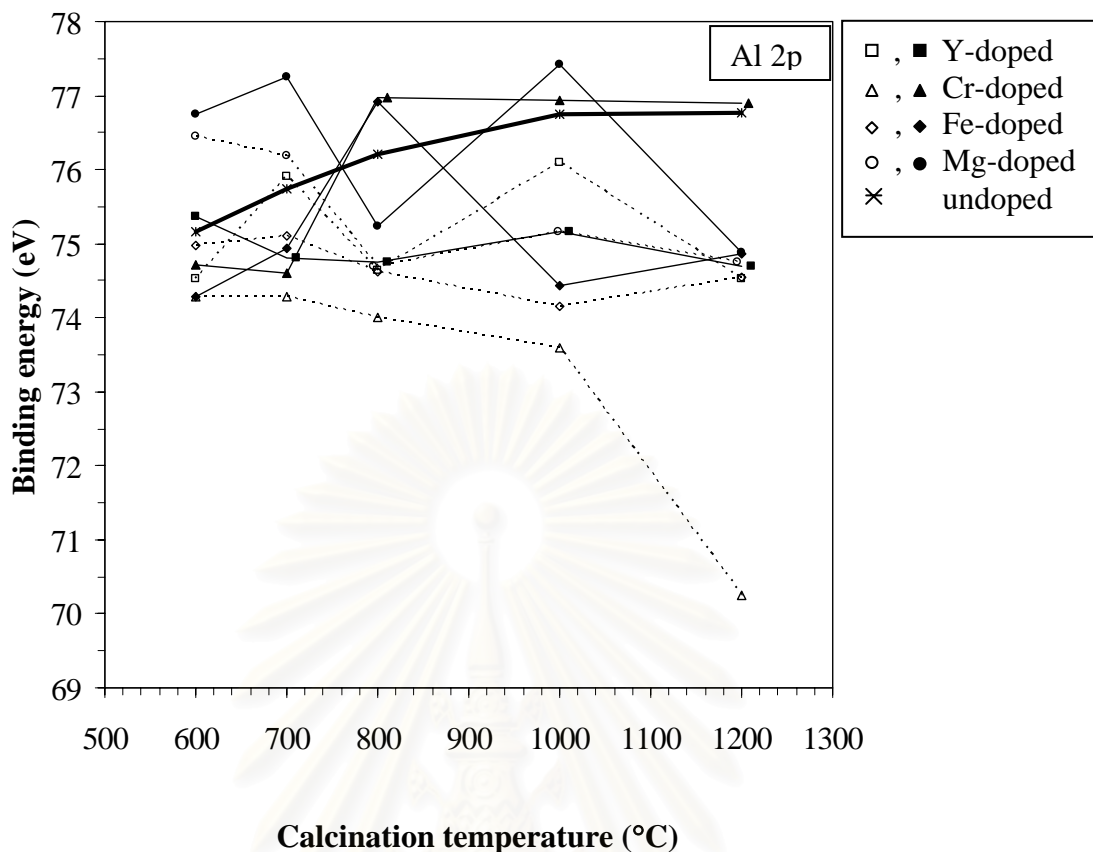
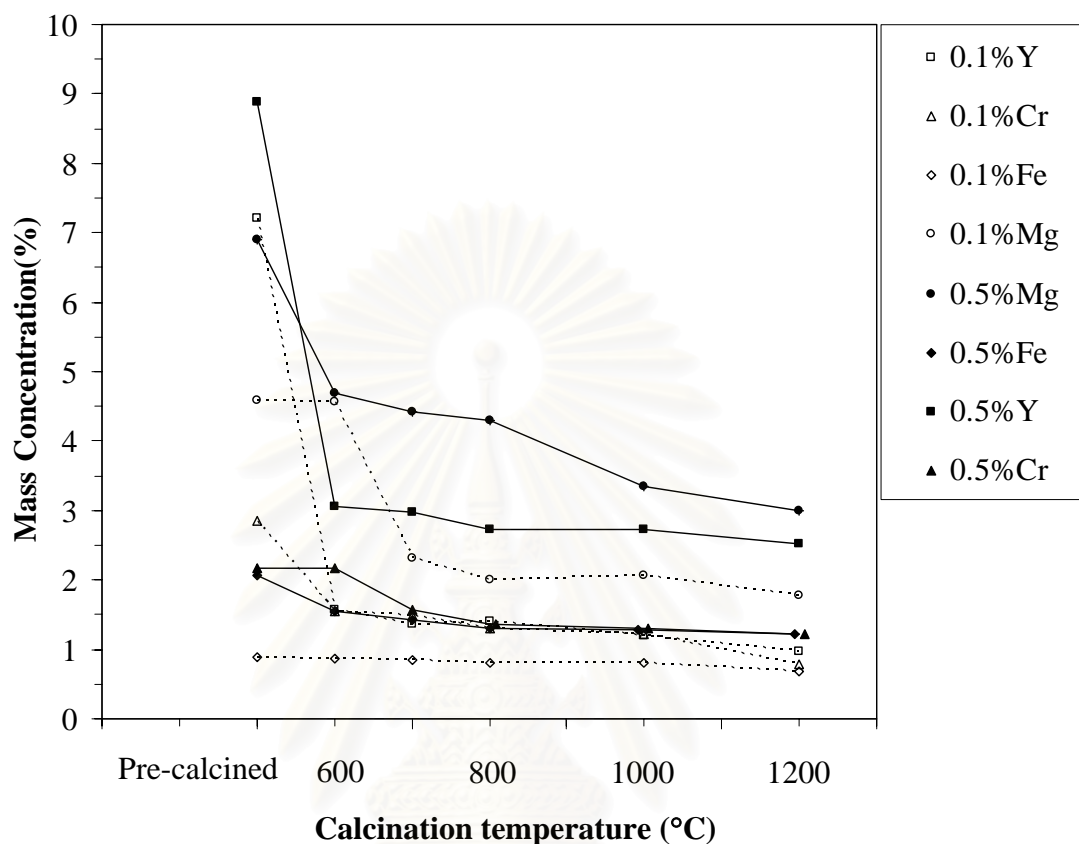


**Figure 4.29** The Al 2p binding energy of the samples calcined at different temperatures: (---) alumina with doping content of 0.1%, (—) alumina with doping content of 0.5%.

For doped samples, the binding energy is varied in the range of 531-535 eV for O 1s electrons and in the range 74-77 eV for Al 2p electrons. It can be seen that doping with different metal results in different shift in binding energy. The most obvious result is the case of 0.1 wt.% chromium doped-alumina, where the binding energy of O 1s and Al 2p electrons are significantly deviated from those in undoped sample. Since binding energy of one species depends strongly on the chemical and/or electronic environment surrounding it [118], the shifts in binding energy observed are the results from the different properties of dopant. For the different content of metal doping, it can be seen that the higher doping content generally causes the binding energy to shift toward higher energy. However, the result is not sufficient to thoroughly understand interaction between dopant and atoms in alumina matrix. It is suggested that the binding energy shifts are characteristic of physical or chemical change in the environment of the analyzed species. Moreover, it has been observed



that the electronegativity of the incorporated metal plays a decisive role on the type of interaction between the metal and alumina [119].



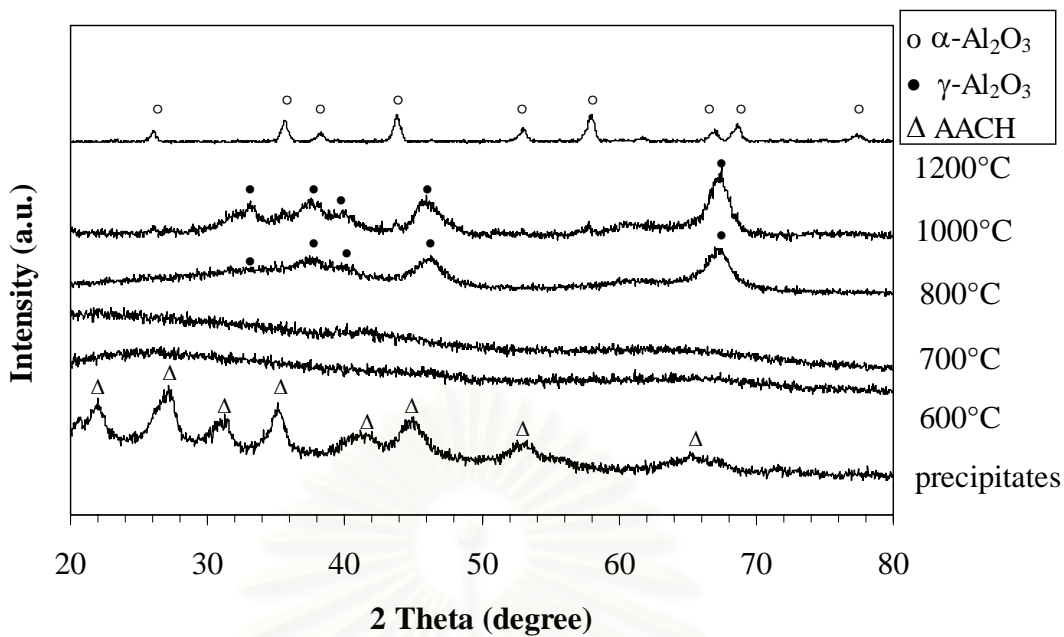
**Figure 4.30** The metal content at the surface of sample calcined at different temperatures: (---) alumina with doping content of 0.1%, (—) alumina with doping content of 0.5%.

Figure 4.30 shows the content of metal species detected on the surface by XPS analysis. It is found that the surface metal content is decreased with increasing calcination temperature. The surface concentration of most metal is significantly decreased from that in pre-calcined powder. After calcined at higher temperature, it shows a slow decrease and almost stable at the calcination temperature higher than 1000°C. From this result, it is indicated that the incorporated metal distributes into the alumina powder since the calcination at low temperature. The ability of metal to incorporate in alumina structure has been related to the ionic radii of the additive. This result is in good agreement with the analysis of lattice parameters.

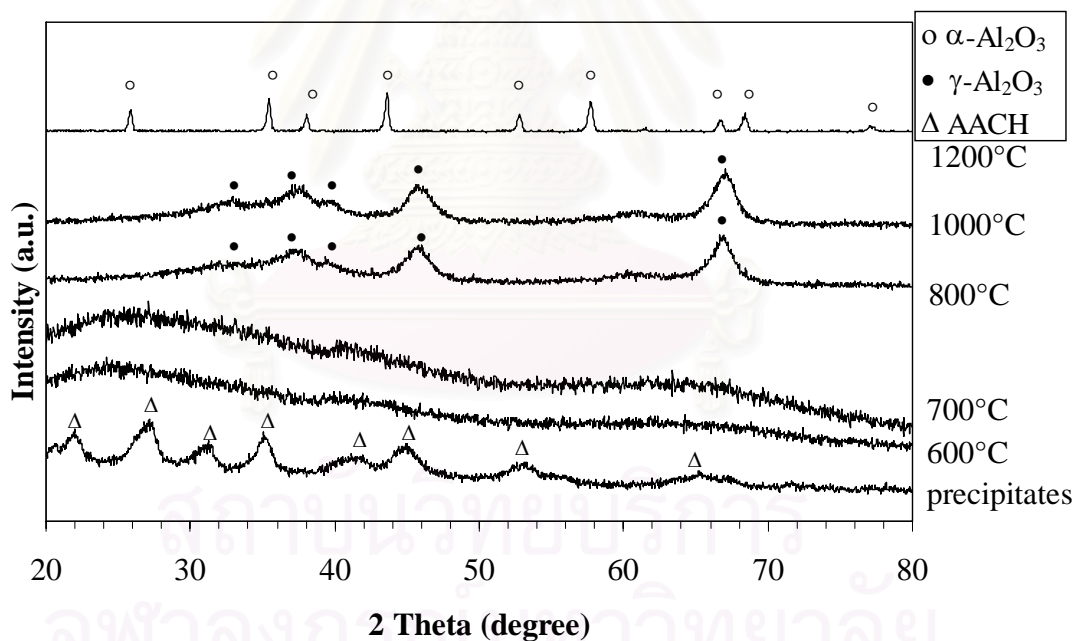
#### 4.2.8 Introduction of both metal and sol-seed to alumina

According to the experimental procedures previously described, doping of the secondary metal investigated in this work was done by 3 routes, i.e. co-precipitation of metal precursor with aluminum salt, co-precipitation of metal precursor with sol-seeded aluminum salt, and incorporation of metal precursor into alumina sol before introducing to aluminum salt. In this section, the results from the last two routes are compared to investigate the combined effect of metal-doping and sol-seeding. The content of the dopant in this study is fixed at 0.5 wt.%.

According to Figure 4.31 to 4.34, it is shown that the phase transformation behavior of the products obtained does not depend upon the procedure to incorporate metal dopant and alumina sol into the precipitate. The result from adding metal precursor to sol-seeded AAS solution is similar to that from using AAS solution with metal-doped sol. Moreover, they are similar to that from using sol-seed alumina. Nevertheless, the results from different metal are different, as previously discussed in section 4.2.1-4.2.5. Thus from this result, it is suggested that sol-seeding has predominately effect on alumina phase transformation behavior.

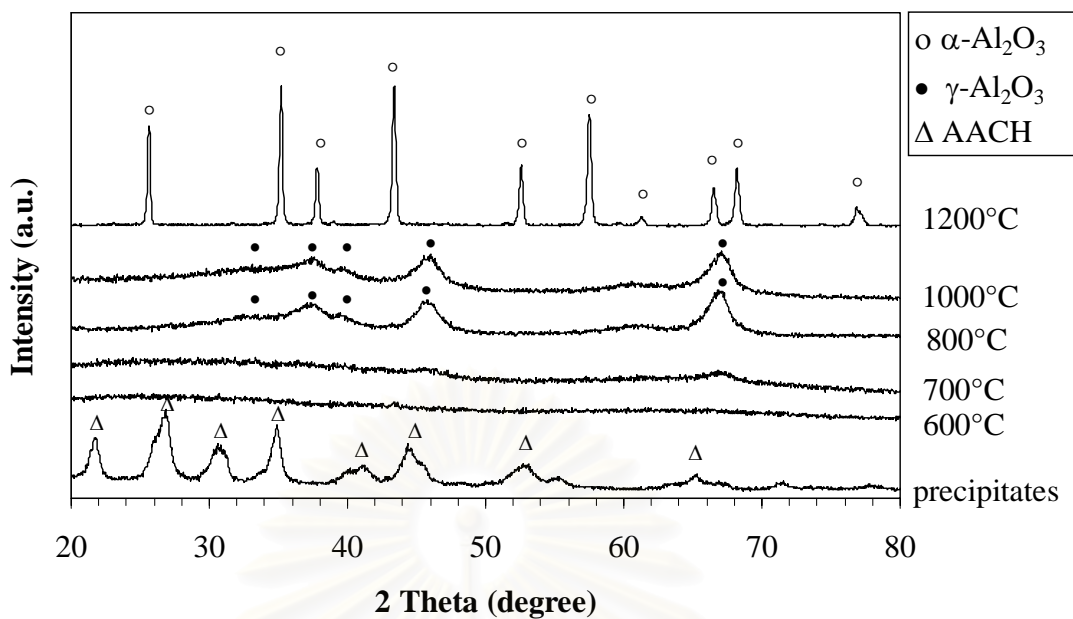


(a)

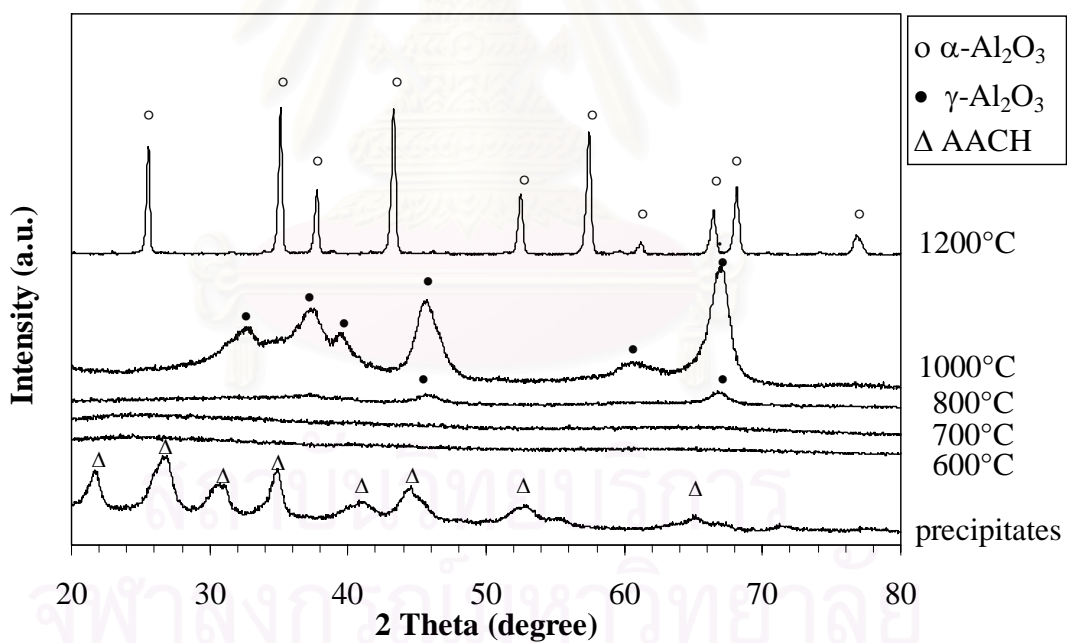


(b)

**Figure 4.31** XRD patterns showing phase transformation of products incorporating both iron-doping and sol-seeding, which were synthesized from: (a) Sol-seeded AAS solution mixed with iron nitrate; (b) AAS solution with iron doped sol.

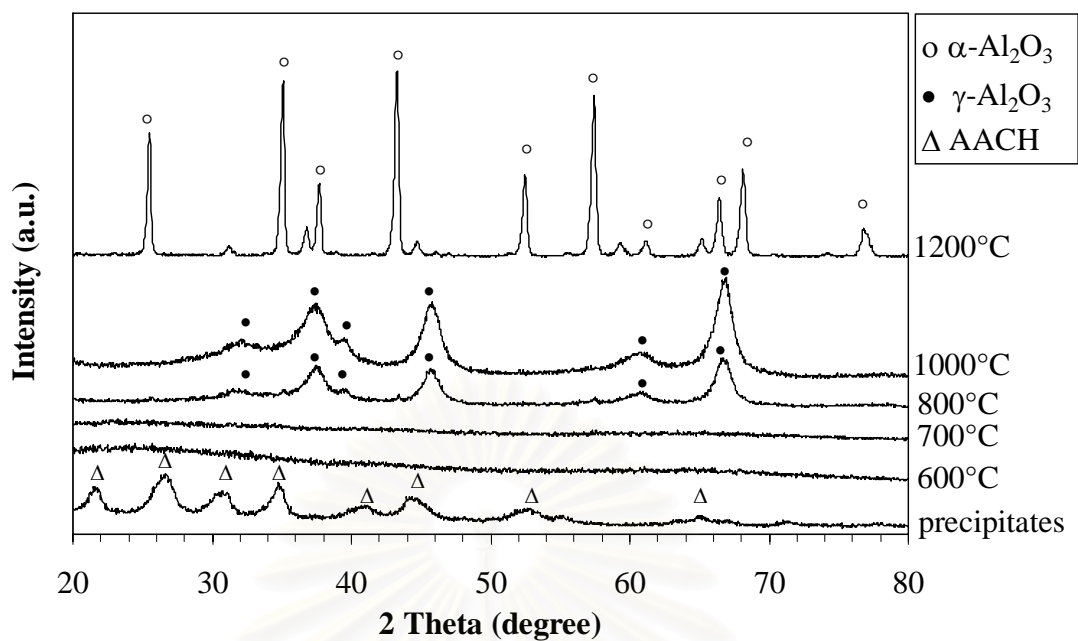


(a)

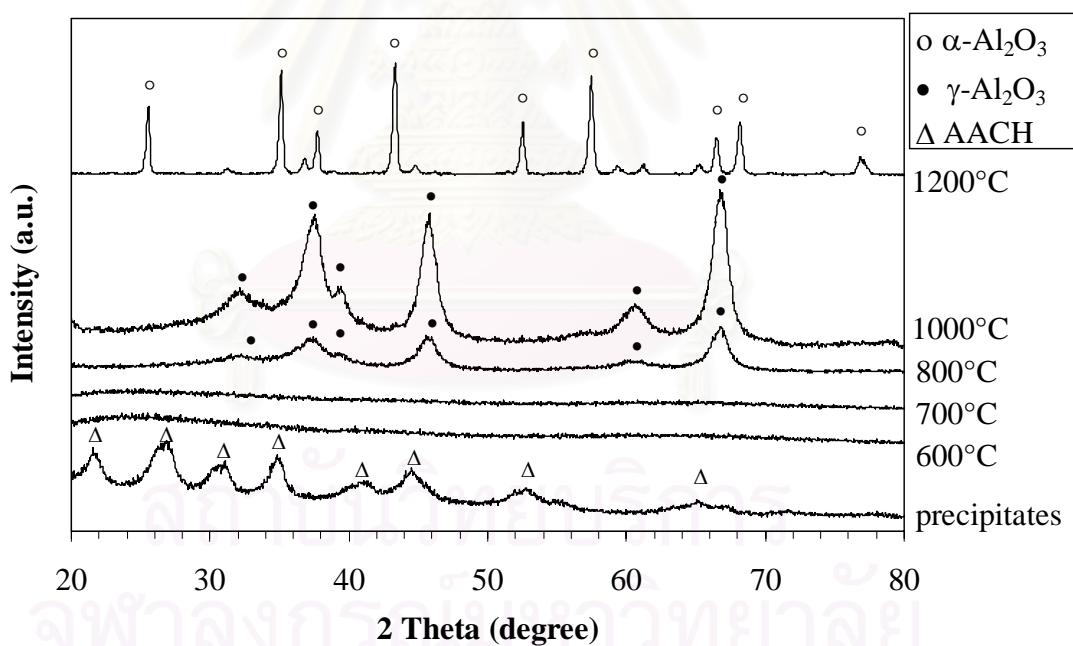


(b)

**Figure 4.32** XRD patterns showing phase transformation of products incorporating both chromium-doping and sol-seeding, which were synthesized from: (a) Sol-seeded AAS solution mixed with chromium nitrate; (b) AAS solution with chromium doped sol.

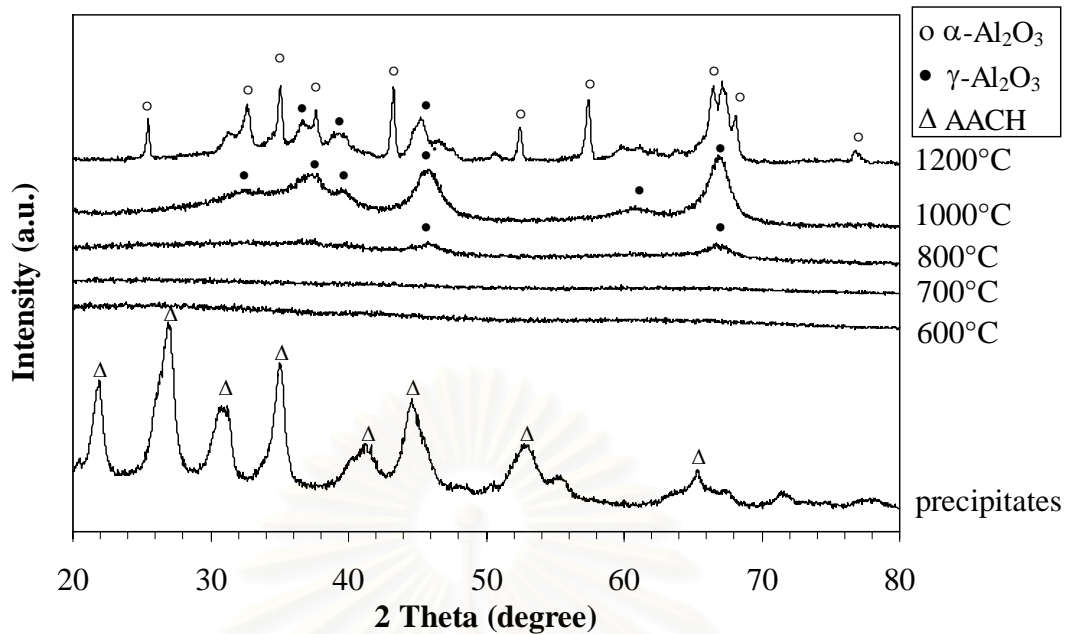


(a)

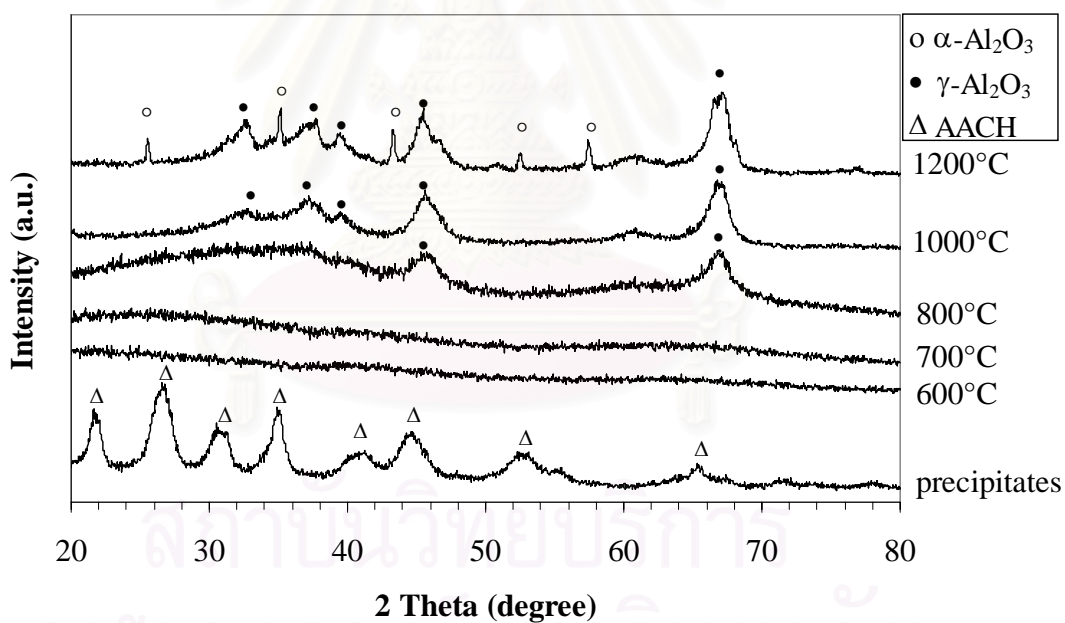


(b)

**Figure 4.33** XRD patterns showing phase transformation of products incorporating both magnesium-doping and sol-seeding, which were synthesized from: (a) Sol-seeded AAS solution mixed with magnesium nitrate; (b) AAS solution with magnesium doped sol.



(a)



(b)

**Figure 4.34** XRD patterns showing phase transformation of products incorporating both yttrium-doping and sol-seeding, which were synthesized from: (a) Sol-seeded AAS solution mixed with yttrium nitrate; (b) AAS solution with yttrium doped sol.

### 4.3 Fabrication of Alumina Powder

Particle size, particle size distribution and state of agglomeration of powder are important factors for fabrication of advanced ceramic. To ensure homogeneity of the starting material, soft agglomerated powders are broken by milling in ball mill to decrease the particle size as well as control the size distribution into narrow range. In this work, the same milling time of 72 h as report literature [112] was selected to applied for undoped, metal-doped and sol-seeded alumina powder. After milling, the powder is fabricated into pellet according to the procedures described in Chapter III. Bulk density and relative density of the sintered specimen fabricated from undoped alumina powder are reported in Table 4.8.

**Table 4.8** Density of sintered alumina specimen.

Sample	Sintered in air at 1300°C		Sintered in air at 1550°C	
	Bulk density (g/cm <sup>3</sup> )	Relative density [%]	Bulk density (g/cm <sup>3</sup> )	Relative density [%]
undoped alumina	3.41	85.7	3.82	95.9
sol-seeded alumina	3.35	84.1	3.73	93.8
0.1%Fe-doped alumina	3.21	80.5	3.69	92.6
0.1%Mg-doped alumina	3.33	83.7	3.72	93.4
0.1%Y-doped alumina	3.45	86.8	3.83	96.3
0.1%Cr-doped alumina	3.19	80.0	3.62	90.6

As shown in Table 4.8, density of sintered specimen is strongly dependent of sintering temperature. Increasing in the sintering temperature results in the increased density of specimen. The density reaches the value higher than 90% theoretical density after sintering at 1550°C in air. It should be noted that the density achieved in this work is relatively low, comparing to that reported in literatures, under same sintering conditions. As previously discussed, all powders synthesized in this work show certain level of agglomeration and presence of large particles, which may results in entrapped pores in the specimen. Among powder synthesized, undoped alumina, sol-seeded alumina and yttrium-doped alumina powders have narrower size

distribution than others. Consequently, the sintered article using these powders has higher density comparing to the others.

Representative SEM micrographs depicting microstructures of the undoped, sol-seeded and metal-doped samples after sintered 2 h at 1550°C are shown in Figure 4.35. The grain structures of all samples show abnormal grain growth, which are the result from various factors such as sintering temperature, particle size distribution of the starting powder and content of sintering additive. The micrographs also reveal lots of isolated pore at triple grain junction. Thus, from this result, it is suggested that abnormal grain growth is generated by character the starting powder, which is mixed between loose and dense agglomeration of fine alumina powder. Fine powder can cause rapid grain growth during the sintering process, while loose packing may result in pores in the specimen. Grain size of the specimen is calculated and show in Table 4.9.

**Table 4.9** Average grain size of sintered specimens

Sample	Average grain size ( $\mu\text{m}$ )
undoped alumina	1.216
sol-seeded alumina	1.490
0.1%Fe-doped alumina	1.074
0.1%Mg-doped alumina	1.152
0.1%Y-doped alumina	1.128
0.1%Cr-doped alumina	1.215

From Table 4.6, grain sizes of the specimens are around 1-1.5  $\mu\text{m}$ . It is found that sol-seeded sample has average grain size significantly larger than other samples. Therefore, it is suggested that sol-seed promotes grain growth. For Fe-doped sample, the additional of Fe is found to inhibit the grain growth. This observation is consistent with the previous finding in the literature [120].



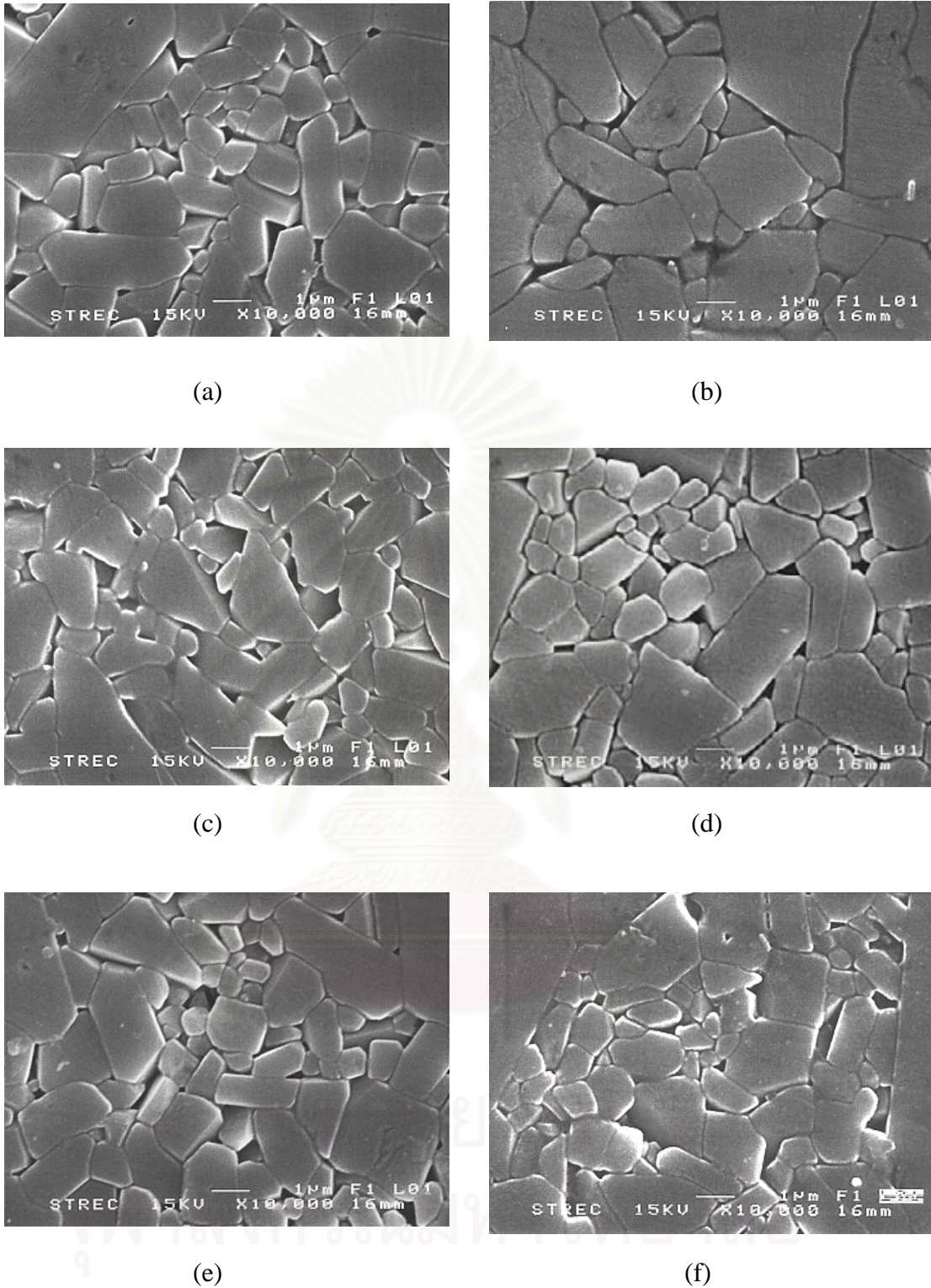


**Figure 4.35** Microstructures of alumina samples sintered for 2 h at 1550°C: (a) undoped alumina, (b) sol-seeded alumina, (c) 0.1 wt.%Cr-doped alumina, (d) 0.1 wt.%Fe-doped alumina, (e) 0.1 wt.%Mg-doped alumina, (f) 0.1 wt.%Y-doped alumina

## CHAPTER V

### CONCLUSIONS AND RECOMMENDATIONS

#### 5.1 Conclusions

In this work, alumina powder is prepared by precipitation method. Effect of doping of various metals and introduction of sol-seed into alumina during preparation procedure on alumina structure and properties are investigated. The conclusions of the study can be drawn as follows:

1. The  $\gamma$ -alumina, a meta-stable phase of alumina, can be stabilized up to 1000°C by the addition small amount of the secondary metal as well as the introduction of alumina sol-seeds to alumina.
2. Metals are co-precipitated with precipitates. The incorporated metal distributes into alumina powder since the calcination at low temperature.
3. Only moderate amount of secondary metal, i.e. less than 0.5 wt.%, can be incorporated into alumina structure by precipitation method. For high content doping, limited amount of metal is incorporated into alumina. The rest of the metal forms oxide compound outside alumina particles.
4. When both alumina sol and metal are incorporated to alumina, phase transformation behavior of the products does not depend upon the incorporation procedure. Moreover, sol-seeding has predominately effect on alumina phase transformation behavior.
5. The additional of Fe is found to inhibit the grain growth during sintering, while alumina sol-seed tends to promote it (relative to the undoped sample). For other metals dopant, it has insignificant effect on the grain size of the sintered alumina article.

## 5.2 Recommendations

1. More characterization techniques such as Rietveld refinement for refining the crystalline structures and XANES spectroscopy for more precise determination of the metal chemical state are required.
2. Sintering conditions should be refined to avoid abnormal grain growth and results in alumina specimen with uniform nanosized grain.
3. The scaling up is recommended to enhance the effectiveness of the production.



สถาบันวิทยบริการ  
จุฬาลงกรณ์มหาวิทยาลัย

## REFERENCES

1. French, R.H., Electronic Band Structure of  $\text{Al}_2\text{O}_3$ , with Comparison to  $\text{AlON}$  and  $\text{AlN}$ . *Journal of the American Ceramic Society*, **73**(3)(1990): 477-489.
2. Scott, W.B. and E. Matijevic, Aluminum hydrous oxide sols : III. Preparation of uniform particles by hydrolysis of aluminum chloride and perchlorate salts. *Journal of Colloid and Interface Science*, **66**(1978): 447.
3. Brinker, C.J. and G.W. Scherer, *Sol-gel science : the physics and chemistry of sol-gel processing*. 1990, Boston: Academic Press. xiv, 908.
4. Dawson, W.H., *Journal of American Ceramic Society Bulletin*, **67**(1998): 1673.
5. Deng, S.G. and Y.S. Lin, Microwave synthesis of mesoporous and microporous alumina powders. *Journal of Materials Science Letters*, **16**(15)(1997): 1291-1294.
6. Sarikaya, Y., I. Sevinc, and M. Akinc, The effect of calcination temperature on some of the adsorptive properties of fine alumina powders obtained by emulsion evaporation technique. *Powder Technology*, **116**(1)(2001): 109-114.
7. Sevinc, I., Y. Sarikaya, and M. Akinc, Adsorption characteristics of alumina powders produced by emulsion evaporation *Ceramic International*, **17**(1991): 1.
8. Inoue, M., H. Kominami, and T. Inui, Thermal Reaction of Aluminum Alkoxide in Glycol. *Journal of the American Ceramic Society*, **73**(1990): 1100-1102.
9. Inoue, M., H. Kominami, and T. Inui, Thermal Reaction of Aluminum Alkoxide in Various Glycols and the Layer Structure of Their Products. *Journal of the Chemical Society, Dalton Transactions*, (1991): 3331-3336.
10. Inoue, M., H. Kominami, and T. Inui, Thermal Transformation of  $\gamma$ - alumina Formed by Thermal Decomposition of Aluminum Alkoxide in organic Media. *Journal of the American Ceramic Society*, **75**(1992): 2597-98.
11. Inoue, M., H. Kominami, and T. Inui, Novel Synthesis Method for The Catalytic Use of Thermally Stable Zirconia: Thermal Decomposition of Zirconium Alkoxide in Organic Media. *Applied Catalysis A-General*, **77**(1993): L25-L30.

12. Inoue, M., H. Kominami, and T. Inui, Novel Synthesis Method for Thermally Stable Monoclinic Zirconia Hydrolysis of Zirconium Alkoxides at High-Temperatures with a Limited Amount of Water Dissolved in Inert Organic-Solvent from the Gas-Phase. *Applied Catalysis A-General*, **121**(1)(1995): L1-L5.
13. Inoue, M., H. Kominami, and T. Inui, Thermal decomposition of alkoxides in an inert organic solvent: Novel method for the synthesis of homogeneous mullite precursor. *Journal of the American Ceramic Society*, **79**(3)(1996): 793-795.
14. Inoue, M., Y. Konko, and T. Inui, Ethylene Glycol Derivative of Boehmite. *Inorganic Chemistry Industry*, **27**(1988): 215-221.
15. Inoue, M., H. Otsu, H. Kominami, and T. Inui, Synthesis of Thermally Stable, Porous Silica-Modified Alumina Via Formation of a Precursor in an Organic Solvent. *Industrial and Engineering Chemistry Research*, **35**(1996): 295-306.
16. Androff, N.W., F. L.F., and V. B.V., Macroporous Ceramics from Ceramic-Polymer Dispersion Methods. *AIChE Journal*, **43**(1997): 2878-2888.
17. Dynys, F.W. and J.W. Hallora, *Journal of American Ceramic Society*, **66**(1983): 655.
18. Hellgardt, K. and D. Chadwick, Effect of pH of Precipitation on the Preparation of High Surface Area Aluminas from Nitrate Solutions. *Industrial and Engineering Chemistry Research*, **37**(1998): 405-411.
19. Hugo, P. and H. Koch, Production of Porous Alumina with Defined Biomodal Pore Structure. *German Chemical Engineering*, **2**(1979): 24-30.
20. Rajendran, S., Production of Ultrafine Alpha-Alumina Powders and Frabrication of Fine-Grained Strong Ceramics. *Journal of Materials Science*, **29**(1994): 5664-5672.
21. Trimm, D.L. and A. Stainslaus, The control of pore size in alumina catalyst supports. *Applied Catalysis A-General*, **21**(1986): 215-238.
22. Ueyama, T., H. Wada, and N. Kaneko, Pulverization and Dispersion Technique for Agglomerated Particles of Alumina Powder in a Slurry. *Journal of American Ceramic Society*, **71**(1988): C-74.
23. Vogel, R., G. Marcellin, and W.L. Kehl, The prepaton of coltrolled pore alumina. *Applied Catalyst*, **12**(1984): 237-248.

24. Cheng, J.P., D. Agrawal, Y.J. Zhang, and R. Roy, Microwave sintering of transparent alumina. *Materials Letters*, **56**(4)(2002): 587-592.
25. Coble, R.L., *Transparent Alumina and Method of Preparation*, in U.S. Patent. 1962.
26. Handwerkwr, C.A., R.M. Cannon, R.H. French, and R.L. Coble, A Retrospective. *Journal of the American Ceramic Society*, **77**(2)(1994): 293-298.
27. Apetz, R. and V. Broggen., Transparent Alumina: A Light-Scattering Model. *Journal of the American Ceramic Society*, **86**(3)(2003): 480-486.
28. Wefers, K. and C. Misra, *Oxides and Hydroxides of Aluminum*, in *Alcoa Technical Paper 1987*, Alcoa Laboratories: Pittsburgh, PA.
29. Gitzen, W.H., *Alumina as a ceramic material*. 1970, Columbus: OH. : The American Ceramic Society. ix, 253.
30. Dynys, F.W. and J.W. Halloran, Alpha alumina Formation in Alum-Derived Gamma Alumina. *Journal of American Ceramic Society*, **65**(1982): 442-448.
31. McArdle, J.L. and G.L. Messing, Transformation Microstructure Development and Densification in Alpha-Fe<sub>2</sub>O<sub>3</sub>-Seeded Boehmite-Derived Alumina. *Journal of American Ceramic Society*, **76**(1993): 214-222.
32. Zielinski, P.A., R. Schulz, S. Kaliaguine, A. Neste, and J. Van, Structural Transformation of Alumina by High-Energy Ball-Milling. *Journal of Materials Research*, **8**(1993): 2985-2992.
33. Ding, J., T. Tsuzuki, and P.G. McCormick, Ultrafine Alumina Particles Prepared by Mechanochemical/Thermal Processing. *Journal of the American Ceramic Society*, **79**(1996): 2956-2958.
34. Djuricic, B., S. Pickering, P. Claude, D. McGarry, and P. Tambuyser, Thermal Stability of Transition Phases in Zirconia-Doped Alumina. *Journal of Materials Science*, **32**(1997): 589-601.
35. Kamiya, K., J. Yotani, R. Senba, J. Matsuoka, and H. Nasu, Sol-gel preparation of alumina gels forming alpha-alumina around 500 degrees C. *Journal of the Ceramic Society of Japan*, **104**(7)(1996): 685-687.
36. Sharma, P.K., M.H. Jilavi, D. Burgard, R. Nass, and H. Schmidt, Hydrothermal synthesis of nanosize alpha-Al<sub>2</sub>O<sub>3</sub> from seeded aluminum

- hydroxide. *Journal of the American Ceramic Society*, **81**(10)(1998): 2732-2734.
37. Tonejc, A., M. Stubicar, A.M. Tonejc, D. Bagovic, and C. Kosanovic, Transformation of Gamma-AlOOH (Boehmite) and Al(OH)<sub>3</sub> (Gibbsite) to Alpha-Al<sub>2</sub>O<sub>3</sub> (Corundum) Induced by High-Energy Ball-Milling. *Materials Science and Engineering*, **1227**(1994): A181-A182.
  38. Yu, Z., Q. Zhao, and Q. Zhang, Effect of Hydrochloric-Acid on The Preparation and Characteristics of Ultrafine Alumina Powder. *Journal of Materials Science Letters*, **14**(1995): 531-532.
  39. Chang, P.L., F.S. Yen, K.C. Cheng, and H.L. Wen, Examinations on the critical and primary crystallite sizes during theta- to alpha-phase transformation of ultrafine alumina powders. *Nano Letters*, **1**(5)(2001): 253-261.
  40. Wen, H.L. and F.S. Yen, Growth characteristics of boehmite-derived ultrafine theta and alpha-alumina particles during phase transformation. *Journal of Crystal Growth*, **208**(1-4)(2000): 696-708.
  41. Morinaga, K., T. Torikai, K. Nakagawa, and S. Fujino, Fabrication of fine alpha-alumina powders by thermal decomposition of ammonium aluminum carbonate hydroxide (AACH). *Acta Materialia*, **48**(18-19)(2000): 4735-4741.
  42. Kumagai, M. and G.L. Messing, Enhanced Densification of Boehmite Sol-Gel by  $\alpha$ -Alumina Seeding. *Journal of the American Chemical Society*, **67**(1984): 230.
  43. Shek, C.H., J.K.L. Lai, T.S. Gu, and G.M. Lin, Transformation evolution and infrared absorption spectra of amorphous and crystalline nano-Al<sub>2</sub>O<sub>3</sub> powders. *Nanostructured Materials*, **8**(5)(1997): 605-610.
  44. Badkar, P.A. and J.E. Bailey, Two-stage densification of ultrafine transition alumina seeded with alpha-phase transition particulates. *Journal of Materials Science*, **11**(1976): 1794-1806.
  45. Jagota, S. and R. Raj, *Journal of Materials Science*, **27**(1992): 2251.
  46. Kumagai, M. and G.L. Messing, Controlled Transformation and Sintering of a Boehmite Sol-Gel by ... Seeding. *Journal of the American Chemical Society* **68**(1985): 500.

47. Chai, M.R., M. Machida, K. Eguchi, and H. Arai, Preparation and Characterization of Sol-Gel Derived Microporous Membranes with High Thermal-Stability. *Journal of Membrane Science*, **96**(3)(1994): 205-212.
48. Long, C., J.J. Richardson, and M. Osawa, Structural phase transformation of rare-earth modified transition alumina to corundum. *Journal of Alloys and Compounds*, **250**(1997): 356-359.
49. Ozawa, M., M. Kimura, and A. Isogai, Thermal Stability and Characterization of Gamma Alumina Modified with Rare Earths. *Journal of The Less-Common Metals*, **162**(1990): 297.
50. Burtin, P., J. Brunelle, M. Pijolat, and M. Soustelle, Influence of surface area and additives on the thermal stability of transition alumina catalyst supports. I : kinetic data. *Applied Catalysis*, **34**(1987): 225-238.
51. Burtin, P., J. Brunelle, M. Pijolat, and M. Soustelle, Influence of surface area and additives on the thermal stability of transition alumina catalyst supports. II : kinetic model and interpretation. *Applied Catalysis*, **34**(1987): 239-254.
52. Lafarga, D., A. Lafuente, M. Menendez, and J. Santamaria, Thermal stability of gamma-alumina/alpha- alumina mesoporous membranes. *Journal of Membrane Science*, **147**(1998): 173-185.
53. Rossignol, S. and C. Kappenstein, Effect of doping elements on the thermal stability of transition alumina. *International Journal of Inorganic Materials*, **3**(1)(2001): 51-58.
54. Levin, I. and D. Brandon, Metastable alumina polymorphs: Crystal structures and transition sequences. *Journal of the American Ceramic Society*, **81**(8)(1998): 1995-2012.
55. Simpson, T.W., Q.Z. Wen, N. Yu, and D.R. Clarke, Kinetics of the amorphous  $\gamma \rightarrow \alpha$  transformations in aluminum oxide: Effect of crystallographic orientation. *Journal of the American Ceramic Society*, **81**(1)(1998): 61-66.
56. Messing, G.L. and M. Kumagai, Low-Temperature Sintering of Alpha-Alumina-Seeded Boehmite Gel. *American Ceramic Society Bulletin*, **73**(10)(1994): 88-91.



57. Urretavizcaya, G., A.L. Cavalieri, J.M.P. Lopez, I. Sobrados, and J. Sanz, Thermal evolution of alumina prepared by the sol-gel technique. *Journal of Materials Synthesis and Processing*, **6**(1)(1998): 1-7.
58. Seabaugh, M.M., I.H. Kerscht, and G.L. Messing, Texture development by templated grain growth in liquid-phase-sintered alpha-alumina. *Journal of the American Ceramic Society*, **80**(5)(1997): 1181-1188.
59. Yoshizawa, Y., M. Toriyama, and S. Kanzaki, Preparation of high fracture toughness alumina sintered bodies from bayer aluminum hydroxide. *Journal of the Ceramic Society of Japan*, **106**(12)(1998): 1172-1177.
60. Baca, L., J. Plewa, L. Pach, and J. Opfermann, Kinetic analysis crystallization of alpha-Al<sub>2</sub>O<sub>3</sub> by dynamic DTA technique. *Journal of Thermal Analysis and Calorimetry*, **66**(3)(2001): 803-813.
61. Kumar, K.N.P., J. Tranto, J. Kumar, and J.E. Engell, Pore-structure stability and phase transformation in pure and M-doped (M=La, Ce, Nd, Gd, Cu, Fe) alumina membranes and catalyst supports. *Journal of Materials Science Letters*, **15**(3)(1996): 266-270.
62. Xia., Z.P., J.W. Lu., Y. Huang., and Y.B. Cheng., Influence of different seeds on transformation of aluminum hydroxides and morphology of alumina grains by hot-pressing. *Materials & Design*, **24**(2003): 209-214.
63. Xia., Z.P., J.W. Lu., Y. Huang., and Y.B. Cheng., Influence of alpha-alumina seed on the morphology of grain growth in alumina ceramics from Bayer aluminum hydroxide. *Materials Letters*, **57**(2003): 2501-2508.
64. Ogihara, T., H. Nakajima, T. Yanagawa, N. Ogata, and K. Yoshida, Preparation of Monodisperse, Spherical Alumina Powders from Alkoxides. *Journal of American Ceramic Society*, **74**(1991): 2263-2269.
65. Youn, H.J., J.W. Jang, I.T. Kim, and K.S. Hong, Low-temperature formation of alpha-alumina by doping of an alumina-sol. *Journal of Colloid and Interface Science*, **211**(1)(1999): 110-113.
66. Lippens, B.C. and J.J. Steggerde, *Physical and Chemical Aspects of Adsorbent and Catalysts*. 1970, New York: Academic Press.
67. Stumpf, H.C., A.S. Russell, J.W. Newsome, and C.M. Tucker, Thermal Transformation of Aluminas and Alumina Hydrates. *Industrial and Engineering Chemistry*, **42**(7)(1950): 1398-1403.

68. Megaw, H.D., *Crystal Structures : A Working Approach*. 1973, Saunders, Philadelphia, London, Toronto.
69. Corbato, C.E., R.T. Tettenhorst, and G.G. Christoph, Structure Refinement of Deuterated Boehmite. *Clays and Clay Minerals*, **33**(1)(1985): 71-75.
70. Yamaguchi, G. and M. Okumiya, Refinement of the Structure of Tohdite ( $5\text{Al}_2\text{O}_3 \cdot \text{H}_2\text{O}$ ). *Bulletin of the Chemical Society of Japan*, **42**(1969): 2247-2249.
71. Yamaguchi, G., H. Yanagida, and S. Ono, New Alumina Hydrate, Tohdite ( $5\text{Al}_2\text{O}_3 \cdot \text{H}_2\text{O}$ ). *Bulletin of the Chemical Society of Japan*, **37**(1964): 1555-1557.
72. El-Mashri, S.M., R.G. Jones, and A.J. Forty, An Electron-Yield EXAFS Study of Anodic Oxide and Hydrated Oxide Films on Pure Aluminum. *Philosophical Magazine A*, **48**(1983): 665.
73. Bourdillon, A.J., S.M. El-Mashri, and A.J. Forty, Application of TEM Extended Electron Energy Loss Fine Structure to the study of Aluminum Oxide Films. *Philosophical Magazine A*, **49**(3)(1984): 341.
74. Bendersky, L.A., A. Roytburd, and W.J. Boettinger, Phase-Transformations in the (Ti,Al)<sub>3</sub>Nb Section of the Ti-Al-Nb System .1. Microstructural Predictions Based on a Subgroup Relation between Phases. *Acta Metallurgica Et Materialia*, **42**(7)(1994): 2323-2335.
75. Waseda, Y., K. Sugiyama, and J.M. Toguri, Direct Determination of the Local Structure in Molten Alumina by High-Temperature X-ray Diffraction. *Zeitschrift fur Naturforschung A: Journal of Physical Sciences*, **50**(8)(1995): 770-774.
76. Lippens, B.D. and J.H.D. Boer, Study of phase transformations during calcination of aluminum hydroxides by selected area electron diffraction. *Acta Crystallographica*, **17**(1964): 1312.
77. Wilson, S.J., Phase transformations and development of microstructure in-derived transition aluminas. *Proceedings of the British Ceramic Society*, **28**(1979): 281-94.
78. Perego, C. and P.L. Villa. *The catalytic process from laboratory to the industrial plant. in: D. SanFilippo (Ed.). in Proceedings of the 3rd Seminar on Catalysis*. 1994. Rimini, Italy: Italian Chemical Society.

79. Nagai, H., Y. Oshima, K. Hirano, and A. Kato, Sintering Behavior of Aluminum-Oxides Derived from Aluminum Hydroxides with Various Morphologies. *British Ceramic Transactions*, **92**(3)(1993): 114-119.
80. Sarikaya, Y. and M. Akinc, Preparation of Alumina Microshells by the emulsion Evaporation Technique. *Ceramic International*, **14**(4)(1988): 239-244.
81. Inoue, M., H. Kominami, and T. Inui, Thermal Decomposition of alkoxides in an inert organic solvent : nevel method for the synthesis of homogeneous mullite precursor. *Journal of the American Ceramic Society*, **75**(1996): 2597-98.
82. Inoue, M., H. Otsu, H. Kominami, and T. Inui, Synthesis of Thermally Stable, Porous Silica-Modified Alumina Via Formation of a Precursor in an Organic Solvent. *Industrial and Engineering Chemistry Research*, **35**(1996): 295-306.
83. P.-, L., Hen and J.-W. Chen, Reactive Cerium (IV) Oxidase Powders by the Homogeneous Precipitation Method. *Journal of the American Ceramic Society*, **76**(1993): 1577.
84. Ertl, G., H. Knozinger, and J. Weitkamp, *Preparation of Solid Catalysts*. 1997: Wiley-VCH.
85. Prasitwuttisak, T., V. Pavarajarn, and P. Praserthdam. *Comparative study of Nanosclaed Alumina and Chromium Doped Alumina Powder Prepared from Various Synthesis Techniques*. in *Proceedings of the Regional Symposium on Chemical Engineering 2004*. 2004. Bangkok, Thailand.
86. Shuzo, K., I. Takeo, H. Shogo, and I. Yuichi, *Method for manufacture of sintered alumina from ammonium aluminum carbonate hydroxide*, in *U.S. Patent* 1975.
87. Dörre, E. and H. Hübner, *Alumina : processing, properties, and applications*. 1984, Berlin ; New York: Springer-Verlag. xiii, 329 p.
88. Smith, F., *Principles of materials science and engineering*. 2 ed, ed. c. 1990. 1996, New York: McGraw-Hill. xiii, 864.
89. Brophy, J.H., R.M. Rose, and J. Wulff, *The structure and Properties of Materials*. Thermodynamics of structure. Vol. 2. 1964: Wiley. 139.

90. Wong, B. and J.A. Pask, Experimental Analysis of Sintering of MgO Compacts. *Journal of the American Ceramic Society*, **62**(3-4)(1979): 141-146.
91. Hughes, R.W., *Ruby & Sapphire*. 1997, RWH Publishing.
92. Fritsch, E. and G.R. Rossman, *An update on color in gems. Gems & Gemology ; Part I : Introduction and colors caused by dispersed metal ions. 23, No.3: 126-139; Part II : Colors involving multiple atoms and color centers. 24 No.1: 3-15; Part III : Colors caused by band gaps and physical phenomena. 24 No.2: 81-103.* 1987, 1988: RWHL.
93. Schmetzer, K., Zur deutung der farbursache blauer Saphire-Einc discussion. *Neues Jahrbuch fur Mineralogie. Monatshefte*, **8**: 337-343.
94. Ferguson, J.C. and P.E. Fielding, The origins of the colours of natural yellow, blue and green sapphires. *Australian Journal of Chemistry*, **25**(1972): 1371-1385.
95. Emmett, J.L. and T.R. Douthit, Heat treating the sapphire of Rockl Creek, Montana. *Gems & Gemology*, **29**(1993): 250-272.
96. Nassau, K. and K. Valente, The seven types of yellow sapphire and their stability to light. *Gems & Gemology*, **23**(1987): 222-231.
97. Koivula, J.I., Internal diffusion. *Journal of Gemmology*, **20**(1987): 474-477.
98. Nassau, K., *Gems made by man*. 1980, Radnor, Pa: Chilton Book Co. xviii, 364.
99. Schmetzer, K. and H. Bank, Explanation of the absorption spectra of natural and synthetic Fe- and Ti- containing corundums. *Neues Jahrbuch fur Mineralogie*, **139**(1980): 216-225.
100. Weibel, M. and R. Wessicken, Hamatit als Einschluss im schwarzen Sternsaphir. *Zeitschrift der Deutschen Gemmologischen Gesellschaft*, **30**(1981): 170-176.
101. Webster, R., *GEMS Their sources, Descriptions and identification*, ed. f. edition. 1994.
102. Fremy, E. and E. Feil, *Compt. rend.*, **85**(1877): 1029.
103. Ballman, A.A., *Method of Growing Corundum Crystals*, in U.S. 1961.
104. Lopez-Navarrete, E., A.R. Gonzalez-Elipse, and M. Ocana, Non-conventional synthesis of Cr-doped SnO<sub>2</sub> pigments. *Ceramics International*, **29**(4)(2003): 385-392.

105. Lopez-Navarrete, E. and M. Ocana, A simple procedure for the preparation of Cr-doped tin sphene pigments in the absence of fluxes. *Journal of the European Ceramic Society*, **22**(2002): 353-359.
106. Lopez-Navarrete, E., A. Caballero, A.R. Gonzalez-Elipe, and M. Ocana, Low-temperature preparation and structural characterization of Pr-doped ceria solid solutions. *Journal of Materials Research*, **17**(4)(2002): 797-804.
107. Lopez-Navarrete, E., A. Caballero, A.R. Gonzalez-Elipe, and M. Ocana, Chemical state and distribution of Mn ions in Mn-doped alpha-Al<sub>2</sub>O<sub>3</sub> solid solutions prepared in the absence and the presence of fluxes. *Journal of the European Ceramic Society*, **24**(10-11)(2004): 3057-3062.
108. Li, J., Y. Pan, C. Xiang, Q. Ge, and J. Guo, Low temperature synthesis of ultrafine alpha-alumina powder by a simple aqueous sol-gel process. *Ceramics International*, (2005).
109. Munoz, R., R. Fornos, Y. Bellmunt, H. Beltran, A. Barrio, and E. Cordoncillo, *Environmental Problem of Chromium-Containing Ceramic Pigments: Optimisation of their Synthesis*. 2002, Qualicer, Spain. 159-174.
110. Iler, R.K., *Fabrillar Colloidal Boehmite; Progressive Conversion to Gamma, Theta, and Alpha-Alumina*. *Journal of American Ceramic Society*, **44**(1961): 618.
111. Mekasuwandumrong, O., P. Prasertdam, M. Inoue, V. Pavarajarn, and W. Tanakulrungsank, Phase transformation behavior of nanocrystalline chi-alumina powder obtained by thermal decomposition of AIP in inert organic solvent. *Journal of Materials Science*, **39**(7)(2004): 2417-2421.
112. Prasitwuttisak, T., *Comparative study of alumina powder synthesis techniques to the physical and optical properties of colored alumina ceramics*, in *Department of Chemical Engineering*. 2004, Chulalongkorn University: Bangkok. p. 104.
113. Peretti, A., FGG, FGA, and E. Geol., in *GRS Gemresearch Swissslab AG: P.O.Box 4028, 6002 Lucerne, Switzerland*.
114. González-Calbet, J.M., M.A. Alario-Franco, and M. Gayoso-Andrade, The porous structure of synthetic akaganeite. *Journal of Inorganic and Nuclear Chemistry*, **43**(1981): 257-264.

115. Yen-Pei, F., S. Tsaob, and H. Chen-Ti, Preparation of  $Y_3Al_5O_{12}:Cr$  powders by microwave-induced combustion process and their luminescent properties. *Journal of Alloys and Compounds*, **395**(2005): 227-230.
116. Music, S., M. Maljkovic, S. Popovic, and R. Trojko, Formation of Chromia from Amorphous Chromium Hydroxide. *Croatica Chemica Acta*, **72**(4)(1999): 789-802.
117. Hongxia Lu, Hongwei Sun, Aixia Mao, Huizhi Yang, Hailong Wang, and X. Hu, Preparation of plate-like nano  $\gamma$ - $Al_2O_3$  using nano-aluminum seeds by wet-chemical methods. *Materials Science and Engineering A*, **406**(2005): 19-23.
118. Lo'pez-Navarrete, E., A. Caballero, A.R. Gonza'lez-Elipse, and M. Ocan' a, Chemical state and distribution of Mn ions in Mn-doped  $\alpha$ - $Al_2O_3$  solid solutions prepared in the absence and the presence of fluxes. *Journal of the European Ceramic Society*, **24**(2004): 3057-3062.
119. Norton, F.H., *Fine ceramics: Technology and Applications*. 1970, New York: Mcgraw-Hill Inc.
120. Drahus, M.D., H.M. Chan, J.M. Rickman, and M.P. Harmer, Densification and Grain Growth of Fe-Doped and Fe/Y Codoped Alumina: Effect of Fe Valency. *Journal of American Ceramic Society*, **88**(12)(2005): 3369-3373.



**APPENDICES**

สถาบันวิทยบริการ  
จุฬาลงกรณ์มหาวิทยาลัย

## APPENDIX A

### CALCULATION OF CONCENTRATION OF BOTH REACTANTS

In this study, ammonium aluminum carbonate hydroxide ( $\text{NH}_4\text{AlCO}_3(\text{OH})_2$ ) has been produced by the reaction of ammonium aluminum sulfate solution (AAS solution) and ammonium hydrogencarbonate solution (AHC solution) as following equation :



Ammonium aluminum carbonate hydroxide(AACH) was prepared with the molar ratio of AAS solution to AHC solution equal to 1:4 as the above reaction and calculation procedure is given here.

#### **Calculation of the amount of ammonium hydrogencarbonate (AHC) and ammonium aluminum sulfate (AAS) for AACH preparation**

Ammonium aluminum sulfate (AAS) and ammonium hydrogencarbonate (AHC) are used as reactants to prepare AACH.

1. Ammonium aluminum sulfate ( $\text{NH}_4\text{Al}(\text{SO}_4)_2 \cdot 12\text{H}_2\text{O}$ ) has an molecular weight of 237.18 g/mol (not included molecule of water)
2. Ammonium hydrogencarbonate ( $\text{NH}_4\text{HCO}_3$ ) has an molecular weight of 79.06 g/mol.



**Example :** Calculation of AACH preparation with concentration of AAS solution to AHC solution equal to 0.5 : 2.0 mol/l and molar ratio of AAS solution to AHC solution is 0.05 : 0.2 , which is equal to 1 : 4 as mentioned before, are as following :

AAS solution 0.05 mol consists of :

$$\text{AAS } 0.05 \times 237.18 = 11.859 \text{ g}$$

To get concentration 0.5 mol/l

$$\text{Distilled water} = 100 \text{ cm}^3$$

AHC solution 0.2 mol consists of :

$$\text{AHC } 0.2 \times 79.06 = 15.812 \text{ g}$$

To get concentration 2.0 mol/l

$$\text{Distilled water} = 100 \text{ cm}^3$$



สถาบันวิทยบริการ  
จุฬาลงกรณ์มหาวิทยาลัย

## APPENDIX B

### CALCULATION OF AMOUNT OF METAL PRECURSOR FOR METAL-DOPED ALUMINA

For precipitation method and sol-seeding, nitrate salt of iron, chromium, yttrium or magnesium were used as secondary metal which incorporated into solution.

Reagents : Ammonium aluminum sulfate ( $\text{NH}_4\text{Al}(\text{SO}_4)_2 \cdot 12\text{H}_2\text{O}$ )

Molecular weight = 237.18 g/mol

(not included molecule of water)

Aluminium nitrate nonahydrate ( $\text{Al}(\text{NO}_3)_3 \cdot 9\text{H}_2\text{O}$ )

Molecular weight = 212.98 g/mol

Precursors : Chromium (III) nitrate nonahydrate ( $\text{Cr}(\text{NO}_3)_3 \cdot 9\text{H}_2\text{O}$ )

Molecular weight = 238 g/mol

( not include molecule of water)

Ferric (III) nitrate nonahydrate ( $\text{Fe}(\text{NO}_3)_3 \cdot 9\text{H}_2\text{O}$ )

Molecular weight = 242 g/mol

( not include molecule of water)

Magnesium (II) nitrate hexahydrate ( $\text{Mg}(\text{NO}_3)_2 \cdot 6\text{H}_2\text{O}$ )

Molecular weight = 148 g/mol

( not include molecule of water)

Yttrium (III) nitrate hexahydrate ( $\text{Y}(\text{NO}_3)_3 \cdot 6\text{H}_2\text{O}$ )

Molecular weight = 275 g/mol

( not include molecule of water)

**Calculation :****Precipitation method****Example :** For 0.1% Metal precursor/Aluminium precursor

From Appendix A, concentration of solution I to solution II equal to 0.5 : 2.0 mol/l and molar ratio of solution I to solution II is 0.05 : 0.2, then AAS 11.859 g was required.

- For 0.1% Chromium precursor/Aluminium precursor

$$\text{Chromium} = (0.1/100) \times 11.859 = 1.1859 \times 10^{-2} \text{ g} = 2.2806 \times 10^{-4} \text{ mol}$$

used chromium (III) nitrate nonahydrate equal to :

$$\begin{aligned} \text{Chromium (III) nitrate nonahydrate} &= (238/52) \times 1.1859 \times 10^{-2} \\ &= 5.4278 \times 10^{-2} \text{ g} \end{aligned}$$

AAS 11.859 g consisted of aluminium equal to :

$$\text{Aluminium} = (26.98/237.18) \times 11.859 = 1.349 \text{ g} = 0.05 \text{ mol}$$

$$\begin{aligned} \text{The mol ratio of Cr/Al} &= 2.2806 \times 10^{-4} / 0.05 = 4.5612 \times 10^{-3} \\ &= 0.45 \text{ mol \% Cr/Al} \end{aligned}$$

- For 0.1% Ferric precursor/Aluminium precursor

$$\text{Ferric} = (0.1/100) \times 11.859 = 1.1859 \times 10^{-2} \text{ g} = 2.1177 \times 10^{-4} \text{ mol}$$

used ferric (III) nitrate nonahydrate equal to :

$$\begin{aligned} \text{Ferric (III) nitrate nonahydrate} &= (242/56) \times 1.1859 \times 10^{-2} \\ &= 5.1248 \times 10^{-2} \text{ g} \end{aligned}$$

AAS 11.859 g consisted of aluminium equal to :

$$\text{Aluminium} = (26.98/237.18) \times 11.859 = 1.349 \text{ g} = 0.05 \text{ mol}$$

$$\begin{aligned} \text{The mol ratio of Cr/Al} &= 2.1177 \times 10^{-4} / 0.05 = 4.2354 \times 10^{-3} \\ &= 0.42 \text{ mol \% Fe/Al} \end{aligned}$$

- For 0.1% Magnesium precursor/Aluminium precursor

$$\text{Magnesium} = (0.1/100) \times 11.859 = 1.1859 \times 10^{-2} \text{ g} = 4.9413 \times 10^{-4} \text{ mol}$$

used magnesium (II) nitrate nonahydrate equal to :

$$\begin{aligned} \text{Magnesium (II) nitrate hexahydrate} &= (148/24) \times 1.1859 \times 10^{-2} \\ &= 7.3131 \times 10^{-2} \text{ g} \end{aligned}$$

AAS 11.859 g consisted of aluminium equal to :

$$\text{Aluminium} = (26.98/237.18) \times 11.859 = 1.349 \text{ g} = 0.05 \text{ mol}$$

$$\begin{aligned} \text{The mol ratio of Cr/Al} &= 4.9413 \times 10^{-4} / 0.05 = 4.9828 \times 10^{-3} \\ &= 1.0 \text{ mol \% Mg/Al} \end{aligned}$$

- For 0.1% Yttrium precursor/Aluminium precursor

$$\text{Yttrium} = (0.1/100) \times 11.859 = 1.1859 \times 10^{-2} \text{ g} = 1.3325 \times 10^{-4} \text{ mol}$$

used yttrium (III) nitrate nonahydrate equal to :

$$\begin{aligned} \text{Yttrium (III) nitrate hexahydrate} &= (275/89) \times 1.1859 \times 10^{-2} \\ &= 3.6643 \times 10^{-2} \text{ g} \end{aligned}$$

AAS 11.859 g consisted of aluminium equal to :

$$\text{Aluminium} = (26.98/237.18) \times 11.859 = 1.349 \text{ g} = 0.05 \text{ mol}$$

$$\begin{aligned} \text{The mol ratio of Cr/Al} &= 1.3325 \times 10^{-4} / 0.05 = 2.6649 \times 10^{-3} \\ &= 0.27 \text{ mol \% Y/Al} \end{aligned}$$

### ***Sol-seeding***

For sol-seeding, 24.0729 g of Aluminium nitrate nonahydrate was used as aluminium precursor.

- For 0.5% Chromium precursor/Aluminium precursor

$$\begin{aligned} \text{Chromium} &= (0.5 / 100) \times 11.859 = 5.9295 \times 10^{-2} \text{ g} = 1.1402 \times 10^{-3} \text{ mol} \\ &\text{in 10 ml of alumina sol (0.1113 mol/l).} \end{aligned}$$

$$\begin{aligned} \text{Chromium} &= (0.1140 \times 50)/1000 = 5.7014 \times 10^{-3} \text{ mol} = 2.9647 \times 10^{-1} \text{ g} \\ &\text{in 50 ml of alumina sol.} \end{aligned}$$

used chromium (III) nitrate nonahydrate equal to :

$$\begin{aligned} \text{Chromium (III) nitrate nonahydrate} &= (238/52) \times 2.9647 \times 10^{-1} \\ &= 1.356 \text{ g} \end{aligned}$$

- For 0.5% Ferric precursor/Aluminium precursor

$$\begin{aligned} \text{Ferric} &= (0.5/100) \times 11.859 = 5.9295 \times 10^{-2} \text{ g} = 1.0588 \times 10^{-3} \text{ mol} \\ &\text{in 10 ml of alumina sol (0.1058 mol/l).} \end{aligned}$$

$$\begin{aligned} \text{Ferric} &= (0.1058 \times 50)/1000 = 5.2941 \times 10^{-2} \text{ mol} = 2.9647 \times 10^{-1} \text{ g} \\ &\text{in 50 ml of alumina sol.} \end{aligned}$$

used ferric (III) nitrate nonahydrate equal to :

$$\begin{aligned}\text{Ferric (III) nitrate nonahydrate} &= (242/56) \times 2.9647 \times 10^{-1} \\ &= 1.2811 \text{ g}\end{aligned}$$

- For 0.5% Magnesium precursor/Aluminium precursor

Magnesium =  $(0.5/100) \times 11.859 = 5.9295 \times 10^{-2} \text{ g} = 2.4706 \times 10^{-3} \text{ mol}$   
in 10 ml of alumina sol (0.2470 mol/l).

Magnesium =  $(0.2470 \times 50)/1000 = 1.2353 \times 10^{-2} \text{ mol} = 2.9647 \times 10^{-1} \text{ g}$   
in 50 ml of alumina sol.

used magnesium (III) nitrate nonahydrate equal to :

$$\begin{aligned}\text{Magnesium (II) nitrate hexahydrate} &= (148/24) \times 2.9647 \times 10^{-1} \\ &= 1.8282 \text{ g}\end{aligned}$$

- For 0.5% Yttrium precursor/Aluminium precursor

Yttrium =  $(0.5/100) \times 11.859 = 5.9295 \times 10^{-2} \text{ g} = 6.6623 \times 10^{-4} \text{ mol}$   
in 10 ml of alumina sol (0.0666 mol/l).

Yttrium =  $(0.0666 \times 50)/1000 = 3.3311 \times 10^{-3} \text{ mol} = 2.9647 \times 10^{-1} \text{ g}$   
in 50 ml of alumina sol.

used yttrium (III) nitrate nonahydrate equal to :

$$\begin{aligned}\text{Yttrium (III) nitrate hexahydrate} &= (275/89) \times 2.9647 \times 10^{-1} \\ &= 0.9160 \text{ g}\end{aligned}$$

สถาบันวิทยบริการ  
จุฬาลงกรณ์มหาวิทยาลัย

## APPENDIX C

### CALCULATION OF THE CRYSTALLITE SIZE

#### Calculation of the crystallite size by Debye-Scherrer equation

The crystallite size was calculated from the half-height width of the diffraction peak of XRD pattern using the Debye-Scherrer equation.

From Scherrer equation:

$$D = \frac{K\lambda}{\beta \cos \theta} \quad (\text{C.1})$$

where  $D$  = Crystallite size, Å  
 $K$  = Crystallite-shape factor = 0.9  
 $\lambda$  = X-ray wavelength, 1.5418 Å for CuK $\alpha$   
 $\theta$  = Observed peak angle, degree  
 $\beta$  = X-ray diffraction broadening, radian

The X-ray diffraction broadening ( $\beta$ ) is the pure width of a powder diffraction free from all broadening due to the experimental equipment.  $\alpha$ -Alumina is used as a standard sample to observe the instrumental broadening since its crystallite size is larger than 2000 Å. The X-ray diffraction broadening ( $\beta$ ) can be obtained by using Warren's formula.

From Warren's formula:

$$\beta = \sqrt{B_M^2 - B_S^2} \quad (\text{C.2})$$

Where  $B_M$  = The measured peak width in radians at half peak height.  
 $B_S$  = The corresponding width of the standard material.

**Example:** Calculation of the crystallite size of  $\alpha$ -alumina

$$\begin{aligned}
 \text{The half-height width of 012 diffraction peak} &= 0.25^\circ \text{ (from the figure C.1)} \\
 &= \left( \frac{2\pi}{360} \right) \cdot (0.26) \\
 &= 0.0045 \text{ radian}
 \end{aligned}$$

The corresponding half-height width of peak of  $\alpha$ -alumina (from the  $B_s$  value at the  $2\theta$  of  $25.88^\circ$  in figure C.2) = 0.0038 radian

$$\begin{aligned}
 \text{The pure width, } \beta &= \sqrt{B_M^2 - B_S^2} \\
 &= \sqrt{0.0045^2 - 0.0038^2} \\
 &= 0.0024 \text{ radian}
 \end{aligned}$$

$$B = 0.0024 \text{ radian}$$

$$2\theta = 25.88^\circ$$

$$\theta = 12.94$$

$$\lambda = 1.5418 \text{ \AA}$$

$$\text{The crystallite size} = \frac{0.9 \times 1.5418}{0.0024 \cos 12.94} = 590 \text{ \AA} = 59 \text{ nm}$$

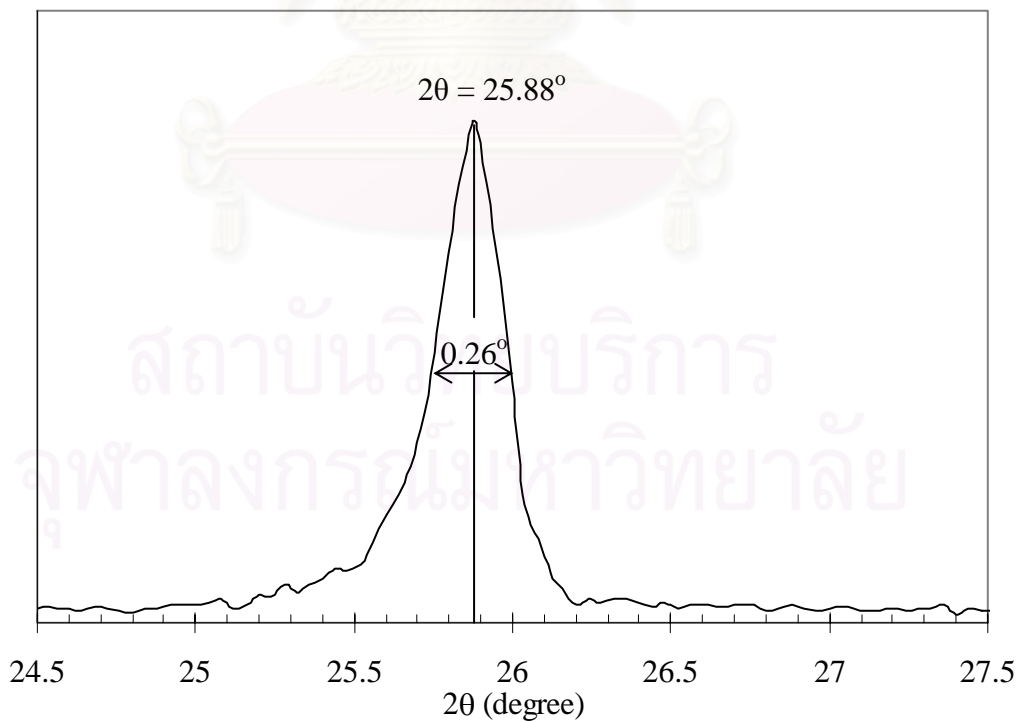


**Figure C.1** The observation peak of  $\alpha$ -alumina for calculating the crystallite size.

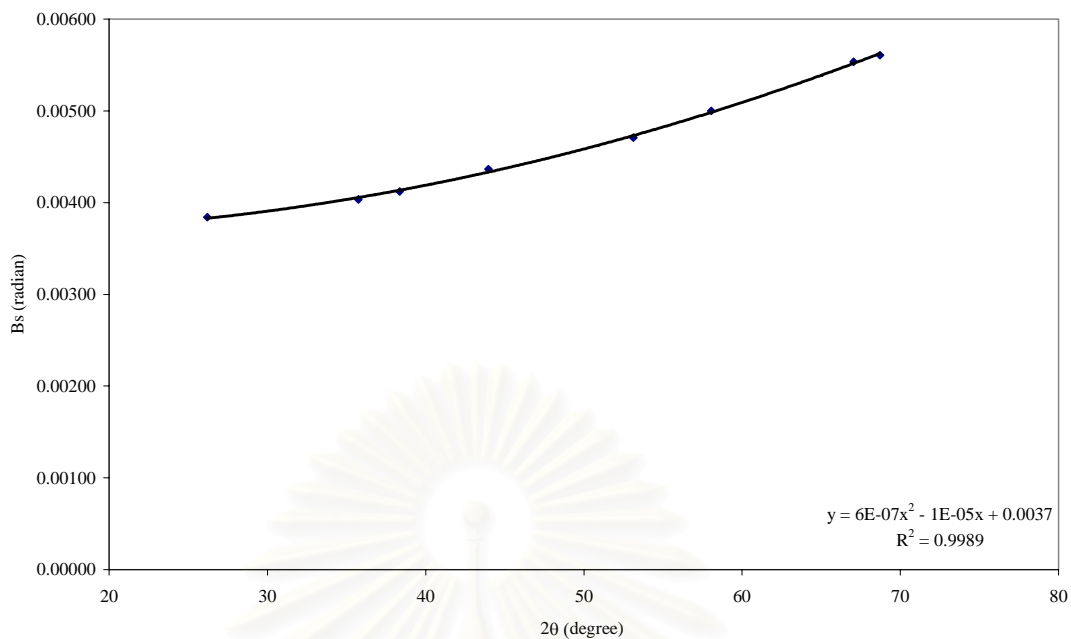


**Figure C.2** The graph indicating that value of the line broadening attribute to the experimental equipment from the  $\alpha$ -alumina standard.

สถาบันวิทยบริการ  
จุฬาลงกรณ์มหาวิทยาลัย



## APPENDIX D

### PHASE TRANSFORMATION BEHAVIOR OF PRODUCTS CALCINED AT VARIOUS TEMPERATURE

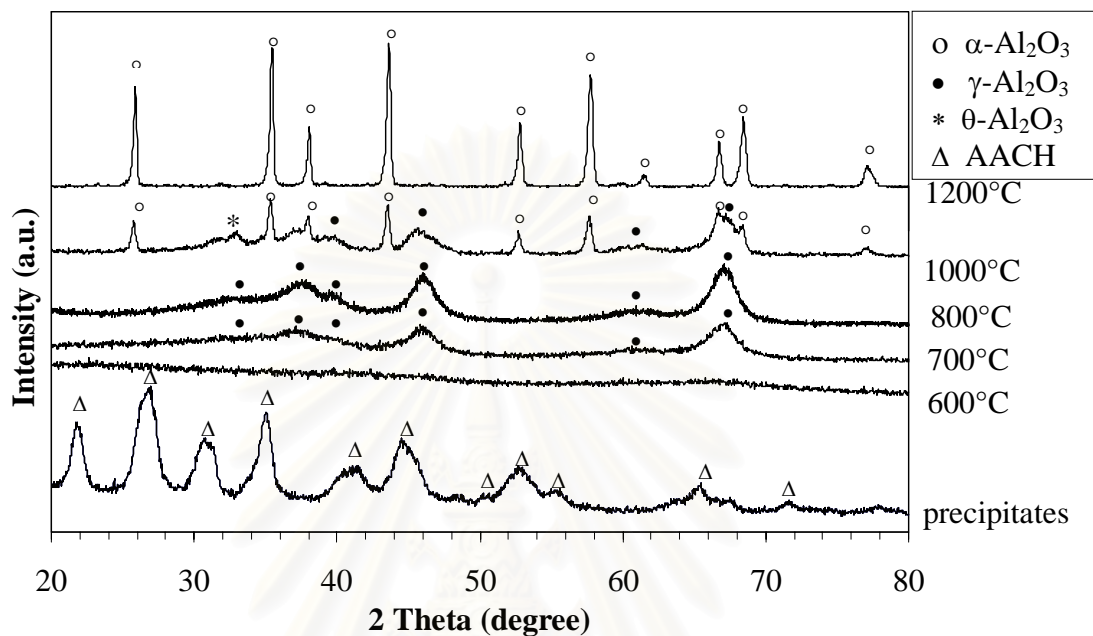


**Figure D.1** XRD patterns of undoped product calcined at various temperatures.

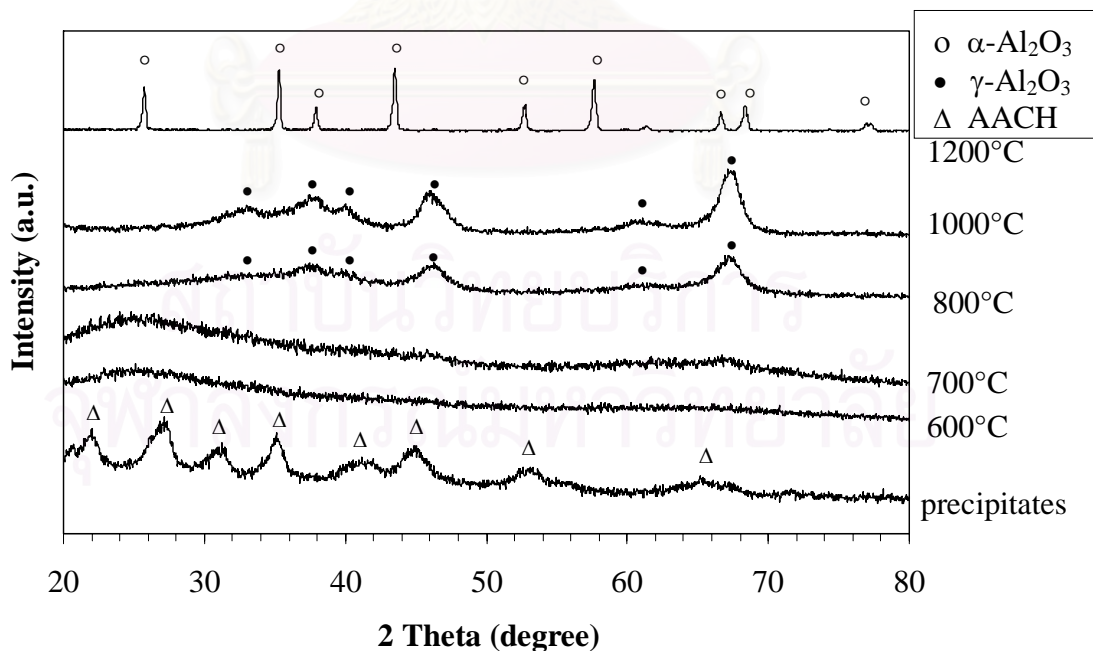


**Figure D.2** XRD patterns of the product synthesized by precipitation accompanied by sol-seeding and calcined at various temperatures.

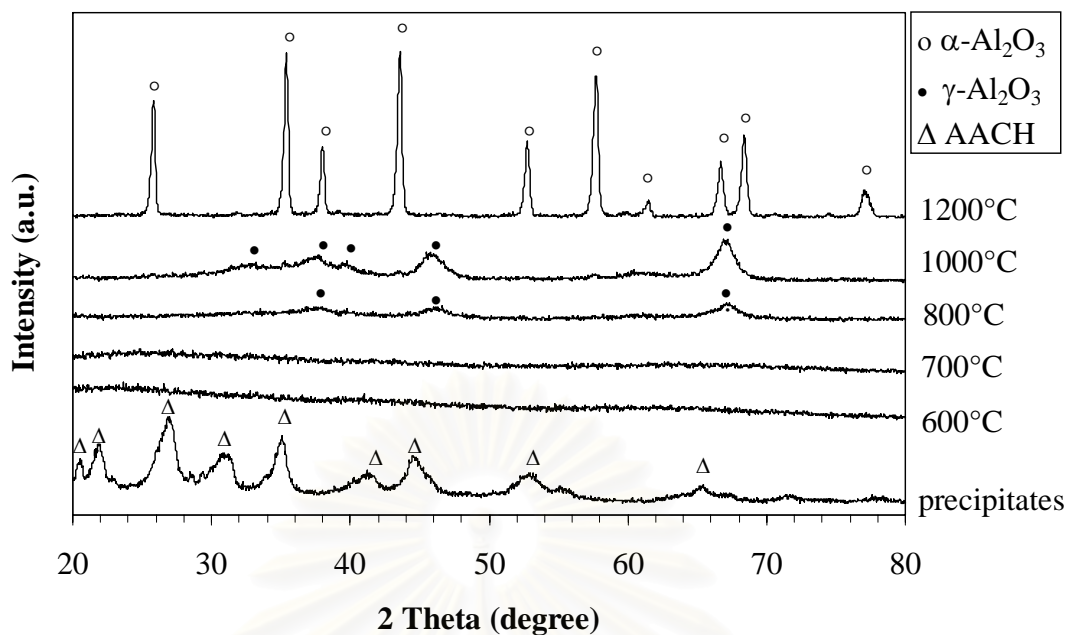


**Figure D.3** XRD patterns of the precipitate and products calcined at various temperatures, which were obtained from precipitation accompanied by iron at 0.1 wt.%

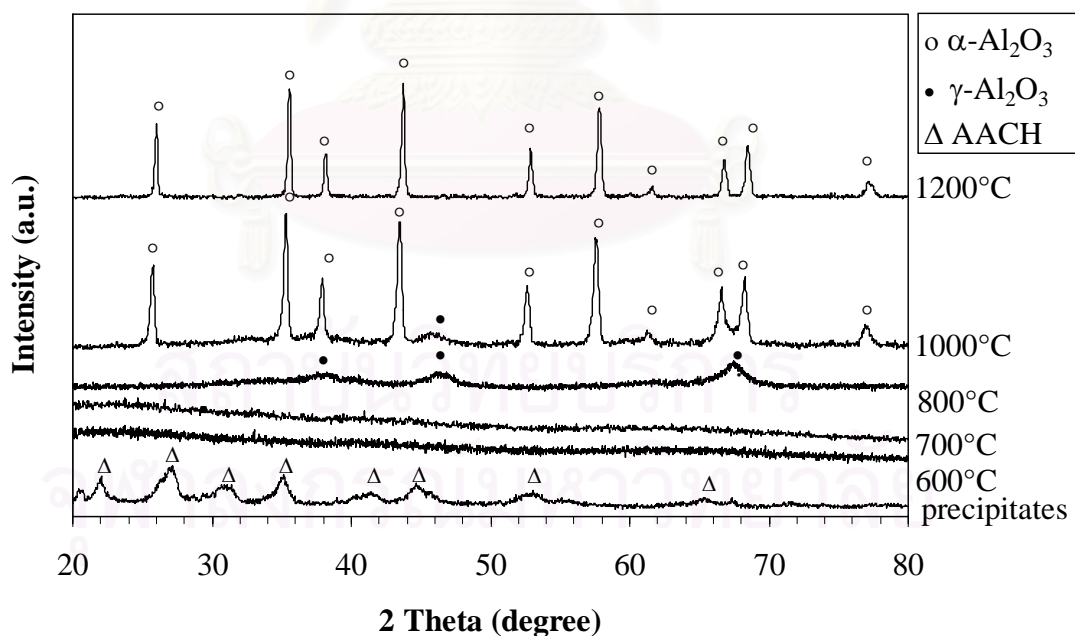


**Figure D.4** XRD patterns of the precipitate and products calcined at various temperatures, which were obtained from precipitation accompanied by iron at 0.5 wt.%

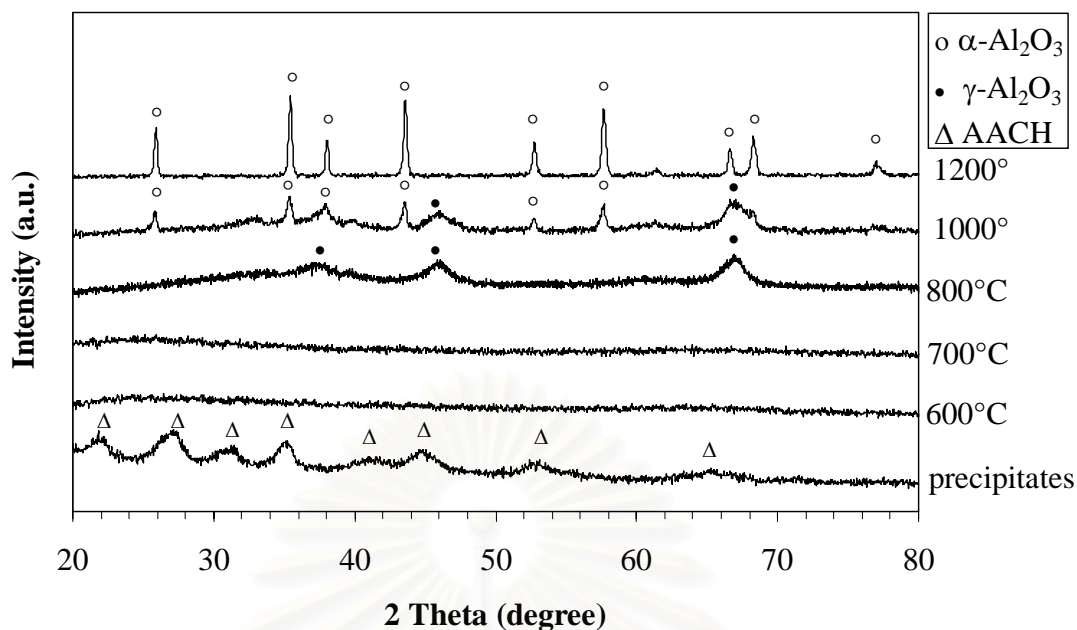


**Figure D.5** XRD patterns of the precipitate and products calcined at various temperatures, which were obtained from precipitation accompanied by iron at 1.0 wt.%

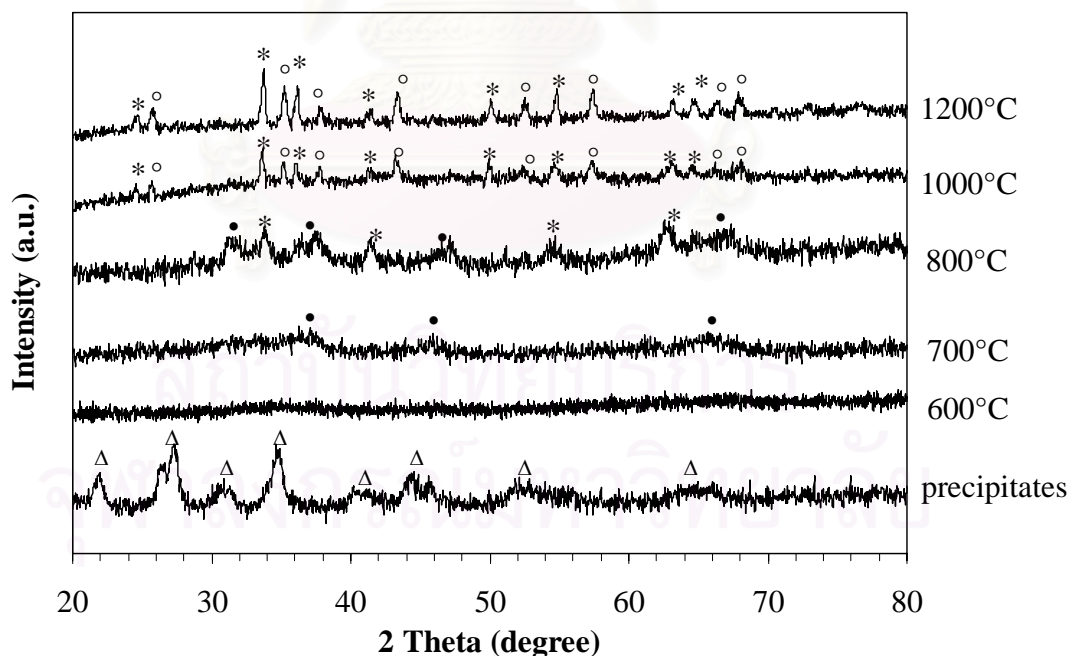


**Figure D.6** XRD patterns of products calcined at various temperatures, which were obtained from precipitation accompanied by iron at 10 wt.%.  
(o  $\alpha$ -Al<sub>2</sub>O<sub>3</sub>, •  $\gamma$ -Al<sub>2</sub>O<sub>3</sub>, \* Fe<sub>2</sub>O<sub>3</sub>, Δ AACH).

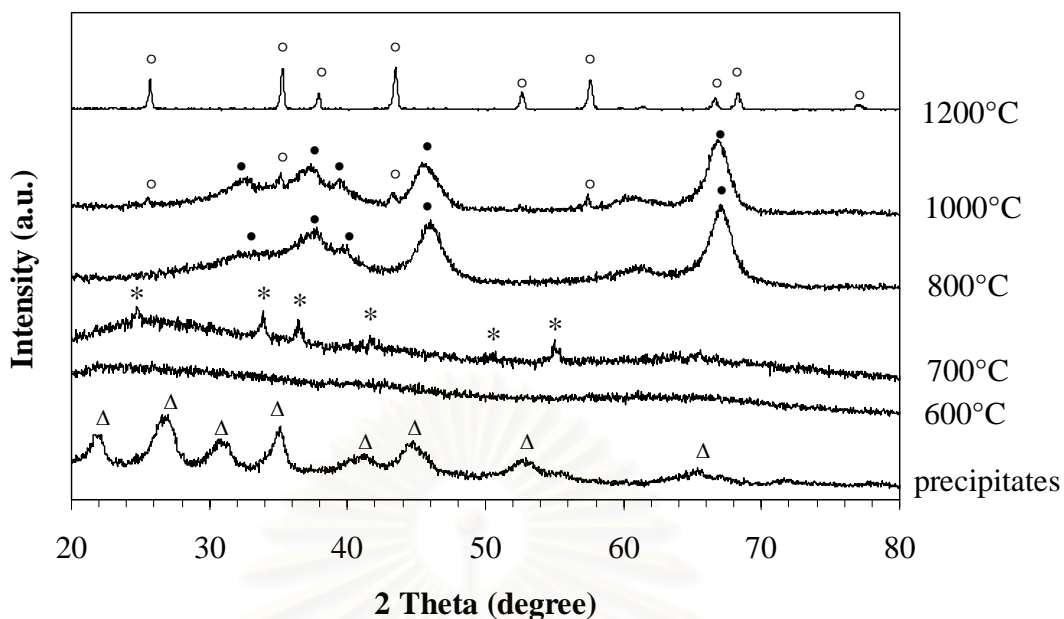


**Figure D.7** XRD patterns of the precipitate and products calcined at various temperatures, which were obtained from precipitation accompanied by chromium at 0.1 wt.%. (o  $\alpha$ -Al<sub>2</sub>O<sub>3</sub>, •  $\gamma$ -Al<sub>2</sub>O<sub>3</sub>, \* Cr<sub>2</sub>O<sub>3</sub>,  $\Delta$  AACH).

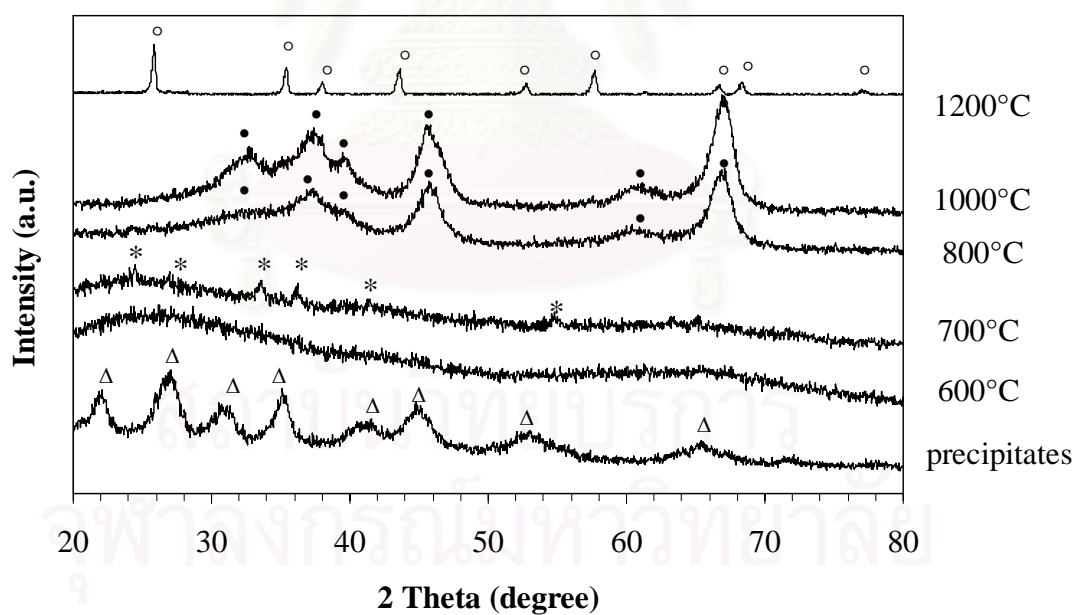


**Figure D.8** XRD patterns of the precipitate and products calcined at various temperatures, which were obtained from precipitation accompanied by chromium at 0.5 wt.%. (o  $\alpha$ -Al<sub>2</sub>O<sub>3</sub>, •  $\gamma$ -Al<sub>2</sub>O<sub>3</sub>, \* Cr<sub>2</sub>O<sub>3</sub>,  $\Delta$  AACH).

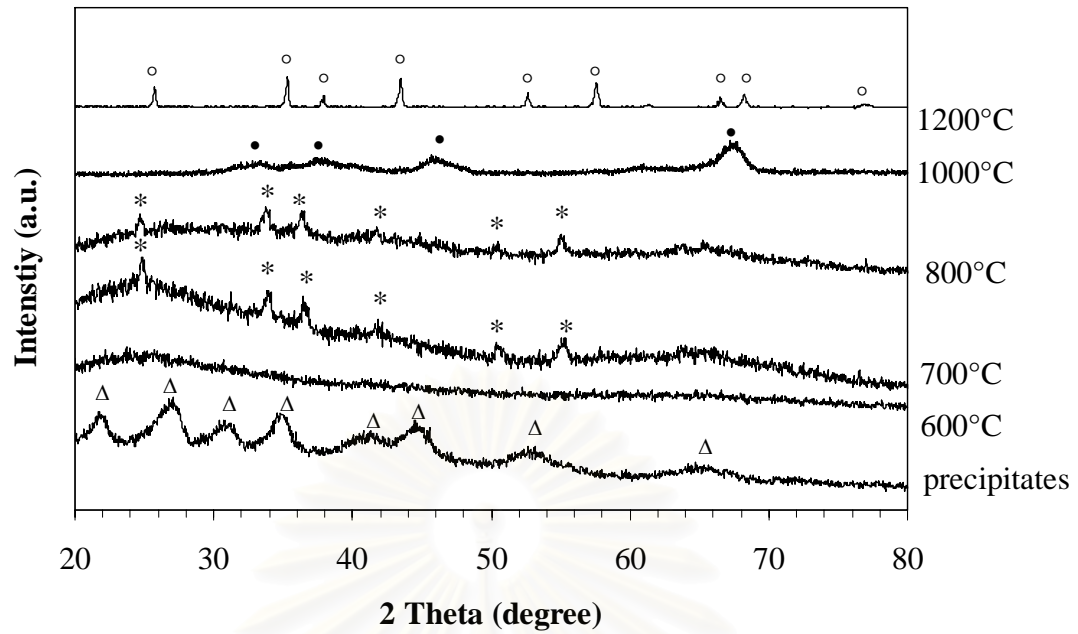


**Figure D.9** XRD patterns of the precipitate and products calcined at various temperatures, which were obtained from precipitation accompanied by chromium at 1.0 wt.%: (○  $\alpha$ -Al<sub>2</sub>O<sub>3</sub>, ●  $\gamma$ -Al<sub>2</sub>O<sub>3</sub>, \* Cr<sub>2</sub>O<sub>3</sub>, Δ AACH).

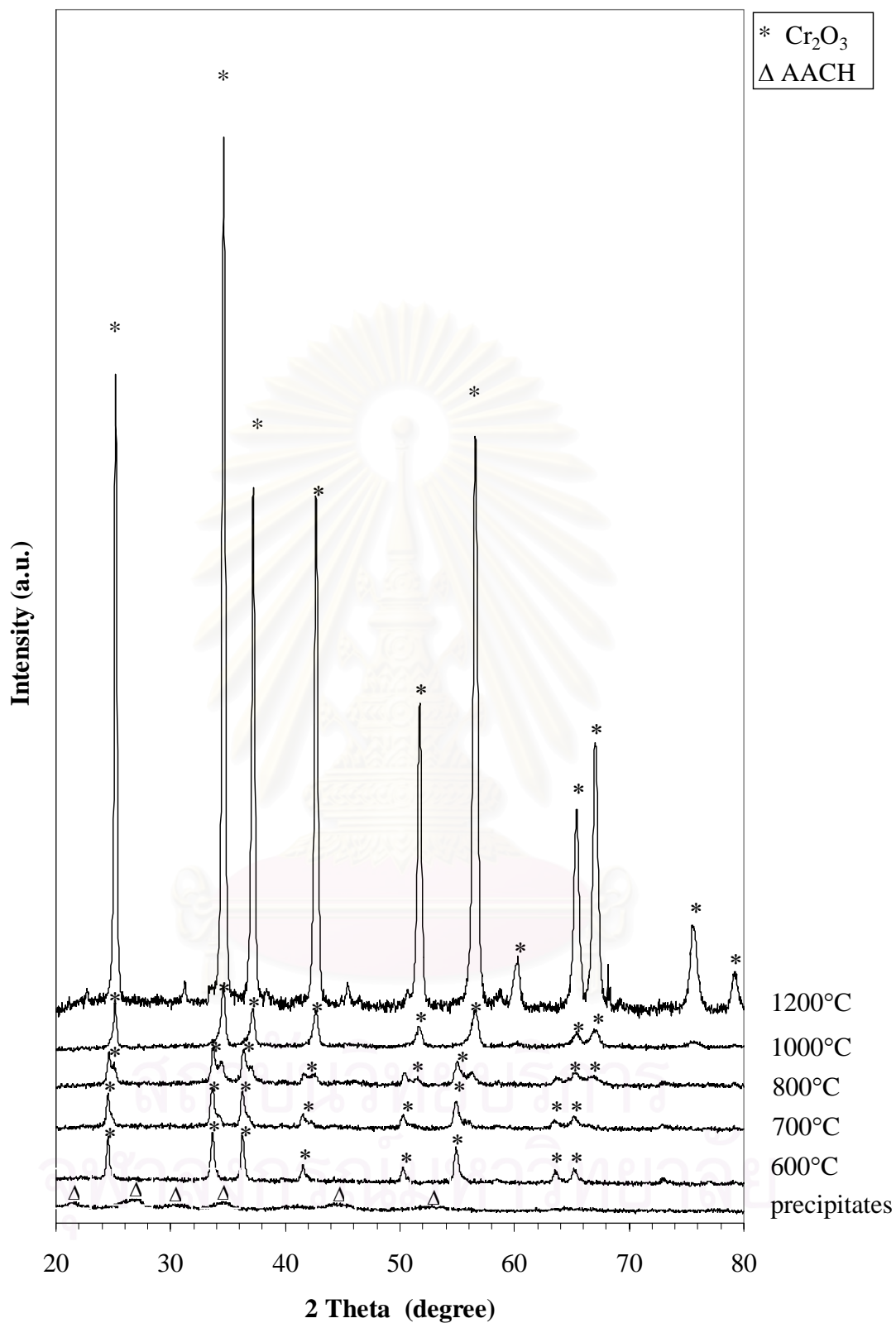


**Figure D.10** XRD patterns of products calcined at various temperatures, which were obtained from precipitation accompanied by chromium at 10 wt.%

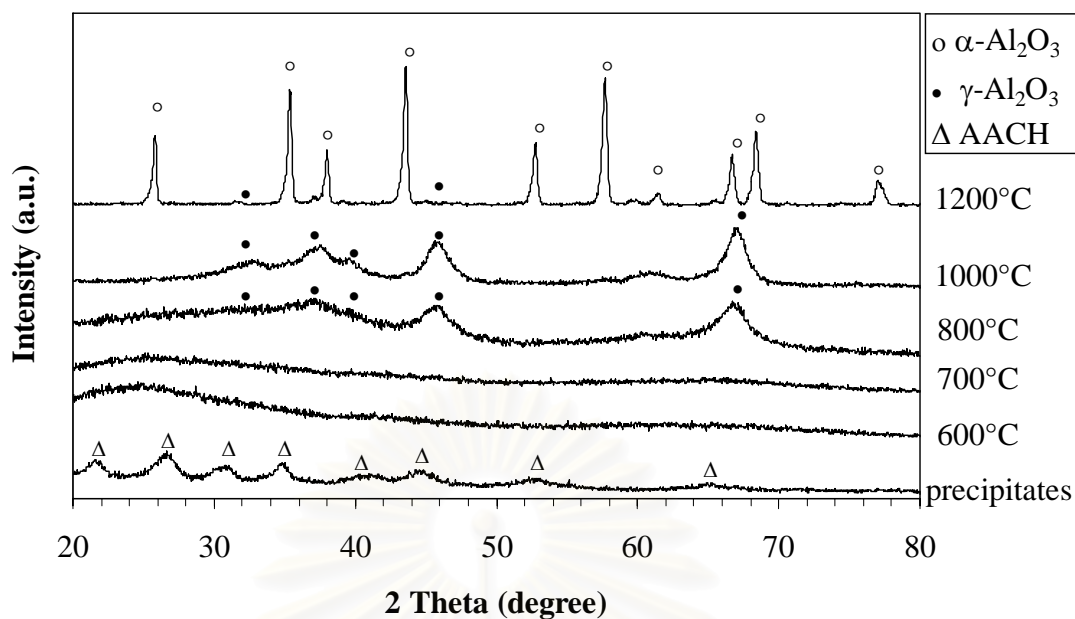


**Figure D.11** XRD patterns of the precipitate and products calcined at various temperatures, which were obtained from precipitation accompanied by magnesium at 0.1 wt.%.

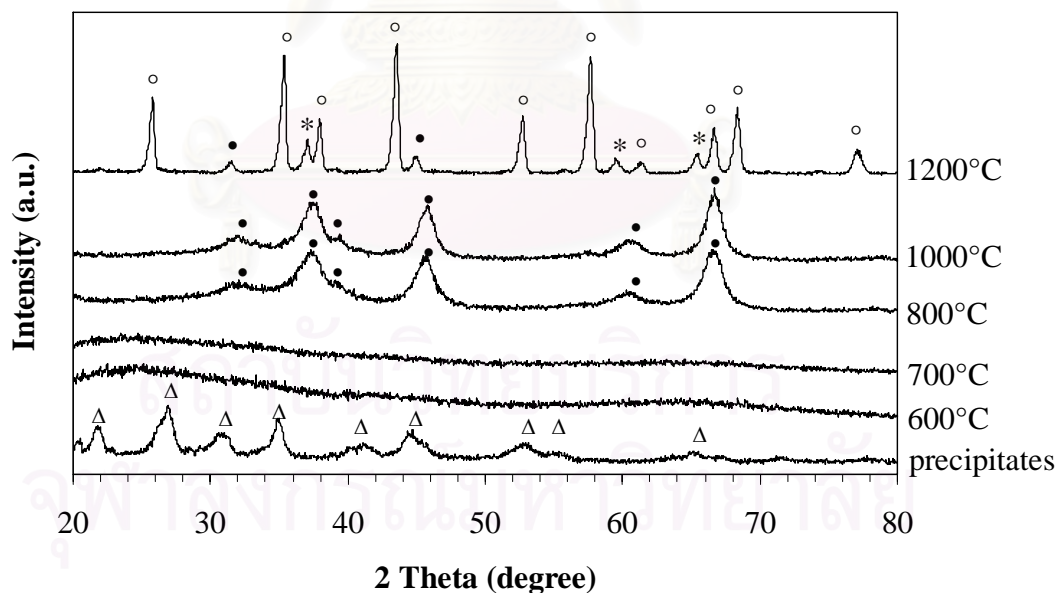


**Figure D.12** XRD patterns of the precipitate and products calcined at various temperatures, which were obtained from precipitation accompanied by magnesium at 0.5 wt.%: (o  $\alpha$ - $\text{Al}_2\text{O}_3$ , •  $\gamma$ - $\text{Al}_2\text{O}_3$ , \* unidentified phase,  $\Delta$  AACH).

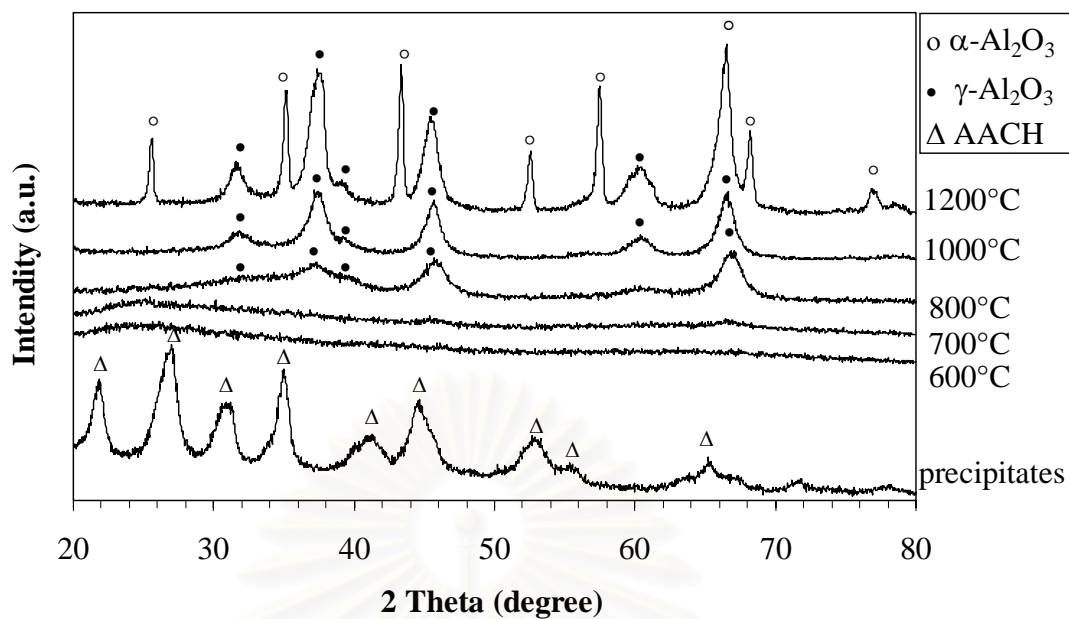


**Figure D.13** XRD patterns of the precipitate and products calcined at various temperatures, which were obtained from precipitation accompanied by magnesium at 1.0 wt.%.

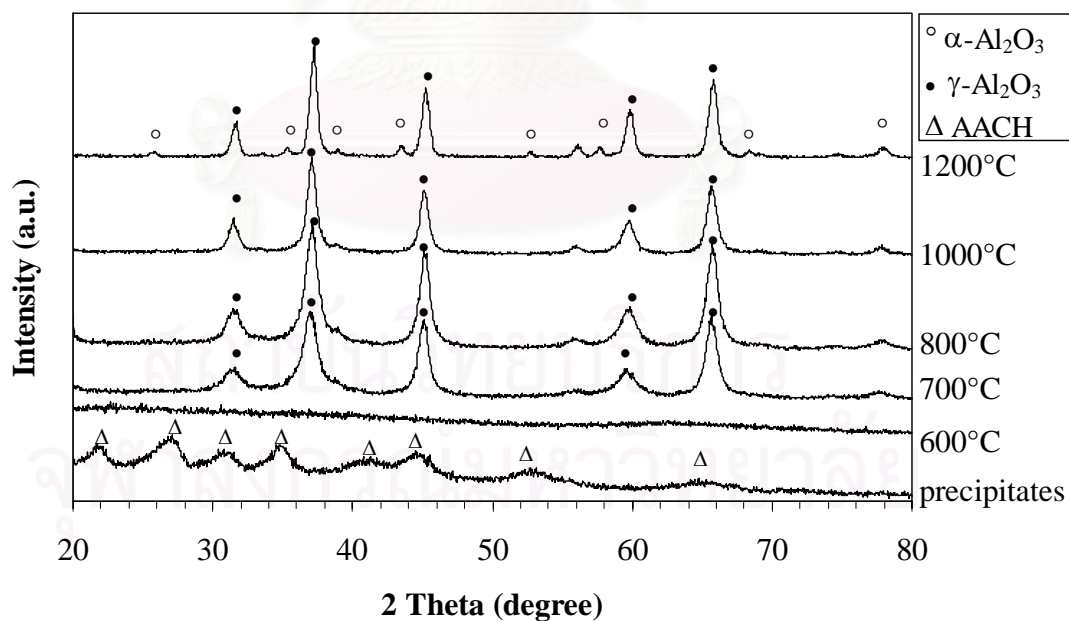


**Figure D.14** XRD patterns of products calcined at various temperatures, which were obtained from precipitation accompanied by magnesium at 10 wt.%.



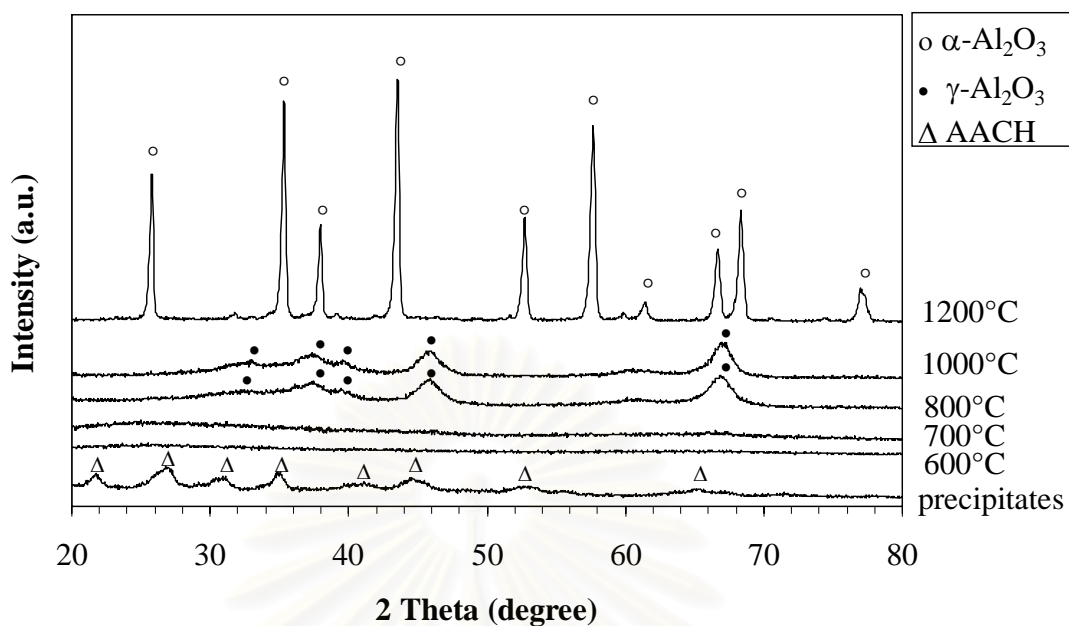


**Figure D.15** XRD patterns of the precipitate and products calcined at various temperatures, which were obtained from precipitation accompanied by yttrium at 0.1 wt.%

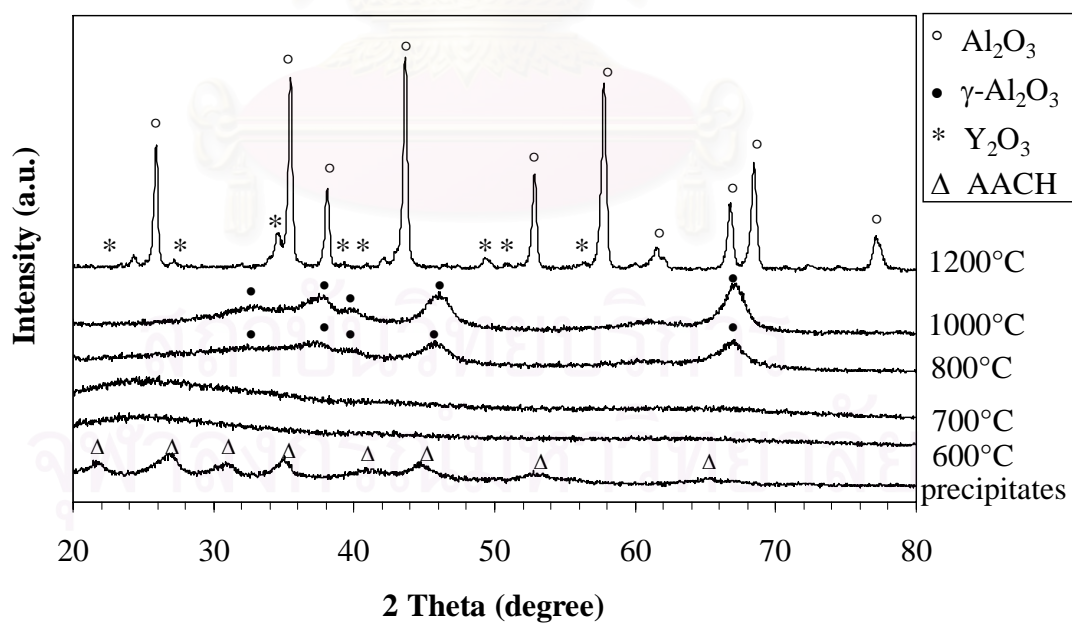


**Figure D.16** XRD patterns of the precipitate and products calcined at various temperatures, which were obtained from precipitation accompanied by yttrium at 0.5 wt.%.

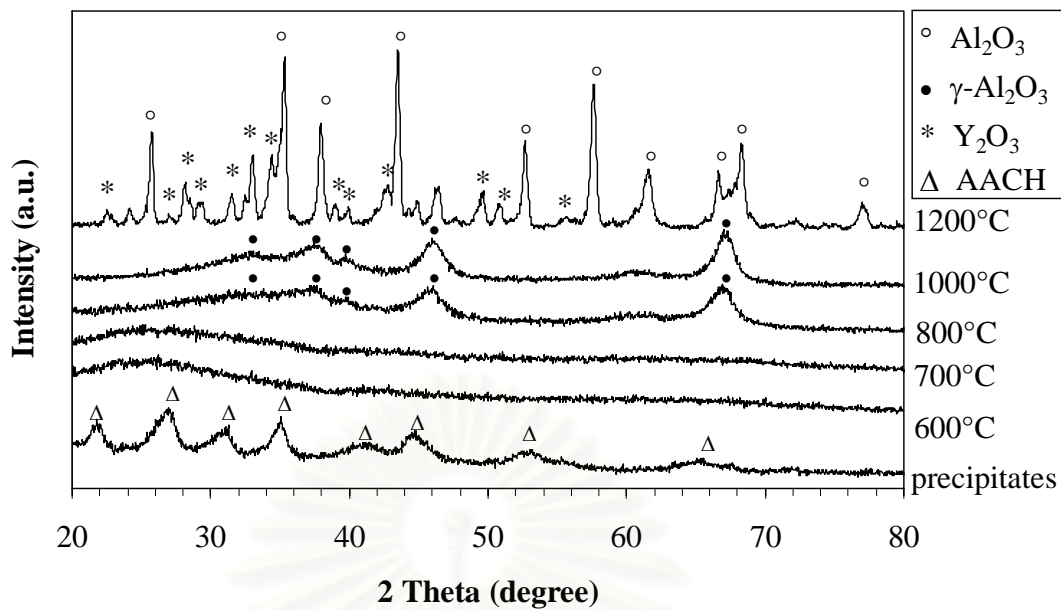


**Figure D.17** XRD patterns of the precipitate and products calcined at various temperatures, which were obtained from precipitation accompanied by yttrium at 1.0 wt.%.

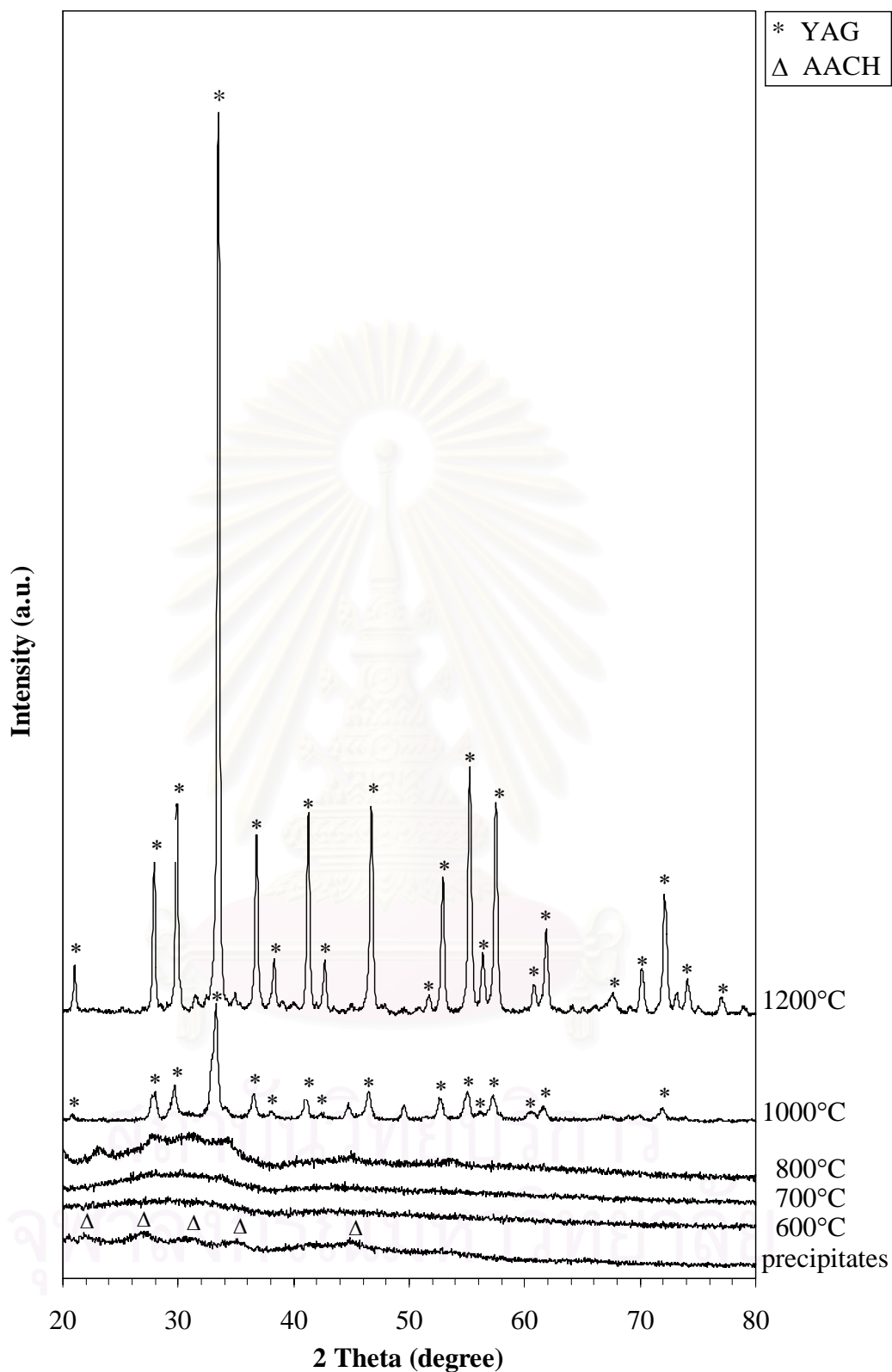


**Figure D.18** XRD patterns of products calcined at various temperatures, which were obtained from precipitation accompanied by yttrium at 10 wt.%.

## APPENDIX E

### CONDITIONS FOR BALL MILL AND DISPERSION OF POWDER

#### **Ball mill**

The particles size can be reduced a by breaking some soft agglomeration of powders by using polypropylene bottle and high purity alumina balls.

Place high purity alumina ball 362 g or half of bottle, alumina powder, and ethanol solution 100 cc into the polypropylene bottle which has volume 250 cc. Mill this bottle with rotating speed 150 rpm at desired time. After milling with ball mill, filter the solution of powder and dry in the oven at 100°C for 24 h.

#### **Dispersion of powder**

Before measuring a particle size distribution of alumina powder, all powders should to be dispersed by following steps :

1. Preparation of dispersion solution with concentration 0.2 wt% by dissolving NaHMP (Sodium Hexa Methaphosphate) 0.2 g in distilled water 99.8 g.
2. Use this solution 50 cc for 0.5 g of powder, then mix this solution with magnetic stirrer for 30 minutes.

After mixing by magnetic stirrer, pour the solution into a bottle and sealed with para-film and place it into ultrasonic apparatus for 30 minutes before measuring their particle size distribution by using Laser Particle Size Distribution Analyzer.

จุฬาลงกรณ์มหาวิทยาลัย

## APPENDIX F

### DENSITY

- **Bulk density**

The bulk density of specimens was measured according to Archimedes' method. The air in open pores of specimen was removed by applying vacuum for 30 min and then water was poured onto specimens until submerged in water. Water was further forced into the opened pores by applying vacuum for 2 h. The dry weight  $W_d$  were measured and used to calculate the bulk density using equation (E.1) following ASTM standard (Designation : C830-93).

$$\text{Bulk density} = \frac{W_d}{W_{\text{sat}} - W_{\text{sus}}} \rho \quad (\text{E.1})$$

Where  $\rho$  is water density at the measurement temperature (0.996512 g/cm<sup>3</sup> at 27°C)

- **Theoretical density**

The theoretical density of sintered pellets was calculated from real density using the following equation.

$$\text{Theoretical density} = \frac{W_{\text{total}}}{W_a/\rho_a + W_b/\rho_b + \dots} \quad (\text{E.2})$$

Where

$W_{\text{total}}$	is total weight of used component.
$W_a, W_b$	are weights of component, a and b, respectively.
$\rho_a, \rho_b$	are real densities of component, a and b, respectively.
a, b, ...	are used components.

In this experiment, the theoretical densities of pure Al<sub>2</sub>O<sub>3</sub> = 3.98 g/cm<sup>3</sup> was used for calculation.

- **Relative density**

The relative density of the sintered specimens was calculated from its bulk density and theoretical density using the following equation :

$$\text{Relative density} = \frac{\text{Bulk density}}{\text{Theoretical density}} \quad (\text{E.3})$$

$$\text{And \% of theoretical density} = \text{Relative density} \times 100$$



สถาบันวิทยบริการ  
จุฬาลงกรณ์มหาวิทยาลัย

## LIST OF PUBLICATION

1. Benjaporn Muangsombut, Piyasan Prasertdam, and Varong Pavarajarn, “Effects of Secondary Metal Doping and Sol-seeding on Phase Transformation of Alumina Prepared by Precipitation Method”, Proceedings of the Regional Symposium on Chemical Engineering 2005, Hanoi, Vietnam, Nov.30-Dec.3, 2005, Ref. No. OCA-02.



สถาบันวิทยบริการ  
จุฬาลงกรณ์มหาวิทยาลัย

## Effects of Secondary Metal Doping and Sol-Seeding on Phase Transformation of Alumina Prepared by Precipitation Method

Benjaporn Muangsombut\*, Piyasan Praserttham and Varong Pavarajarn<sup>+</sup>

Center of Excellence on Catalysis and Catalytic Reaction Engineering,  
Department of Chemical Engineering, Faculty of Engineering, Chulalongkorn University,  
Bangkok 10330 Thailand.

<sup>+</sup> Corresponding author (Tel: +66-02-2186890, Fax: +66-02-2186877, Email: fchvvp@eng.chula.ac.th)

### Abstract

The objective of this research is to study the influence of secondary metal doping and sol-seeding on phase transformation of alumina. Nanocrystalline alumina was prepared by precipitation method, using ammonium aluminium sulfate and ammonium hydrogen carbonate aqueous solutions as starting materials. The secondary metal doping was done by incorporating nitrate salt of iron, chromium, yttrium or magnesium into the solution. The obtained precipitation was dried at 120°C for 24 h before heat treatment at temperature in the range of 600-1200°C for 3 h. Physical properties as well as phase composition of the products were investigated by X-ray diffraction (XRD), scanning electron microscope (SEM), thermogravimetric and infrared spectroscopy analysis (IR) and UV-Visible spectroscopy techniques. XRD analysis revealed that the precipitate transformed to  $\alpha$ -alumina upon the calcination at high temperature via the formation of metastable  $\gamma$ -alumina. It was found that small amount of the secondary metal doping was sufficient to increase the phase transformation temperature, from  $\gamma$ - to  $\alpha$ -alumina, up to 1000°C. In the other words,  $\gamma$ -alumina could be stabilized up to 1000°C by addition of the secondary metal. The doped metal altered the sintering behavior and crystallite size of the product. The effects of type of metal as well as amount of metal doped on the phase transformation behavior of alumina were discussed. The effects of metal-doping were also compared with seeding effect from an addition of alumina sol into the precipitates.

**Keyword:** Alumina; Metal doping; Phase transformation; Precipitation method.

### Introduction

Alumina ( $\text{Al}_2\text{O}_3$ ) has been considered as one of the most promising advanced materials for variety of applications because of its distinctive chemical, mechanical and thermal properties. Alumina is widely used as ceramic, ceramic coating, catalyst, catalyst support, wear-resistance material, soft abrasive, medicinal material, filler, crucible, sagger and adsorbent. Many techniques have been developed to synthesize alumina powder with required characteristics, such as precipitation from solution, sol-gel synthesis, hydrothermal synthesis, microwave synthesis, emulsion evaporation and solvothermal synthesis. In such methods, the characteristics of alumina are tailored-made by controlling crystalline phase, crystal size, particle shape, particle size distribution, degree of agglomeration and porosity of particles [1-4].

Alumina can exist in many metastable phases before transforming to the stable  $\alpha$ -alumina (corundum form). There are six principal metastable phases of alumina designated by the Greek letters chi ( $\chi$ ), kappa ( $\kappa$ ), eta ( $\eta$ ), theta ( $\theta$ ), delta ( $\delta$ ), and gamma ( $\gamma$ ), respectively. Many industrial solid catalysts are made up from active centers anchoring on transition alumina supports, which have good characteristics such as high porosity, high surface area, good mechanical strength and thermal stability.

Many studies on alumina, in material aspect, have focused on the relationship between phase transformation from transition aluminas to  $\alpha$ -alumina and sinterability of the final material [5-8]. Nevertheless, stabilization of transition alumina is also a challenge for other applications, especially in catalytic applications. To prevent or delay alumina phase transformation, addition of doping elements has been extensively used [9-11].

It is a challenge to find the method to synthesize transition alumina that is thermally stable at high temperature, in order to extend its range of applications. In this research, the main purpose is to study the effect of secondary metals doping and seeding on the phase transformation of alumina synthesized by precipitation method.

### Materials and Methods

In the precipitation method, alumina powder is obtained from calcination of ammonium aluminum carbonate hydroxide ( $\text{NH}_4\text{AlCO}_3(\text{OH})_2$ ), which is produced from the reaction between the solution of ammonium hydrogencarbonate and aluminum salt solution.



Ammonium aluminium sulfate aqueous solution (AAS solution) was gradually added, at the rate of 3 ml/min, to ammonium hydrogencarbonate aqueous solution (AHC solution). The concentration ratio of AAS solution to AHC solution was 0.5:2.0 mol/l. The mixture was rigorously agitated with magnetic stirrer. The temperature and pH of the mixture were controlled to be 40-45°C and pH = 9, respectively. After the mixed solution was aged for 15 minutes, white precipitates formed were separated from the solution by centrifuge, repeatedly washed by methanol and dried at 110°C for 12 h. Doping of the secondary metal was done by incorporating nitrate salt of iron, chromium, yttrium or magnesium into AAS solution in the predetermined amount.

For sol-seeding, 24 g of aluminum nitrate was dissolved in 50 ml of ethanol at room temperature. The solution was transferred into a reactor equipped with a reflux-condenser and kept at temperature in the range of 70-80°C for 18 h. The obtained liquid containing alumina sol was mixed with AAS solution before dropping into AHC solution, according to the procedure previously described.

All of the dried precipitates were calcined in air in a box furnace. The product was heated at a rate of 10°C/min to the desired temperature and held at that temperature for 3 h. The obtained products were characterized by using X-ray diffraction (XRD), scanning electron microscope (SEM), thermogravimetric and differential thermal analysis (TG-DTA) and UV-Visible spectroscopy techniques.

## Results and Discussion

### Alumina Prepared by the Precipitation Method

The XRD analysis of undoped samples, as shown in Figure 1a, reveals that the precipitate obtained from the reaction between AAS and AHC is in fact ammonium aluminium carbonate hydroxide (AACH). All diffraction peaks are broad, indicating that the crystals are very small and imperfect, which agrees with AACH reported in the previous finding in literature [12].

Upon the calcination at low temperature, AACH is decomposed and transformed to amorphous materials. At calcination temperature of 700°C,  $\gamma$ -Al<sub>2</sub>O<sub>3</sub> is observed. It should be noted that the diffraction peaks corresponding to  $\gamma$ -Al<sub>2</sub>O<sub>3</sub> are weak in intensity, which indicates that it is under transition from amorphous phase. The crystallinity of  $\gamma$ -Al<sub>2</sub>O<sub>3</sub> phase improves as the calcination is increased to 800°C. Phase transformation to  $\alpha$ -Al<sub>2</sub>O<sub>3</sub> takes place at temperature lower than 1000°C, as evidenced from the fact that the powder calcined at 1000°C is mixture of  $\alpha$ - and  $\gamma$ -phase. However, trace amount of  $\theta$ -Al<sub>2</sub>O<sub>3</sub> detected from the sample calcined at this temperature suggests that  $\gamma$ - to  $\theta$ -phase transformation also takes place. At temperature higher than 1000°C, only peaks corresponding to  $\alpha$ -Al<sub>2</sub>O<sub>3</sub> are observed. Sharp and high-intensity XRD peaks of  $\alpha$ -Al<sub>2</sub>O<sub>3</sub> suggest the growth of crystallite grains upon the completion of phase transition [13].

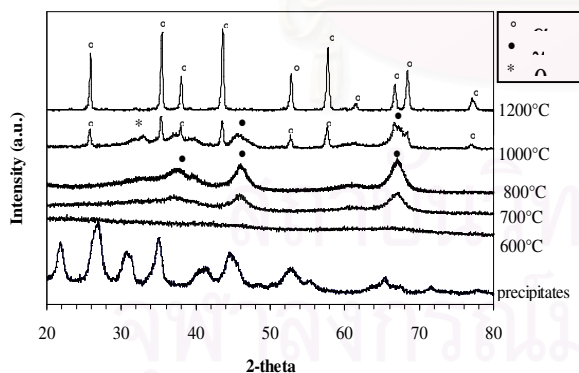


**Figure 1-** XRD patterns of the undoped precipitate and undoped products calcined at various temperatures.

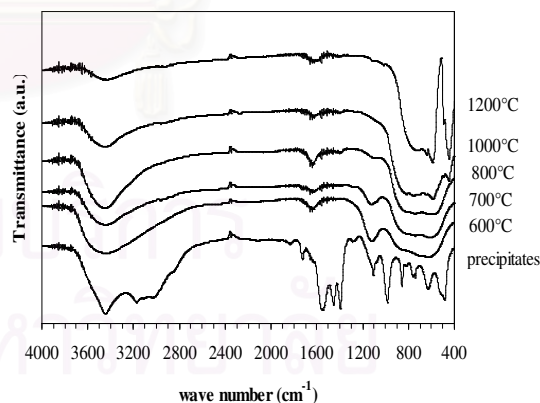


**Figure 2-** FTIR spectra of the undoped precipitate and undoped products calcined at various temperatures.

The crystallite size of  $\gamma$ -Al<sub>2</sub>O<sub>3</sub> in all samples, calculated from XRD peak broadening using Scherrer equation, is approximately 4-6 nm. As the calcination temperature is increased over 1000°C, phase transformation takes place and the  $\alpha$ -Al<sub>2</sub>O<sub>3</sub> grows rapidly. The crystallite size of  $\alpha$ -Al<sub>2</sub>O<sub>3</sub> obtained is around 50 nm. It should be noted that no significant growth of  $\gamma$ -Al<sub>2</sub>O<sub>3</sub> crystallites was observed prior to the  $\gamma$ - to  $\alpha$ -phase transformation. SEM micrographs of the synthesized powder (not shown) reveal that grains of alumina powder agglomerate into the secondary particle about 10  $\mu$ m in size. However, it is suggested that the secondary

particles are resulted from soft aggregates, since the average size of the secondary particles can be easily decreased by milling.

The FTIR spectra of sample calcined at different temperatures are shown in Figure 2. The presence of organic moiety in the pre-calcined precipitate can be clearly observed, e.g. the absorption from  $\text{CO}_3^{2-}$  and  $\text{NH}_4^+$  at wave number 800 and 1425  $\text{cm}^{-1}$ , respectively. These organic groups are eliminated upon the calcination. After calcination at 600°C, a broad and smooth absorption band in the wave number ranging from 500 to 900  $\text{cm}^{-1}$ , which indicates the formation of amorphous nanosized alumina, was observed. This band has been attributed to the disordered distribution of vacancies and broad distribution of bond length in amorphous material [11]. At 700 and 800°C, the infrared spectra of the products show absorption bands at 615 and 747  $\text{cm}^{-1}$  that are specific to tetrahedral Al-O vibration from  $\gamma$ -phase. Finally, when the calcination temperature is increased to 1000°C, the absorption bands at 443, 590 and 639  $\text{cm}^{-1}$  appear. These bands are identified to be characteristic absorption bands of octahedral Al-O vibration from  $\alpha$ - $\text{Al}_2\text{O}_3$ . It can be seen that the FTIR results are in good agreement with XRD observation.

### Effects of Sol-Seeding

For the precipitation accompanied by sol-seeding, it is found that the precipitate is still AACH (see Figure 3). However, the product from the decomposition of AACH in this case remains amorphous even after calcination at 700°C. Notable amount of  $\gamma$ - $\text{Al}_2\text{O}_3$  is detected only after the precipitate is calcined at 800°C, which is higher than the case of precipitation without sol-seeding. The  $\gamma$ -phase is still the sole crystalline phase observed in the product calcined at 1000°C. The results clearly show that the introduction of seeds results in  $\gamma$ - $\text{Al}_2\text{O}_3$  with improved thermal stability. Nevertheless, at 1200°C, all  $\gamma$ -phase completely transforms into  $\alpha$ - $\text{Al}_2\text{O}_3$ . This result is in good agreement with previous report by Youn *et al.* that the sol-effect does not reduce the finishing temperature for the  $\alpha$ - $\text{Al}_2\text{O}_3$  conversion [13]. The sol-effect may be regarded as  $\alpha$ - $\text{Al}_2\text{O}_3$  self seeding.

The FTIR spectra of the precipitate obtained by reaction system with sol-seeding is quite different than that of the precipitate without sol-seed (Figure 4). The absorption bands corresponding to organic moieties are no longer apparent. Instead, the characteristic absorption bands of nitrate ion at 1465  $\text{cm}^{-1}$  [1] is observed. Moreover, the bands at 615 and 773  $\text{cm}^{-1}$ , which are characteristic bands of boehmite,  $\text{Al}(\text{OOH})$ , [13] are observed. However, after calcination, only absorption bands associated with  $\gamma$ - or  $\alpha$ -alumina, depending on the calcination temperature were observed. The FTIR results were consistent with XRD analysis.

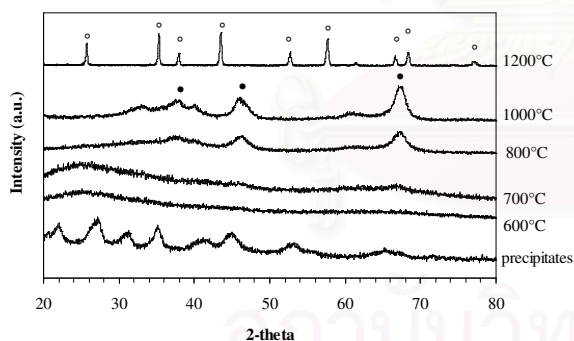


**Figure 3-** XRD patterns of the precipitate and products calcined at various temperatures, which were obtained from precipitation accompanied by sol-seeding

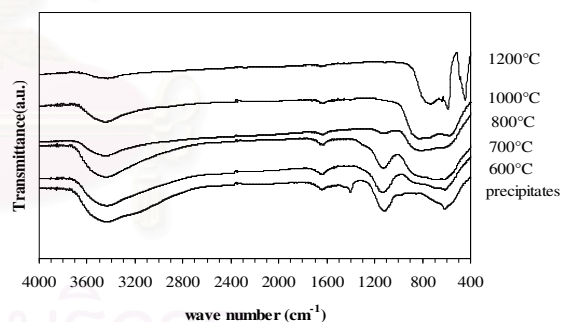


**Figure 4-** FTIR spectra of the precipitate and products calcined at various temperatures, which were obtained from precipitation accompanied by sol-seeding

### Effect of Secondary Metal Doping

The secondary metal was doped into alumina by co-precipitation method described earlier. By using low content of the dopant (0.1 wt.%), no crystalline phase other than alumina could be detected by XRD analysis, with an exception in the case of chromium doping. Nevertheless, the presence of metal in alumina powder was confirmed by the X-ray photoelectron spectroscopy analysis. It was found that the phase transformation behavior of the products doped with 0.1 wt.% of iron, magnesium or yttrium is similar to that of alumina introduced with seeds, i.e. the thermal stability of  $\gamma$ -alumina is significantly enhanced.

For chromium-doped alumina,  $\text{Cr}_2\text{O}_3$  was found mixed with  $\gamma$ - $\text{Al}_2\text{O}_3$  in the product calcined at temperature in the range of 700 to 800°C. The higher the chromium content, the higher the temperature at which  $\text{Cr}_2\text{O}_3$  was detected. However, the signal from  $\text{Cr}_2\text{O}_3$  disappeared after the product was calcined at temperature near the transformation temperature to  $\alpha$ -alumina. It should be noted that chromium-doped powder which is

calcined at 600-1000°C is green, due to  $\text{Cr}^{3+}$  from the presence of  $\text{Cr}_2\text{O}_3$ . After the calcination at temperature higher than 1000°C, the obtained powder is pink, which indicates dissolution of Cr species into the corundum structure.

For iron doping, the thermal stability of  $\gamma\text{-Al}_2\text{O}_3$  doped 0.5 or 1.0 wt.% iron is slightly lower than the product with only 0.1 wt.% iron. The direct phase transformation of alumina from  $\gamma$ - to  $\alpha$ -phase takes place at temperature lower than 1000°C if moderate amount (1.0 wt.%) of iron is used. No iron-containing compound, such as iron oxide, was found after the heat treatment. On the contrary, when extremely high amount of iron, e.g. 10 wt.%, is co-precipitated with AACH, formation of  $\alpha\text{-Fe}_2\text{O}_3$  as well as  $\text{FeAl}_2\text{O}_4$  is evolved during the calcination at 800 and 1000°C, respectively. These phases remain mixed with alumina product even after calcination at higher temperature.

For magnesium- and yttrium-doped alumina, no significant change in the effect of metal content on thermal stability of  $\gamma$ -phase, was observed. Doping of magnesium or yttrium in the amount corresponding to 0.5 or 1.0 wt.% results in the same effect as 0.1 wt.% doping. However, oxides of both compounds, i.e. MgO and  $\text{Y}_2\text{O}_3$  were formed after calcination at 1200°C.

### Conclusion

In this work, phase transformation of alumina powder prepared by the precipitation method, using AAS and AHC aqueous solution as reagents, is investigated. The white precipitate formed from the reaction is identified as ammonium aluminium carbonate hydroxide, which decomposes to amorphous alumina upon the calcination. Further increase in calcination temperature results in phase transformation to  $\alpha$ -alumina, via the formation of metastable  $\gamma$ -phase. It is found that small amount of the secondary metal doping, as well as the introduction of alumina sol-seeds, is sufficient to raise the temperature at which  $\gamma$ - to  $\alpha$ -phase transformation takes place to 1000°C. In the other words,  $\gamma$ -alumina can be stabilized up to 1000°C by the addition of the secondary metal or alumina sol seeds. The secondary particles of the calcined powder are soft aggregates of 4-6 nm alumina grains, which can be broken off by ball milling.

### Acknowledgements

The authors would like to acknowledge partial support from the Thailand Research Fund (TRF) and the Graduate School, Chulalongkorn University.

### References

- [1] Trimm D.L. and Stanislaus A., The Control of Pore Size in Alumina Catalyst Supports: A Review, *Applied Catalysis* 1986; 21: 215-400.
- [2] Rajendran S., Production of Ultrafine  $\alpha$ -Alumina Powders and Fabrication of Fine-Grained Strong Ceramics, *Journal of Materials Science* 1994; 29: 5664-72.
- [3] Androff N.W., Francis L.F. and Velamakanni B.V., Macroporous Ceramics from Ceramic-Polymer Dispersion Methods, *AIChE Journal* 1997; 43: 2878-88.
- [4] Hellgardt K. and Chadwick D., Effect of pH of Precipitation on the Preparation of High Surface Area Aluminas from Nitrate Solutions, *Industrial & Engineering Chemistry Research* 1998; 37: 405-11.
- [5] Badkar P.A. and Bailey J.E., *Journal of Materials Science* 1976; 11: 1794.
- [6] Jagota N.K. and Raj R., *Journal of Materials Science* 1992; 27: 2251.
- [7] Kumagai M., and Messing, G. L., Enhanced Densification of Boehmite Sol-Gels by  $\alpha$ -Alumina Seeding, *Journal of the American Ceramic Society* 1984; 67: C230.
- [8] Kumagai M. and Messing G.L., Controlled Transformation and Sintering of a Boehmite Sol-Gel by Seeding, *Journal of the American Ceramic Society* 1985; 68: 500.
- [9] Burtin P., Brunelle J.P., Pijolat M. and Soustelle M., Influence of Surface Area and Additives on the Thermal Stability of Transition Alumina Catalyst Supports. I: Kinetic Data, *Applied Catalysis* 1987; 34: 225-38.
- [10] Burtin P., Brunelle J.P., Pijolat M. and Soustelle M., Influence of Surface Area and Additives on the Thermal Stability of Transition Alumina Catalyst Supports. II: Kinetic Model and Interpretation, *Applied Catalysis* 1987; 34: 239-54.
- [11] Lafarga D., Lafuente A., Menendez F. and Santamaria J., Thermal Stability of Gamma- $\text{Al}_2\text{O}_3$ /Alpha- $\text{Al}_2\text{O}_3$  Mesoporous Membranes, *Journal of Membrane Science* 1998; 147: 173-85.
- [12] Prasitwuttisak T., Pavarajarn V. and Praserttham P., Comparative Study of Nanoscaled Alumina and Chromium Doped Alumina Powder Prepared from Various Synthesis Techniques, *Proceedings of the Regional Symposium on Chemical Engineering 2004, Bangkok, Thailand, Dec. 1-3, 2004.*
- [13] Youn H.J., Jang J.W., Kim I.T. and Hong K.S., Low-Temperature Formation of  $\alpha$ -Alumina by Doping of an  $\alpha$ -Sol, *Journal of Colloid and Interface Science* 1999; 211: 110-3.

## VITA

Miss Benjaporn Muangsombut was born in Bangkok, Thailand, on April, 1982. She received bachelor's degree in Chemical Engineering from the department of Chemical Engineering, Faculty of Engineering, King Mongkut's Institute of Technology Ladkrabang, Bangkok, Thailand on May, 2004.



สถาบันวิทยบริการ  
จุฬาลงกรณ์มหาวิทยาลัย